NITROGEN AND HYDROGEN INDUCED TRAP PASSIVATION AT THE SiO_2/4H-SiC INTERFACE

By

Sarit Dhar

Dissertation

Submitted to the Faculty of the

Graduate School of Vanderbilt University

in partial fulfillment of the requirements

for the degree of

DOCTOR OF PHILOSOPHY

in

Interdisciplinary Materials Science

May, 2005

Nashville, Tennessee

Approved:

Professor Leonard C. Feldman
Professor Sokrates T. Pantelides
Professor Daniel M. Fleetwood
Professor Bridget R. Rogers
Professor John R. Williams

ACKNOWLEDGEMENTS

This work would not have been possible without the involvement and assistance of other individuals, to all of whom I am deeply indebted. I am highly grateful to my advisor Prof. Leonard C. Feldman for his invaluable guidance and encouragement throughout this work. I would like to thank Prof. John R. Williams of Auburn University for his continual involvement with this work. I wish to acknowledge the technical guidance and assistance I received from Dr. Anthony B. Hmelo and Mr. Walter Augustyniak with all lab activities. Working with these gentlemen and other fellow scientists at Vanderbilt was a pleasure and certainly a very intellectually satisfying experience.

This acknowledgement would be incomplete without thanking my family. I thank their constant support and love that I have received throughout this work. Finally, I would like to acknowledge Vanderbilt University, ONR and DARPA for the financial support I received during this research work.

TABLE OF CONTENTS

Page

LIST OF TABLES

LIST OF FIGURES

CHAPTER I

INTRODUCTION

Development of wide band-gap semiconductor devices is a key to highly efficient technologies for high-temperature and/or high-power electronics applications. Such applications are widespread; some important areas would be electric power conditioning/transmission/ distribution, industrial motor control, electric vehicles, aircraft and ships, well logging, and radiation hardened instrumentation**.** Replacement of conventional Si-based systems with cost-efficient wide-band gap technologies in such niche application areas could lead to substantial socio-economic gains.

Silicon is the most technologically developed and widely studied semiconductor material and is the basis of the modern electronics revolution. However, owing to its fundamental material properties it is not suitable for high temperature and/or high power environments. Semiconductors with a band-gap greater than 2 eV such as SiC, the group III-nitrides (GaN, AlN and BN) and diamond are the potential candidates that promise improved performance under such extreme conditions. Among these materials, SiC is the most mature from the development standpoint. High quality single crystal wafers are commercially available; wafer cost is decreasing rapidly, wafer size and substrate quality is increasing. SiC Schottky diodes are available commercially, and other devices have been projected to be marketed within the next few years.

Compared to other wide band-gap materials, SiC has the unique advantage that it can thermally oxidize to form SiO_2. This property has motivated the development of the

SiC power metal-oxide-semiconductor field effect transistor (power MOSFET), along the lines of Si power MOSFETs. In MOS devices, the quality of the insulator (i.e. oxide)/ semiconductor interface plays a significant role in determining the overall device performance. However, the electronic properties of the SiO_2/SiC interface are inferior compared to the SiO_2/Si interface. This problem has been a major obstacle for the realization of reliable SiC power MOSFETs. The fundamental understanding and modification of this critical SiC interface is the subject of this thesis. A summary of the work undertaken as a part of this dissertation has been presented in the next section. The rest of the chapter is devoted to addressing fundamental problems at the SiO_2/SiC interface that motivate this work. In order to proceed in a systematic manner, a basic introduction to power MOSFET operation is provided. This is followed by a brief description of the physical properties of SiC and Si and properties of oxide layers thermally grown on SiC. The SiO_2/SiC interface problem has been discussed from the standpoint of fundamental materials science research. Chapters II-VI consist of detailed scientific investigation of this materials system. These are presented in a 'journal' format.

Summary of research

With a motivation of developing SiO_2/4H-SiC interfaces with low trap densities, we have focused on the following issues in this dissertation:

(i) Crystal face dependency of oxidation and nitridation. Three crystal faces of 4H-SiC have been studied, namely the (0001) Si-, $(11\bar{2}0)$ a- and $(000\bar{1})$ C-faces.

(ii) Effect of nitridation of oxide films grown on $(11\bar{2}0)$ a- and the $(000\bar{1})$ C-faces.

(iii) Effect of hydrogenation of nitridated interfaces for the (0001) Si, $(11\bar{2}0)$ a- and the $(000\bar{1})$ C-faces.

An overview of the various measurements performed on the different crystals faces studied is presented in Table 1.1, according to the layout of this thesis.

We have observed dramatic reduction of interface trap densities for all three crystal faces ((0001) Si, $(11\bar{2}0)$ a-face and the $(000\bar{1})$ C-face) via nitridation by NO post-oxidation annealing. Further reduction of trap densities has been achieved by using sequential anneals in NO and H_2. Record low interface trap densities were achieved on the (0001) Si face and $(11\bar{2}0)$ a-face using this process. Excellent field effect mobilities were obtained on MOSFETs fabricated by this process - the maximum mobilities being ~55 cm^{-2} $V^{-1}s^{-1}$ and ~100 cm^{-2} $V^{-1}s^{-1}$ for the (0001) Si face and $(11\bar{2}0)$ a-face respectively, as shown in Fig. 1.1. To the author's knowledge, this is one of the best results obtained on the $(11\bar{2}0)$ a-face. These promising results definitely add to the technological relevance of the work presented in this dissertation. The following is a summary of the major accomplishments of this work:

(i) First demonstration of the effectiveness of NO in passivating traps on the $(11\bar{2}0)$ a- and $(000\bar{1})$ C-face.

(ii) Record low trap densities on the $(11\bar{2}0)$ a- and $(000\bar{1})$ C-face using sequential passivation anneals in NO and H_2.

(iii) First observation of nitridation anisotropy on 4H-SiC.

(iv) First measurements of hydrogen incorporation at the SiO_2/SiC interface, incorporated via post-metallization annealing in H_2.

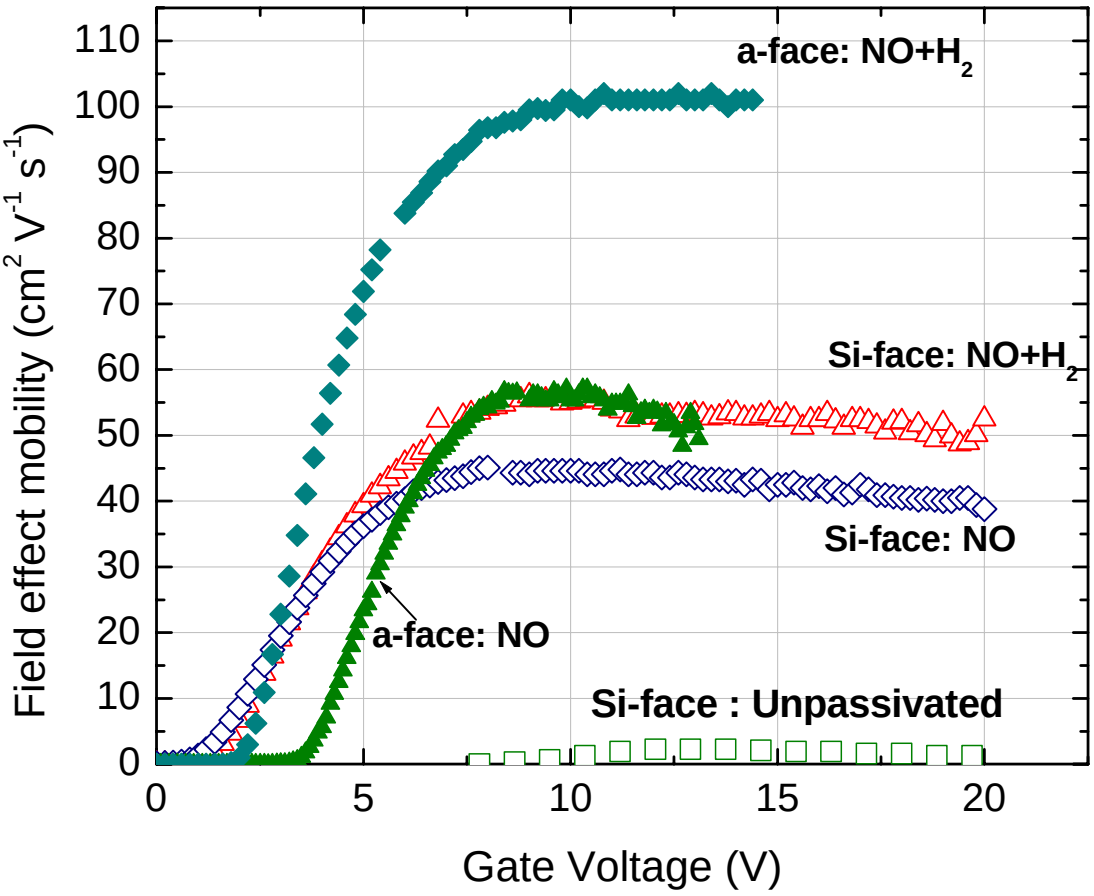

FIG 1. 1 Field effect mobilities of lateral test MOSFETs fabricated on the (0001) Si-face and (11$\bar{2}$ 0) a-face using different passivation procedures.

Table 1.1 Overview of different measurements performed on the different crystal faces of 4H-SiC.

Crystal face in bold (if any) signifies the emphasis of that face in that particular chapter. RBS: Rutherford backscattering spectrometry, SE: Spectroscopic ellipsometry, CV: Capacitance-voltage measurements, MEIS: Medium energy ion scattering, NRA: Nuclear reaction analysis, EELS: Electron energy loss spectroscopy

Chapter (Paper)	**Measurement**	**Crystal face studied**
II	Oxide growth (RBS, SE)	Si, a, C
III	NO passivation (CV) Interface composition (MEIS)	**a,** Si
IV	NO passivation (CV) H passivation (CV)	Si, a, **C**
V	Interfacial N uptake (NRA, EELS)	Si, a, C
VI	H passivation (CV) Interfacial H up-take measurements (NRA)	**Si**

Power MOSFET

A schematic diagram of an n-channel vertical power MOSFET[1] is shown in Fig.1.2. This type of a device is most commonly employed for power switching applications. Common fabrication procedures involve high dose N and low dose Al ion implantation into n-type SiC (usually N doped) to form the n+ source and p-well regions, respectively. The starting SiC substrate is highly doped (N_d~10^{19} cm^{-3}) on the drain side, with a lowly doped (N_d~10^{16} cm^{-3}) 'drift' layer on top. In this three-terminal device, the

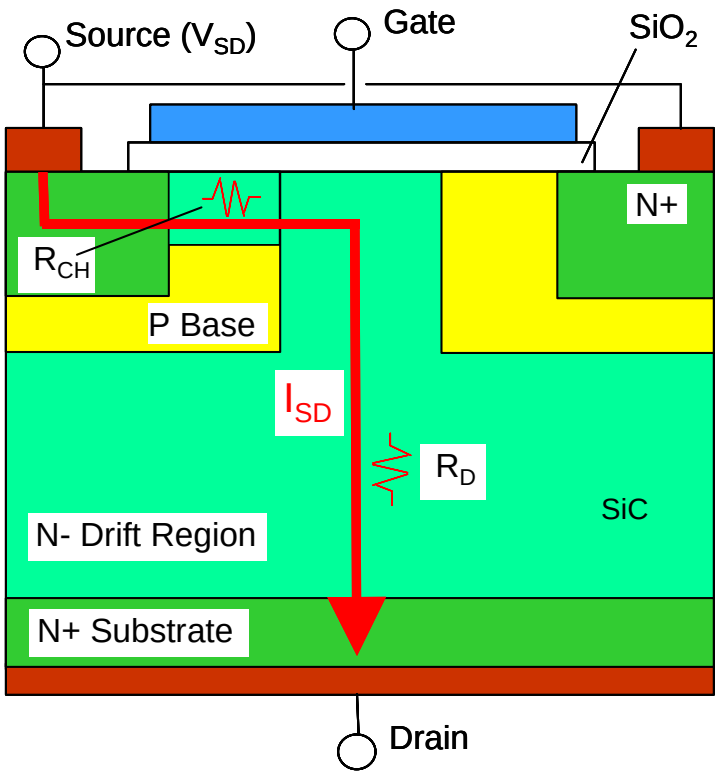

FIG 1. 2 Schematic of vertical power MOSFET. *n*-inversion channel formed by the application of a positive gate voltage. The arrow indicates the flow of electrons from source to drain.

current flow between the source and drain is controlled by the voltage applied at the gate. During device operation, a positive voltage is applied to the drain (denoted by V_{SD} in Fig. 1.2) with the source grounded. In the absence of a positive gate voltage (off-state), no current flows and the source-drain voltage is supported entirely across the depletion region of the pn junction formed by the base and the drift regions. When a positive voltage is applied to the gate, the electric field repels holes and attracts electrons in a shallow region (~1-2 nm) at the surface of the p-base known as the 'inversion channel'. The inversion channel forms a conducting path for current flow, and the 'on-state' of the device is achieved. In the 'on-state', the total resistance to current flow is represented by the 'on-resistance' R_{ON}. This term determines the total internal power loss in the device and determines the maximum current rating of a device. R_{ON} represents the sum of the various internal resistances in the current path, with two important components being the channel resistance R_{CH} and the resistance of the drift layer R_D (as shown in Fig. 1.2). For vertical MOSFETs, the theoretical minimum value for the on-resistance is determined by the parameter "specific on-resistance" or "resistance-area product" of the drift region.[2]

$$R_{on,sp} \sim \frac{V_B^2}{\mu_N \varepsilon_S E_C^3} \tag{1.1}$$

Here V_B is the voltage blocked by the MOSFET, μ_N is the bulk electron mobility perpendicular to the semiconductor / oxide interface, ε_S is the permittivity of SiC and E_C is the critical field. This parameter represents the 'ideal' on-resistance of the drift layer, neglecting any other resistances in the device. The great promise of SiC can be seen in the expression for $R_{on,sp}$, where E_C is approximately seven times larger for SiC than for Si. Lower on-resistance by a factor of more than 300 should be possible with SiC as

shown in Fig. 1.3. Significant improvements in performance can be realized compared to Si MOSFETs for devices that operate near this theoretical performance limit.[3]

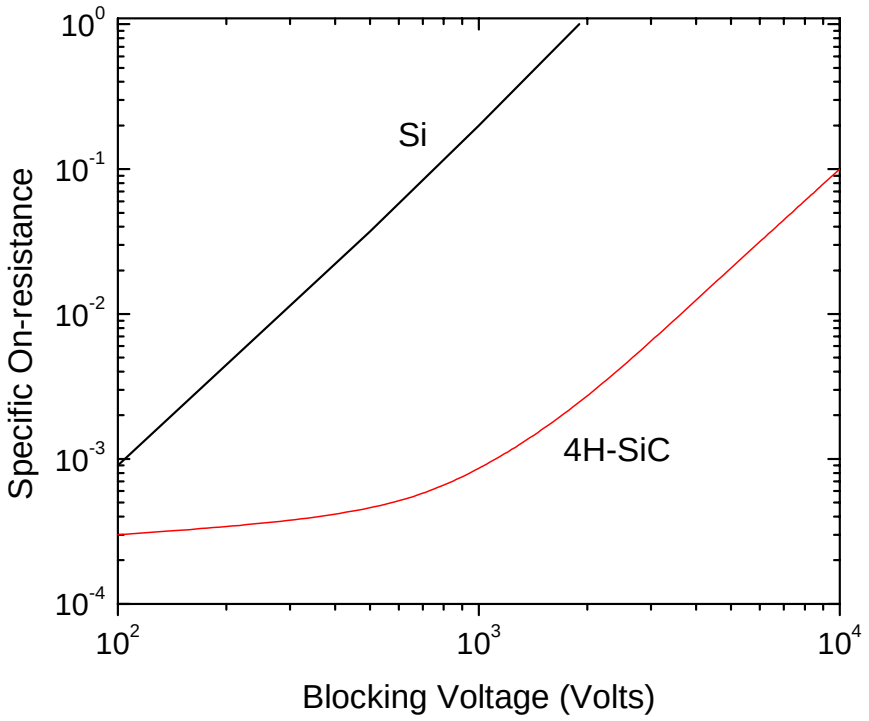

FIG 1. 3 Specific on-resistance as a function of blocking voltage for Si and 4H-SiC power devices.

The low field channel resistance R_{CH}, is given by:

$$R_{CH} = \frac{L}{WQ_N \mu^{CH}{}_N} \tag{1.2}$$

where L and W are the length and width of the channel respectively; Q_N is the inversion layer charge available for current conduction and $\mu^{CH}{}_N$ is the mobility of the electrons in the inversion channel. The quality of the SiO_2/SiC interface determines $\mu^{CH}{}_N$ and Q_N,

which in turn determine R_{CH}. Clearly Q_N and μ^{CH}_{N} should be as high as possible so that $R_{CH} << R_D$. A major problem in SiC MOSFETs has been high interface defect densities at the SiO_2/SiC interface. Such defects can limit Q_N by trapping and μ^{CH}_{N} by interface scattering, severely degrading the trans-conductance of a power MOSFET. This problem will be discussed in further detail in a later section.

Silicon Carbide

Crystal structure and polytypism

The SiC crystal is composed of bilayers of tetrahedrally bonded silicon and carbon atoms. The tetrahedral co-ordination where each Si atom is surrounded by four C atoms (and vice versa) is shown in Fig.1.4 (a) where the Si-C bond length is 1.89 $\overset{0}{A}$. SiC exhibits a one-dimensional polymorphism called polytypism. Polytypes are crystals with same stoichiometry but variable stacking sequence along the stacking direction (c-axis). If we consider Si-C pairs as spheres, then there are three possible occupation sites denoted by A, B and C (as shown in Fig.1.4 (b)) for achieving hexagonal close packing. Two simple stacking sequences are the ABCABC… and and ABAB… for the "zincblende" and "wurtzite" structures, respectively. Different polytypes of SiC are determined by such stacking sequences and, in principle there could be infinite variations. The most popular polytypes for electronic applications are the 3C, 4H, 6H and 15R, but the commercial availability of large single-crystal wafers is restricted to the 4H and 6H

polytypes. The stacking sequences for 3C (ABC…), 4H (ABCB…) and 6H (ABCACB) are shown in Fig 1.4. The nomenclatures for the polytypes, commonly

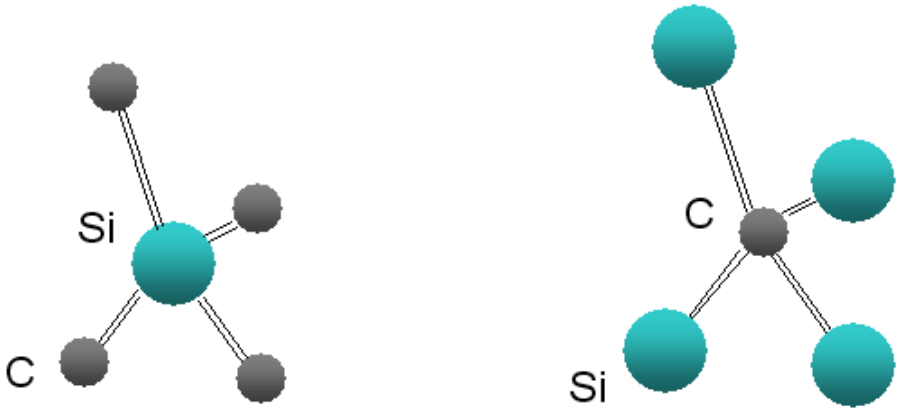

(a)

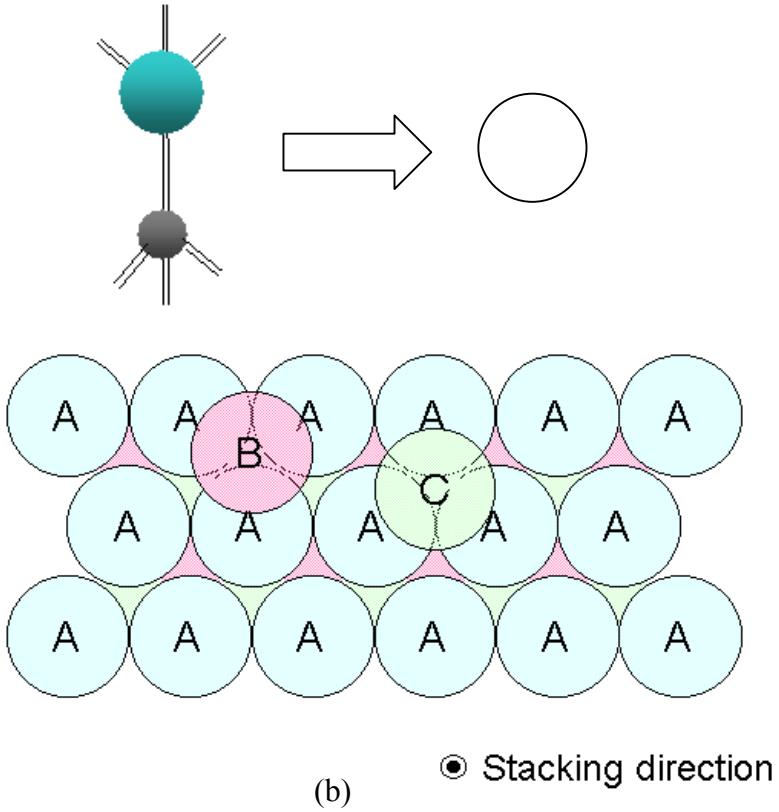

(b)

FIG 1. 4 (a) Tetrahedral bonding arrangement among Si and C atoms in SiC . (b) Close packing of system of spheres illustrating the stacking sequence AB and AC. For SiC, each sphere represents a pair of Si and C atoms.

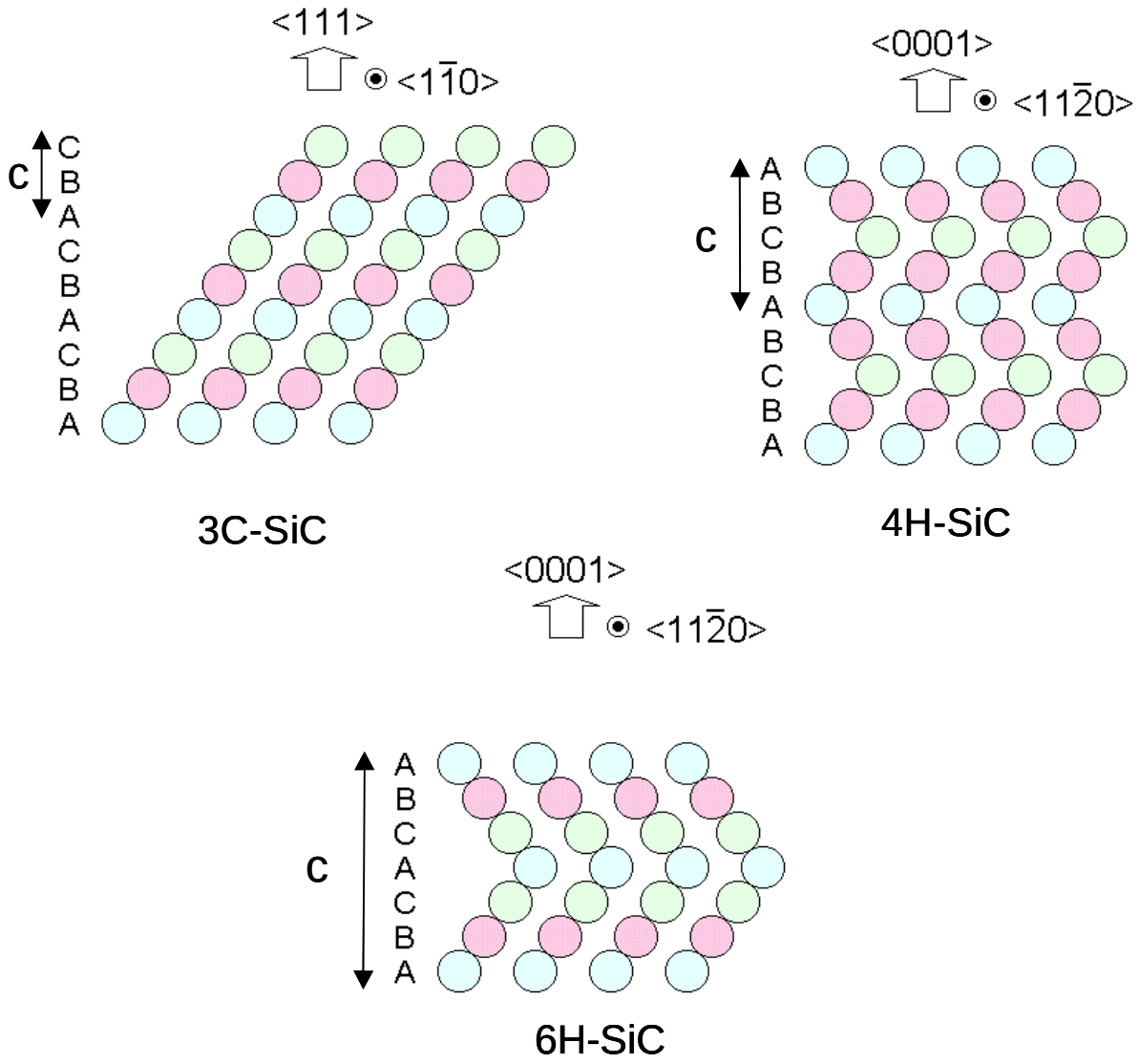

FIG 1. 5 The (11$\bar{2}$0) planes of the three different poltypes 3C, 4H and 6H-SiC, showing the stacking sequence of Si-C bilayers. The height c of the unit cell are 4.36 $\mathring{A}$ for 3C, 10.05 $\mathring{A}$ for 4H and 15.08 $\mathring{A}$ for 6H-SiC. (Figures adopted from http://matsunami.kuee.kyoto-u.ac.jp)

known as the Ramsdell's notation is as follows - polytypes are designated according to their crystal structure (C), hexagonal (H) or rhombohedral (R), and their stacking periodicity along the c-axis. Different polytypes exhibit different electronic properties, for example, the band-gap changes from 2.4 eV (3C) to 3.3 eV (4H). In this dissertation, all work has been carried out on the 4H-polytype.

SiC crystal growth

Due to the greater thermal and physical stability of SiC, it is very difficult to grow SiC single crystals by crystal pulling or seeded solidification from melt, processes used for crystal growth of common semiconductor materials like Si and Ge. The standard method used for growing large diameter (up to 100 mm) bulk crystals is a physical vapor transport process commonly known as 'seeded sublimation growth' or 'modified Lely technique'.[4] In this process, vapors produced by the sublimation of polycrystalline SiC at around 2200°C are transported over a temperature gradient and deposited on a seed crystal of desired orientation held at a lower temperature. High quality epitaxial layers can also be grown using chemical vapor deposition techniques or molecular beam epitaxy commonly referred to as step-controlled epitaxy. Using "off-axis" substrates (3.5° off (0001) for 6H and 8° for 4H) for homoepitaxial growth results in high quality smooth surfaces at lower growth temperatures (~1500°C). Extensive details of SiC bulk growth and epitaxy can be found in the review article by Powell et. al.[5] and references therein. Low defect densities in wafers are vital for industrial level production of SiC devices. Two major defects in SiC crystals are micropipes and polytype inclusions. Micropipes are defects unique to SiC that are physical holes aligned along the c-axis that often

penetrate through the entire wafer. Control of polytype during growth is also an important issue for crystal growth, as inclusions of different polytypes can degrade device performance. Due to the continuing development of SiC materials, such defect densities are getting lower (for example, the micropipe density in production grade SiC wafers is down to 10 cm^{-2}). Such an improved scale of development is essential for successful realization of a SiC electronics industry.

Physical properties

SiC has several attractive physical properties compared to other semiconductors for power electronics applications. Properties can be different for different polytypes, the most significant difference being the band-gap, as mentioned earlier. A comparison of some important properties among Si, 4H and 6H-SiC is shown in Table 1.2.[6-8]The higher critical field of SiC compared to Si is a key advantage for significant reduction of on-resistance in power devices. The larger band-gap, higher critical field and higher thermal conductivity make SiC a very promising material for high temperature applications. Due to the higher band-gap, significantly lower leakage currents can be achieved in devices working at high temperatures. The higher thermal conductivity allows the efficient transfer of heat generated by Joule heating. The high saturation velocity enables high frequency and high speed operation. Other impressive material properties include high hardness value, excellent chemical resistivity and transparency to optical wavelengths. These attributes, in conjunction with the ability to grow a thermal oxide, illustrate the great potential of SiC MOS devices for a wide range of applications.

4H-SiC is the preferred polytype for power MOSFETs due to its wider band-gap and a higher and more isotropic electron mobility. Historically, however, due to higher interface defect densities near the conduction band-edge of 4H-SiC, the effective channel mobilities in n-4H-SiC MOSFETs have been considerably lower than n-6H-SiC MOSFETs. This issue forms the central focus of the problem undertaken in this dissertation work.

Table 1.2 Physical properties of 4H- and 6H-SiC compared to Si

Property	Si	4H-SiC		6H-SiC	
Lattice constants (^{0}A)	a = 5.43	a = 3.073 c = 10.05		a = 3.083 c = 15. 11	
Band gap (eV)	1.1	3.26		3.02	
Intrinsic carrier density (cm^{-3})	1.45×10^{10}	8.2×10^{-9}		2.0×10^{-6}	
Dielectric constant (ε_r)	11.9	9.7		9.7	
Electron mobility ($cm^2\ V^{-1}s^{-1}$)	1417	$\mu_{e \perp c}$	$\mu_{e \parallel c}$	$\mu_{e \perp c}$	$\mu_{e \parallel c}$
		880	800	360	97
Hole mobility ($cm^2\ V^{-1}s^{-1}$)	471	≤ 120		≤ 90	
Electron effective mass ($m_{\perp e}/m_0$) (for density of states calculations)	1.08	0.45		0.45	
Hole effective mass ($m_{\perp e}/m_0$) (for density of states calculations)	0.55	0.66*		0.66	
Thermal conductivity ($W\ cm^{-1}\ s^{-1}$)	1.5	4.5		4.5	
Saturation carrier velocity ($cm\ s^{-1}$)	1.0×10^7	2.0×10^7		2.0×10^7	
Critical field ($MV\ cm^{-1}$)	0.3	2.0		2.4	
Specific on-resistance (relative to Si)		3×10^{-3}		4×10^{-3}	

* Value used same as 6H-SiC

All numbers apply to room temperature conditions and a dopant concentration of 10^{16} cm^{-3}

The SiO_2/SiC interface

Oxidation of SiC and oxide compostion

The simplest way to create an insulating layer on SiC is by thermal oxidation via dry (O_2) or wet (H_2O) oxidation – as is also the case for Si. The interaction of oxygen on SiC surfaces is a complex one, exhibiting regimes of oxidation and etching under different temperature and pressure conditions.[9] Oxidation for MOS fabrication is usually performed in the temperature range 1100°C-1300°C in a flowing oxidizing ambient. In this thermodynamic regime, the overall macroscopic chemical reaction for dry oxidation is given by:

$$SiC + 1.5\ O_2 \longleftrightarrow SiO_2 + CO \qquad (1.3)$$

Oxide growth on SiC is slower than on Si at the same temperature. Moreover, the oxide growth rates on different crystal faces of SiC are significantly different. A simple 'Deal-Grove' model[10] used extensively for Si cannot explain SiC oxidation kinetics and rate anisotropy. The oxidation of SiC is indeed more complex than in the case of Si due to the involvement of two kinds atoms, i.e. Si and C. The unit steps that have a key role in SiC oxidation have been described in detail in chapter II of this thesis. A modified Deal Grove model has been presented for explaining the difference in oxidation rates among the different crystal faces.

Reaction (1.3) has a dual outcome, i.e. formation of SiO_2 and out-diffusion of carbonaceous species. There could other reactions[11] such as:

$$SiC + O_2 \longleftrightarrow SiO_2 + C \qquad (1.4)$$

This reaction produces free carbon at the surface or in an interfacial reaction layer. The amount of carbon left in the oxide will be determined by the reactions:

$$SiC + 2\,CO \longleftrightarrow SiO_2 + 3\,C \qquad (1.5)$$

$$2\,C + O_2 \longleftrightarrow 2\,CO \qquad (1.6)$$

Characterization of the oxide by various optical, x-ray, electron and ion beam spectroscopy techniques show that the bulk of the oxide is stoichiometric SiO_2 and 'carbon free' within the sensitivity of current analytical techniques. Stoichiometry measurements of oxide films of different thickness on 4H and 6H-SiC using Rutherford backscattering spectrometry (RBS), performed in our laboratory, are shown in Fig. 1.6 (thickness is represented as areal density of O atoms in the figure). The measurements clearly show that the ratio of Si : O in the films is close to 1:2. The C concentration is independent of the film thickness indicating that the source of C is at or near the SiO_2/SiC interface. The interfacial C or Si concentration in these measurements (represented by the intercept of the straight line on the vertical axis) is close to that expected for an ideal SiC surface.[12] In ion scattering experiments, the intrinsic surface intensity arises from the interaction of the probing ion beam with the first few monolayers of substrate atoms. Taking the intrinsic surface peaks into account, an upper limit for non-stoichiometric oxide (or oxycarbide) can be determined to be $<< 10\,\mathring{A}$.

'Excess' interfacial C as determined by high resolution medium energy ion scattering (MEIS)[13] analysis of etched-back thin oxides on the (0001) and $(11\bar{2}0)$ surfaces of 4H-SiC are shown in Fig 1.7. These experiments set a limit to the maximum amount of excess carbon at the interface to about a monolayer (considering 1×10^{15} atoms cm^{-2} as a 'monolayer'). Interface composition measurements by other techniques such as

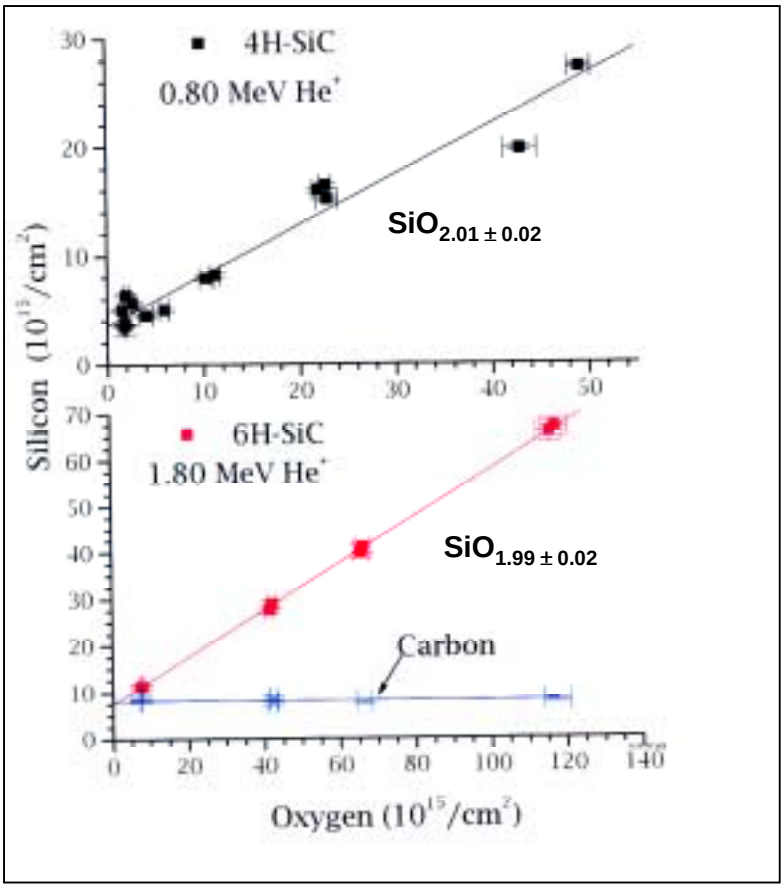

FIG 1. 6 Stoichiometry measurements on oxide layers thermally grown on 4H-SiC and 6H-SiC

electron energy loss spectroscopy (EELS),[14] X-ray photo-electron spectroscopy (XPS)[15] and surface enhanced Raman spectroscopy (SERS)[16] have also detected the presence of a near-interfacial region (~10 Å) that contains excess C (EELS) in the form of free C (SERS) or C containing sub-oxides (EELS). It is important to note that such deviations (~ one monolayer of disorder) from an ideal SiO_2/SiC interface is almost at the detection limits of most physical analysis tools. However, if electrically active, such defects can be important from the standpoint of device physics.

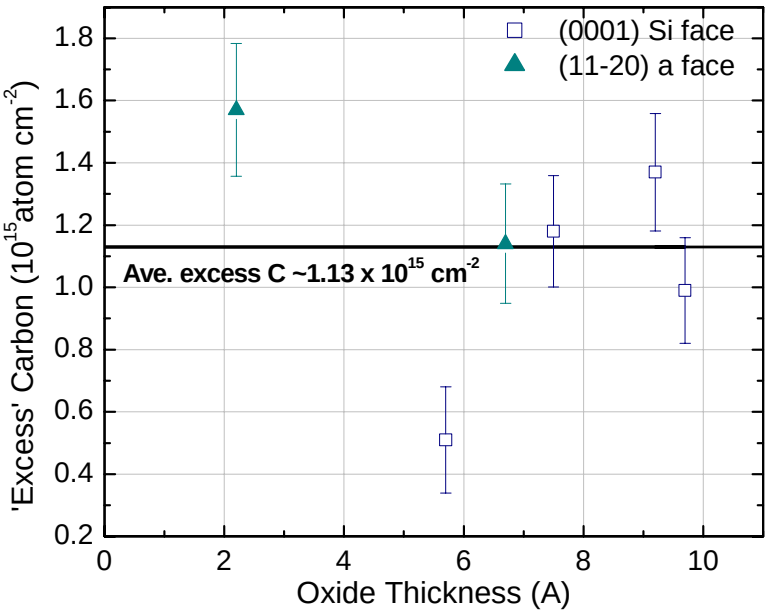

FIG 1.7 'Excess' interfacial C at the SiO_2/4H-SiC interface as determined by MEIS. The measurement set an limit to the amount of 'excess' C to ~ 1 monolayer (~10^{15} atoms cm^{-2})

The Metal/SiO_2/SiC system

As mentioned earlier, the ability of SiC to produce both a semiconductor (single crystal SiC) and an insulator (SiO_2) by compatible technologies as in the case of Si , is the advantage that SiC possesses over other wide band-gap materials. The reason for this is simply because deposition of a metal on the oxide (to provide an electrode where voltage can be applied) results in the formation of a metal-oxide-semiconductor (MOS) capacitor. The MOS capacitor structure shown schematically in Fig.1.8(a) forms the operational core of the MOSFET. MOS capacitors are routinely used as test structures for characterization of the bulk oxide and oxide/semiconductor interfaces without fabricating complete MOSFETs. Energy levels of the three separated components in this

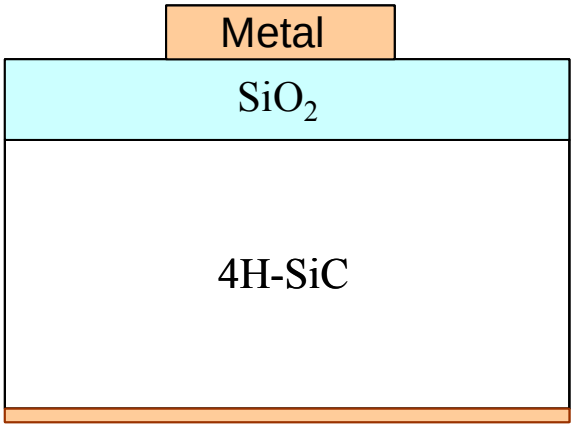

(a)

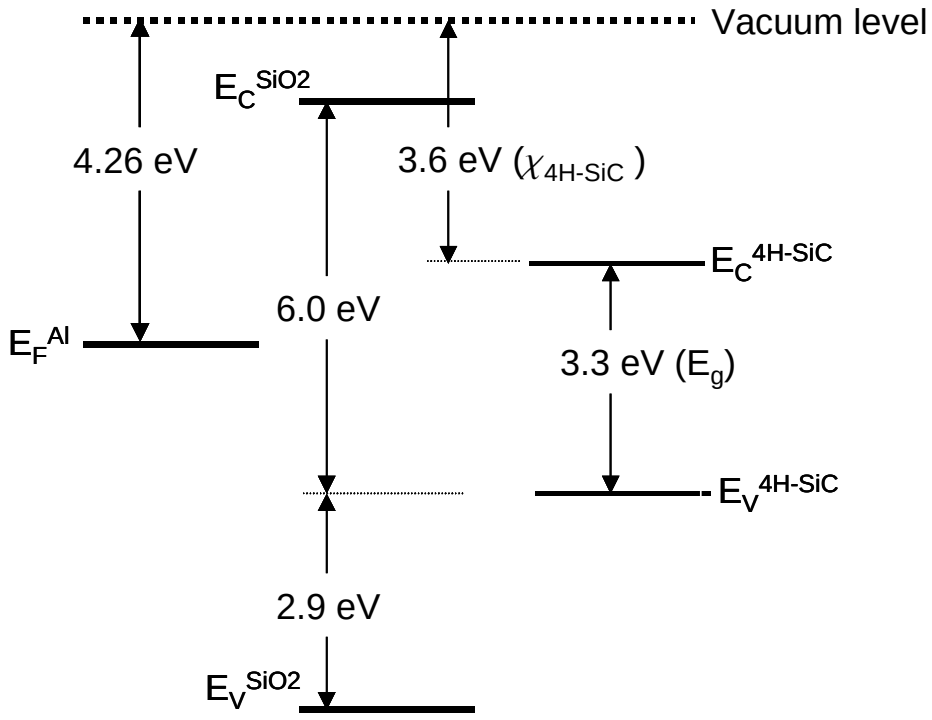

(b)

FIG 1. 8 (a) Schematic of 4H-SiC MOS capacitor (b) Band offsets in 4H-SiC MOS structures (refs. 16 and 17).

system and the band-offsets between SiO_2 and 4H-SiC[17,18] are shown in Fig. 1.8 (b). For an ideal SiO_2/SiC interface as shown in the figure, there are no states in the forbidden gap and the interface consists of a plane free of charges. However, deviations from such an ideal interface can have significant impact on device characteristics as discussed in the following section.

Problems at the SiO_2/SiC interface - Interface defects and channel mobility

For a semiconductor, charge transport in the material can be expressed as

$$J = ne\mu E \tag{1.7}$$

where J is the current density, n is the free carrier density in the channel, e is the electron charge, μ is the mobility of the carriers in the channel. μ is determined by the various scattering processes that occur during carrier transport.[19,20] In general, the mobility of a carrier subjected to several scattering mechanisms can be found by combining the reciprocal mobilities as determined by each scattering process.

$$\frac{1}{\mu} = \sum_i \frac{1}{\mu_i} \tag{1.8}$$

Due to the reciprocal nature of the relationship, the resultant mobility is dominated by a process for which μ_i is smallest (scattering is most severe). The bulk mobility μ_{bulk} of moderately doped semiconductors is thus limited by phonon scattering at room temperature. Phonon scattering increases with applied electric field. Thus, the value used for μ_{bulk} in any semiconductor is usually the 'low-field' value. In the inversion channel of a MOSFET (see Fig. 1.2), the mobility μ_{inv} of carriers can be determined in a similar manner -

$$\frac{1}{\mu_{inv}} = \frac{1}{\mu_{bulk}} + \sum_i \frac{1}{\mu_i} \tag{1.9}$$

where μ_i are mobilities from scattering processes occurring in the channel, most notably scattering from defects at the oxide/semiconductor interface and scattering from interface roughness. For smooth and near-perfect interfaces, where such effects are small, the penetration of the electron wave-function into the oxide may also contribute to reduced channel mobility.[21]

Presence of large interfacial defect densities not only degrades the channel mobility by scattering but, if electrically active, can also cause trapping of carriers. Note that the mobility expressions stated above are for the 'true' mobility (Hall mobility) of the carriers in the channel. However, in a MOSFET, the effective channel mobility of carriers is determined by measuring current, which in turn is a product of the 'true' mobility and the number of carriers available for conduction. In the presence of electrically active interface defects, interface states appear in the forbidden semiconductor band-gap, and these states can act as carrier traps.[22-24] This reduces the number of carriers and contributes to further degradation of the effective mobility.

Historically, SiC MOSFETs exhibited surprisingly low effective mobilities – typically less than 10cm^2 V s^{-1}, which is approximately 1/100 of the 'low-field' bulk mobility. This situation may be compared to Si MOSFETs, for which the electron channel mobility can be 40-50% of the 'low-field' value. Interestingly, the channel mobility for 6H-MOSFETs was considerably higher. Schorner, et al.[25] first suggested that the problem with 4H-SiC was caused by a large number of interfacial defects that produce interface states near the conduction band of 4H-SiC (around 2.9 eV above the

valence band edge). These states are 'acceptor' lik,e as they are neutral when empty and negatively charged when filled with an electron. To first order, interface (electron) traps are filled below the Fermi level and empty above. When an n-channel MOSFET is biased to inversion, the Fermi-level approaches the conduction band-edge of 4H-SiC, and the interface states below the Fermi level fill with electrons. The filling up occurs by 'trapping' of electrons that otherwise would contribute to conduction. As a result, the number of inversion electrons available for conduction is drastically reduced. This process is schematically illustrated in Fig. 1.9. Additionally, the large trapped charge gives rise to Coulomb scattering that reduces the 'true' mobility of the remaining free carriers. The overall result is a dramatic degradation of field-effect mobility. In the case of 6H-SiC, the majority of these states reside in the conduction band levels in 6H-SiC (E_g ~ 3eV), thus they do not affect carrier mobility in the inversion layer.

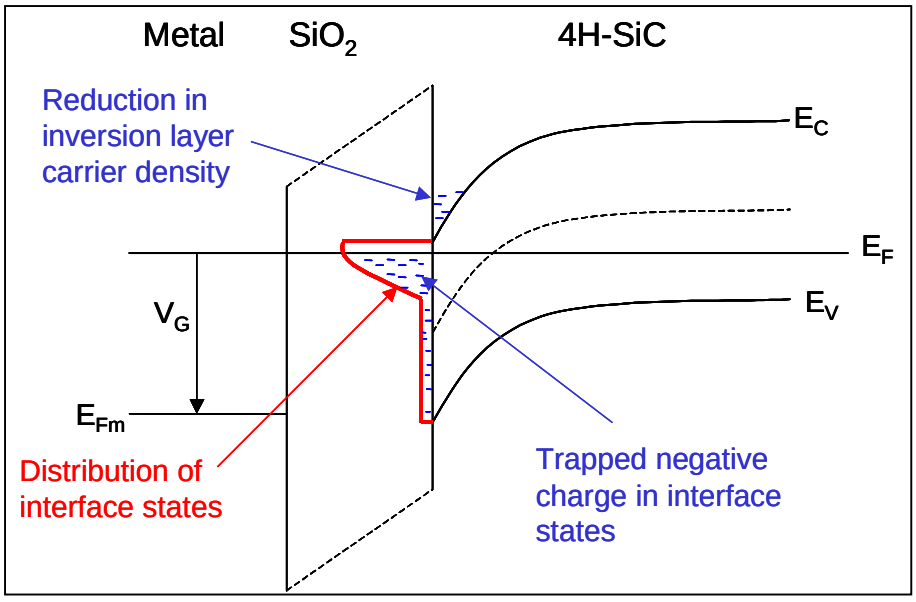

FIG 1. 9 MOS band diagram of an n-channel 4H-SiC MOSFET biased to strong inversion. The figure illustrates electron trapping by the high density of interface traps near the conduction band-edge of 4H-SiC.

Origin of interface states

An overview of interfacial imperfections that are suspected to cause the high density of traps at the SiO_2/SiC interface is shown in Fig. 1.10. According to the 'carbon cluster' model,[26,27] C in the form of small sp^2 bonded clusters or larger 'graphitic' flakes can contribute to a large part of the interface states in the band-gap. The valence band of small clusters is located in the band-gap of 4H-SiC and is thus prone to create 'donor' like (positively charged when empty, neutral when filled with electrons). The conduction band of such clusters lies well beyond the conduction band-edge of 4H-SiC (see Fig. 1.10), thus not producing any traps. Larger graphitic structures however, can indeed produce acceptor like states (neutral when empty, negatively charged when filled with electrons) near the conduction band-edge of 4H-SiC. Afanasev et. al[27] however, suggest that large clusters are statistically less likely to form compared to smaller clusters. They attribute the high density of acceptor like states ($> 10^{13}$ cm^{-2} eV^{-1}) to near-interfacial oxide traps that are located ~2.8 eV below the SiO_2 conduction band-edge[28] . These traps are also observed in the case of the superior SiO_2/Si interface[29] but they have a less detrimental influence on the inversion layer mobility as they lie well within the conduction band of Si. These oxide traps are usually attributed to oxygen vacancies in the near-interfacial region i.e sub-oxides. Apart from such defects, inclusions of other polytypes such as 3C in the 4H material could also possibly contribute to the trap density.[27] In particular, localized polytype conversion during oxidation[30] could bring about this situation.

One of the main reasons the physical nature of the defects remains a topic of discussion was mentioned earlier - the difficulty in using standard materials

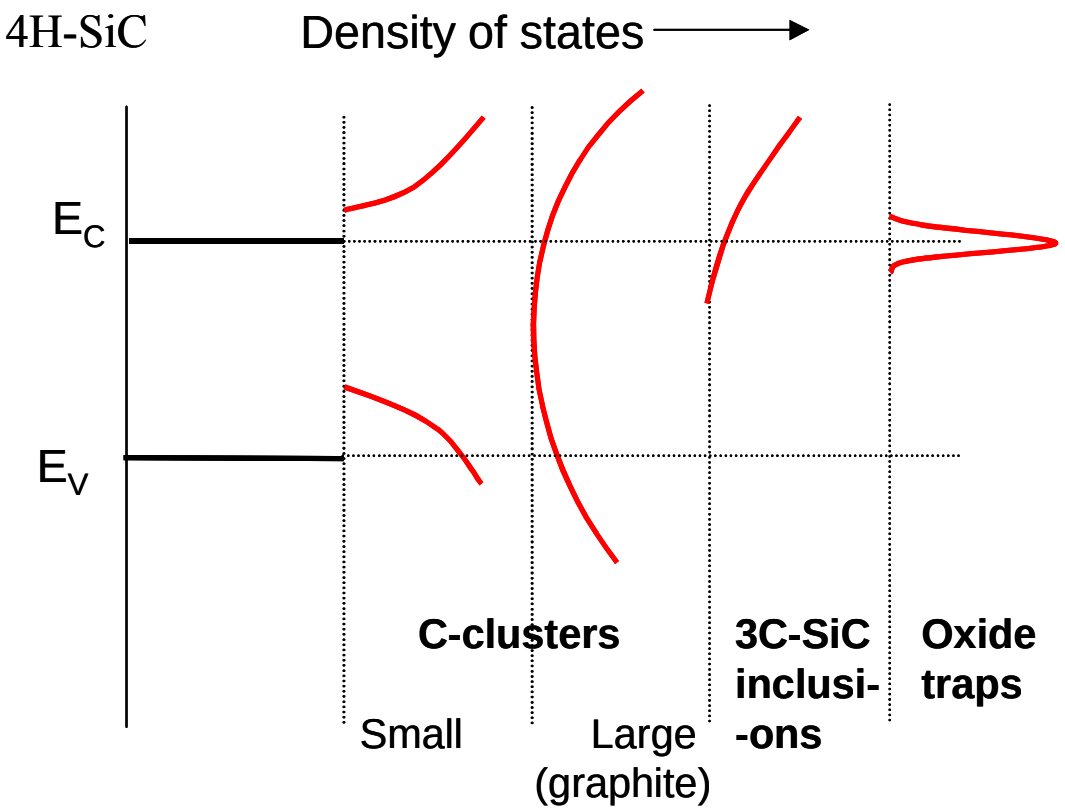

FIG 1. 10 Schematic of interfacial and near-interfacial defects that could contribute to the density of states within the band-gap of 4H-SiC

characterization tools to identify them. The defect densities are small (~10^{13} cm^{-2} ≈ $\frac{1}{1000}$th of a monolayer) from a physical characterization point of view, but their effects at the device level are enormous. It is worthwhile here to note that trap densities in an optimally processed SiO_2/Si interface are ~10^{10} cm^{-2}. The considerably higher trap densities observed at the SiO_2/SiC interface could be due to non-optimal processing, 'intrinsic' to the SiO_2/SiC interface (e.g. carbon related) or inherent in a SiO_2-semiconductor interface (such as oxide traps) that are revealed only because of the very

large band-gap of 4H-SiC. In any case, achieving lower trap densities is absolutely essential to realize the full potential of a SiC power MOSFET.

Improving the quality of the SiO_2/4H-SiC interface

(i) Annealing ambients:

Efforts to improve the SiO_2 / 4H-SiC interface have focused primarily on oxidation procedures (e.g., dry, wet, pyrogenic, deposited) and post-oxidation anneals in various ambients such as NO, N_2O, NH_3, H_2. Hydrogen has received much attention because of its ability to 'passivate' Si dangling bonds at the SiO_2/Si interface. For dry oxidized SiO_2 on Si, a significant reduction of interface state densities occurs following passivation with H_2 - from 10^{12} $cm^{-2}eV^{-1}$ to 10^{10} $cm^{-2}eV^{-1}$ near mid-gap.[31] However, the best passivation results for SiO_2/4H-SiC have been achieved by introducing nitrogen at the interface using post-oxidation anneals in NO[32,33] and N_2O.[34] Following nitridation, interface trap densities near the conduction band are reduced significantly (from > 10^{13} cm^{-2} eV^{-1} to ~10^{12} cm^{-2} eV^{-1}) with little apparent dependence on the procedure used for oxidation. As a direct consequence, nitridation using NO and N_2O has produced effective channel mobilities that are now approaching high values (80 cm^2/V-s) for 4H-SiC MOSFETs.[35-37] Nitridation is widely recognized as an essential processing step for MOS fabrication by most SiC researchers. However, the mobility values are still low compared to the SiO_2/Si interface (~50% of bulk mobility). The ultimate inversion mobility of 4H-SiC MOSFETs is an open question. By comparison with Si, one can make a conservative estimate on achievable mobility of ~250 cm^{-2} V s^{-1}. In order to achieve this, further improvements of the interface is mandatory. In the present work, we

have focused on the development and characterization of passivation processes involving NO (chapters III, IV and V) and H_2 (chapters IV and V) on different crystal faces of 4H-SiC.

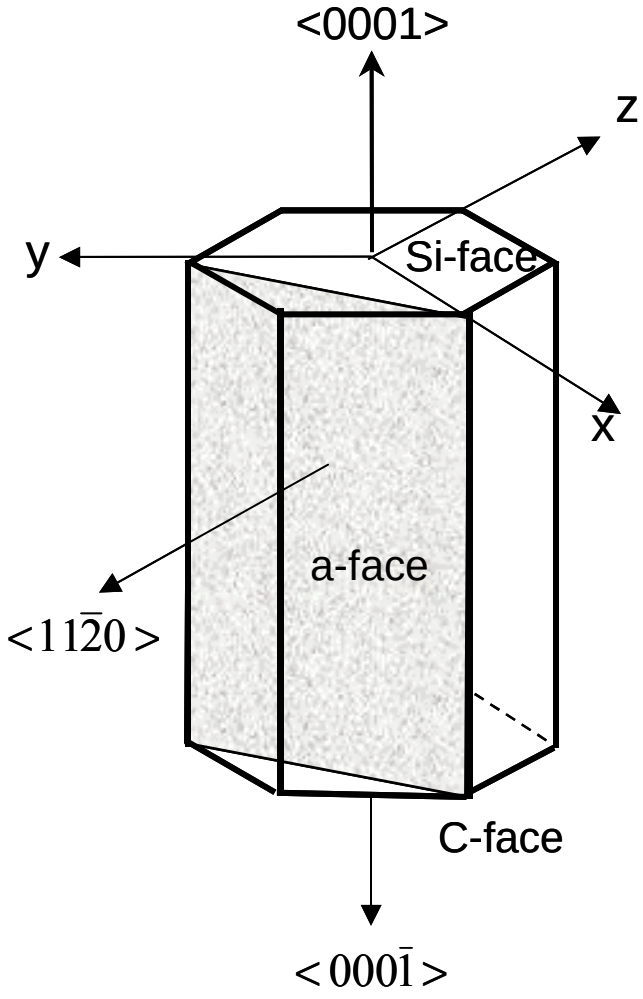

FIG 1. 11 The (0001) Si-, (11$\bar{2}$0) a- and (000$\bar{1}$) C- faces of SiC

(ii) Alternate crystal faces:

Most of the work reported to date has been on the (0001) Si-terminated crystal face of SiC. The main reason the off-axis Si-face is preferred is that epitaxial growth techniques are more developed on this face. Recently however, other crystal faces have aroused considerable interest. In particular, high channel mobilities of MOSFETs fabricated on the $(11\bar{2}0)$ a- face and the $(000\bar{1})$ C-face have been demonstrated.[38,39]

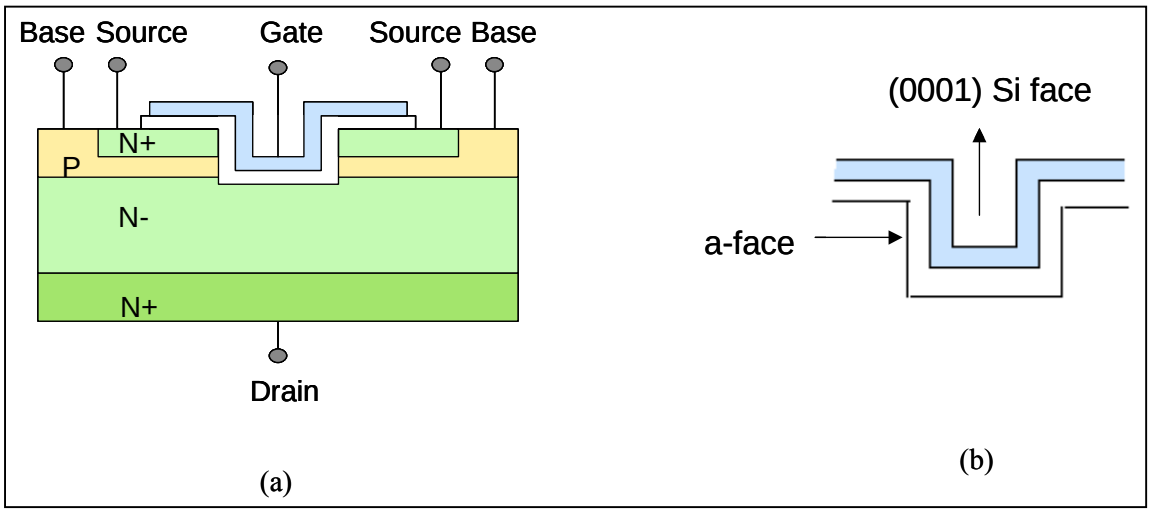

FIG 1. 12 (a) UMOSFET structure (b) The gate is 'U' shaped and the inversion layer forms parallel to the $(11\bar{2}0)$ a-face (or the $(1\bar{1}00)$.

These crystal faces are schematically shown in Fig.1.11. The (0001) Si terminated face is a basal plane in the hexagonal unit cell, in which all surface atoms are Si. The $(000\bar{1})$ C-face is the other basal plane which is C-terminated. The $(11\bar{2}0)$ a-face is a non-polar face that has equal numbers of carbon and silicon atoms in a plane, represented by the shaded area in Fig.1.11. One of the major advantages of using 'alternate' faces such as the $(11\bar{2}0)$ a-face and the $(000\bar{1})$ C-face is the significantly higher oxidation rates compared

to the (0001) Si face (see chapter II). Use of these faces can potentially reduce the thermal budget for fabrication. Furthermore, absence of micropipes penetrating the device is a very promising property of the $(11\bar{2}0)$ a-face material. Study of these faces is also important from the standpoint of new devices. For example, in the UMOSFET[2] structure shown in Fig.1.12, the inversion channel lies along the $(11\bar{2}0)$ or $(1\bar{1}00)$ plane. Interface studies are interesting since the oxidation rates differ greatly on the crystal faces, suggesting a possibility of different interfacial defects. (It is important to note that in the case of Si, different crystal faces show different interface trap densites according to the areal density of Si dangling bonds on these surfaces). A major part of this work (chapters II-V) is devoted to the interface studies for 'alternate' crystal faces of SiC.

References

1 B. J. Baliga, *Power semiconductor devices* (PWS publisher, Boston, 1996).

2 J. A. Cooper Jr, M. R. Melloch, R. Singh, A. Agarwal, and J. W. Palmour, IEEE Trans. Elect. Dev. **49,** 658 (2002).

3 B. J. Baliga, IEEE Trans. Elect. Dev. **10,** 455 (1989).

4 Y. M. Tairov and V. F. Tsvetkov, J. Cryst. Growth **52,** 146 (1981).

5 A. R. Powell and L. B. Rowland, Proceedings of the IEEE **90,** 942 (2002).

6 T. P. Chow, V. Khemka, J. Fedison, N. Ramungul, K. Matocha, Y. Tang, and R. J. Gutmann, Solid-State Electron. **44,** 277 (2000).

7 R. S. Muller and T. I. Kamins, *Device electronics for integrated circuits* (Wiley, New York, 1986).

8 G. L. Harris, *Properties of silicon carbide* (INSPEC, London, 1995).

9 Y. Song and F. W. Smith, Appl. Phys. Lett. **81,** 3061 (2002).

10 B. E. Deal and A. S. Grove, J. Appl. Phys. **36,** 3770 (1965).

[11] C. I. Harris and V. V. Afanas'ev, Microelectr. Eng. **36,** 167 (1997).

[12] L.C.Feldman, J.W.Mayer, and S.T.Picraux, *Materials analysis by ion channeling: submicron crystallography* (Academic press, New York, 1982).

[13] T. Gustafsson, H. C. Lu, B. W. Busch, W. H. Schulte, and E. Garfunkel, Nucl Instrum Methods Phys Res Sect B **183,** 146 (2001).

[14] K.-C. Chang, N. T. Nuhfer, L. M. Porter, and Q. Wahab, Appl. Phys. Lett. **77,** 2186 (2000).

[15] C. Virojanadara and L. I. Johansson, J. Phys. Condens. Matter **16,** 1783 (2004).

[16] W. Lu, L. C. Feldman, Y. Song, S. Dhar, W. E. Collins, W. C. Mitchel, and J. R. Williams, Appl. Phys. Lett. **85,** 3495 (2004).

[17] V. V.Afanas'ev, M. Bassler, G. Pensl, M. J. Schulz, and E. S. vonKamienski, J. App. Phys.l **79,** 3108 (1996).

[18] V. V. Afanas'ev and A. Stesmans, Appl. Phys. Lett. **77,** 2024 (2000).

[19] R.S.Muller and T.I.Kamins, *Device electronics for integrated circuits* (Wiley, New York, 1986).

[20] S.M.Sze, *Physics of semiconductor devices* (Wiley, New York, 1981).

[21] I. Polishchuk and C. Hu, *IEEE Symposium on VLSI Circuits, Digest of Technical Papers*, n TECHNOLOGY SYMP., 2001, p 51-52

[22] N. S. Saks and A. K. Agarwal, Appl. Phys. Lett. **77,** 3281 (2000).

[23] K. Chatty, S. Banerjee, T. P.Chow, R. J. Gutmann, E. Arnold, and D. Alok, Matls. Sci. Forum **389-393,** 1041 (2002).

[24] K.Chatty, S.Banerjee, T. P.Chow, R. J.Gutmann, E.Arnold, and D.Alok, Matls. Sci. Forum **389-393,** 1041 (2002).

[25] R. Schorner, P. Friedrichs, D. Peters, and D. Stephani, IEEE Electron Device Lett. **20,** 241 (1999).

[26] M. Bassler, G. Pensl, and V. Afanas'ev, Diamond Relat. Mat. **6,** 1472 (1997).

[27] V. V. Afanas'ev, F. Ciobanu, S. Dimitrijev, G. Pensl, and A. Stesmans, J Phys Condens Matter **16,** 1839 (2004).

[28] V. V. Afanasev, M. Bassler, G. Pensl, and M. Schulz, Phys. Status Solidi a **162,** 321 (1997).

[29] V. V. Afanas'ev and A. Stesmans, Phys. Rev. Lett. **78,** 2437 (1997).

[30] R. S. Okojie, M. Xhang, P. Pirouz, S. Tumakha, G. Jessen, and L. J. Brillson, Appl. Phys. Lett. **79,** 3056 (2001).

[31] E. H. Nicollian and J. R. Brews, *MOS (Metal Oxide Semiconductor) physics and technology* (John Wiley & Sons, New York, 1982).

[32] G. Y. Chung, C. C. Tin, J. R. Williams, K. McDonald, M. D. Ventra, S. T. Pantilides, L. C. Feldman, and R. A. Weller, Appl. Phys. Lett. **76,** 1713 (2000).

[33] H.-F. Li, S. Dimitrijev, H. B. Harrison, and D. Sweatman, Appl. Phys. Lett. **70,** 2028 (1997).

[34] L. A. Lipkin, M. K. Das, and J. W. Palmour, Matls. Sci. Forum **389-393,** 985 (2002).

[35] G. Y. Chung, C. C. Tin, J. R. Williams, K. McDonald, R. K. Chanana, R. A. Weller, S. T. Pantelides, L. C. Feldman, O. W. Holland, M. K. Das, and J. W. Palmour, IEEE Electron Device Lett. **22,** 176 (2001).

[36] M. K. Das, Matls. Sci. Forum **457-460,** 1275 (2004).

[37] C.-Y. Lu, J. A. Cooper Jr, T. Tsuji, G. Chung, J. R. Williams, K. McDonald, and L. C. Feldman, IEEE Trans. Electron Devices **50,** 1582 (2003).

[38] J. Senzaki, K. Kojima, S. Harada, R. Kosugi, S. Senzaki, T. Suzuki, and K. Fukuda, IEEE Elect. Dev. Lett. 23(1) (2002) 13.

[39] K. Fukuda, M. Kato, K. Kojima, and J. Senzaki, Appl. Phys.Lett. **84,** 2088 (2004).

CHAPTER II

MODIFIED DEAL GROVE MODEL FOR THE OXIDATION OF SiC

Y. Song,[a)] S. Dhar,[a)] L. C. Feldman,[a)] G. Chung,[b)] and J. R. Williams[c)]

a) Dept. of Physics and Astronomy & Interdisciplinary Program in Materials Science
Vanderbilt University, Nashville, TN 37235, USA

b) Dow Corning Inc., Tampa, FL 33619

c) Dept. of Physics, Auburn University, Auburn, Alabama 36849

Published in Journal of Applied Physics, May (2004)

Abstract

A modified Deal Grove model for the oxidation of 4H-Silicon Carbide (SiC) is presented, which includes the removal of the carbon species. The model is applied to new data on the oxidation rates for the (0001) Si, (0001) C and (11 20) a-faces, which are performed in 1 atm dry oxygen and in the temperature range 950 °C~ 1150 °C . Analysis within the model provides a physical explanation for the large crystal-face dependent oxidation rates observed.

Introduction

Silicon carbide is a wide band gap semiconductor possessing attractive properties for applications in electronic devices operating under high power, high frequency and high temperature. Among the numerous polytypes of SiC, the 4H polytype has been

recognized as the most promising material for such applications. One of the major advantages SiC holds over other wide bandgap semiconductors is the ability to thermally oxidize to SiO_2 which has lead to the development of SiC power MOSFETS, analogous to the Si/SiO_2 based technology.

Numerous studies[1-8] have been conducted on the oxidation of SiC. There are several models to explain the oxidation of SiC.[2,6] However, there are wide variations in the reported oxidation rates and the strong crystal face dependence of the oxidation is not fully understood. Compared to oxidation of Si, thermal oxidation of SiC is considerably more complicated. The following reaction governs the oxidation of SiC:

$$SiC + 1.5\ O_2 \leftarrow\rightarrow SiO_2 + CO \qquad (2.1)$$

As opposed to the relatively simple oxidation of Si, there are 5 steps in the thermal oxidation of SiC (Fig. 2.1),

i) Transport of molecular oxygen gas to the oxide surface;

ii) In-diffusion of oxygen through the oxide film;

iii) Reaction with SiC at the oxide/SiC interface;

iv) Out-diffusion of product gases *(e.*g. CO) through the oxide film; and

v) Removal of product gases away from the oxide surface.

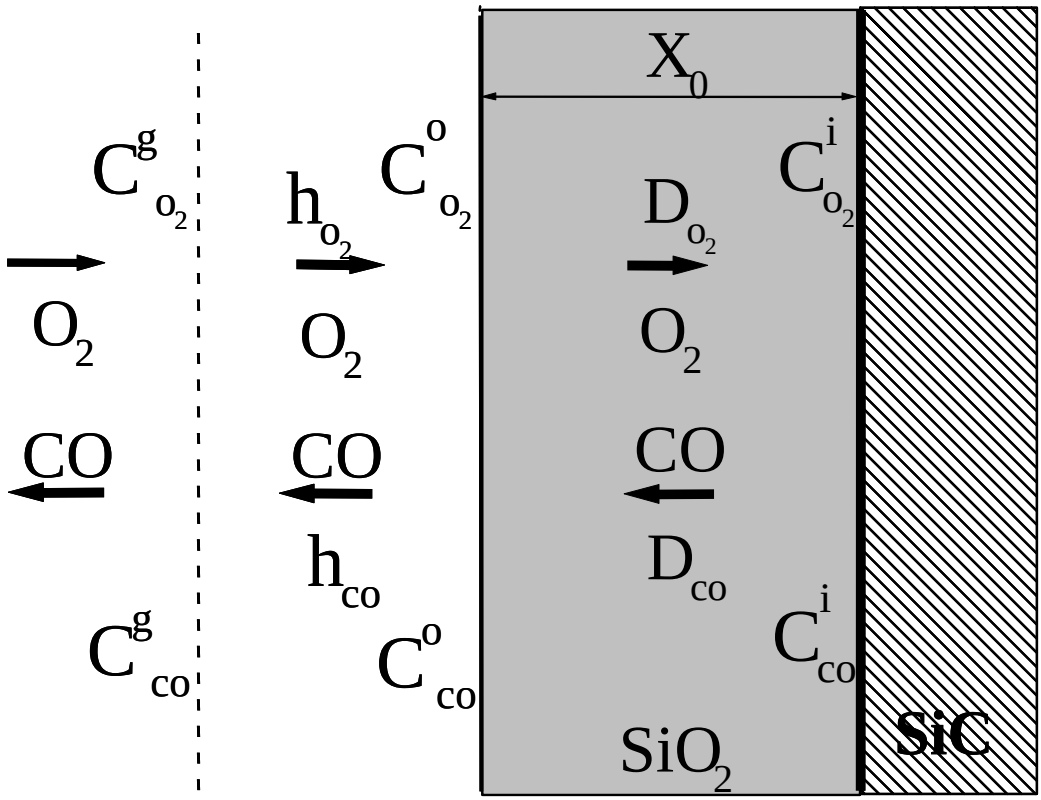

FIG. 2. 1 Five steps involved in the oxidation of SiC

The last two steps are not involved in the oxidation of Si. The oxidation of SiC is about one order of magnitude slower than that of Si under the same conditions. The first and last steps are rapid and are not rate-controlling steps. But among the remaining steps, the rate-controlling step is still uncertain. as discussed in several articles. [9-11]

Based on the great success of the Deal Grove model[12] for the oxidation of Si, it is attractive to apply a modified form of this model to the oxidation of SiC. In the Deal Grove model of silicon, growth follows the following relation:

$$X^2 + AX = B(t + \tau) \qquad (2.2)$$

where X is thickness of oxide and t is oxidation time. τ is related to an initial thickness. B and B/A are parabolic and linear rate constants, respectively. If the growth rate is linear, the interface reaction is the rate-controlling step. If parabolic behavior is dominant, oxygen in-diffusion through the oxide film is the rate-controlling step. The Deal Grove model is not directly applicable to SiC as is it does not include CO out-diffusion. Also for SiC, the oxidation rate dependence on crystal orientation is far greater than that observed for Si. The oxidation rate on the $(000\bar{1})$ C-face is almost one order of magnitude higher than that on the (0001) Si-face.

In this article, we present a modified Deal Grove model by considering the product gas out-diffusion during oxidation. With this model, we try to illustrate which step is the rate- controlling step for the SiC oxidation. We apply the model to our experimental results on the $(11\bar{2}0)$ a-face of SiC, and make comparison with the $(000\bar{1})$ C- and (0001) Si-face. An explanation for the crystal face dependence of the oxidation rate is also proposed.

Modified Deal Grove Model

Following the Deal-Grove approach, we consider SiC covered by a SiO_2 layer of thickness as X_0, as indicated in Fig.2.1

The oxygen flux from the gas to vicinity of the outer silica surface is taken to be:

$$F_{O_2} = h_{O_2}(C^{*}_{O_2} - C^{O}_{O_2}) \qquad (2.3)$$

where h_{O_2} is the gas-phase transport coefficient *in terms of concentrations in the solid* $C^{O}_{O_2}$ is the concentration of the oxidant at the outer surface of the oxide at any given

time, and $C^{*}_{O_2}$ is the equilibrium concentration of oxygen gas in the oxide (see appendix).

Under steady state, the flux of the oxygen across the oxide layer is given by:

$$F_{O_2} = D_{O_2} \frac{C^{O}_{O_2} - C^{i}_{O_2}}{X_0} \tag{2.4}$$

where D_{O_2} is the diffusion coefficient in the oxide and $C^{i}_{O_2}$ is the concentration of the oxygen near the oxide-SiC interface.

For the carbon species out-diffusion, we have:

$$F_{CO} = D_{CO} \frac{C^{i}_{CO} - C^{O}_{CO}}{X_0} = h_{CO} (C^{O}_{CO} - C^{*}_{CO}) \tag{2.5}$$

where D, C^{O}, C^{i} ,and C^{*} and h have the same meaning as above and we use subscripts to distinguish O_2 or CO.

Reaction (2.1) occurs at the SiO_2/SiC interface. The flux corresponding to the oxidation reaction is expressed as the following:[13]

$$F = K_f C^{i}_{O_2} - K_r C^{i}_{CO} \tag{2.6}$$

where K_f and K_r are the rate constants of the forward and reverse reactions, respectively. In the experimental section, we find that K_f is related to local concentration of carbon in the SiC. K_r can be also related to the local concentration of SiO_2. For the steady-state condition, $F : F_{O_2} : F_{CO} = 1 : 1.5 : 1$.

The rate of growth of the SiO_2 layer is described by:

$$\frac{dX_0}{dt} = \frac{F}{N_0} \tag{2.7}$$

where N_0 is the number of oxidant molecules incorporated into a unit volume of the oxide layer.

Combining the equations (see appendix), we find the solution of Eq. (2.7) is in the same form as Eq. (2.2). But the coefficients A and B are different from that in the Deal Grove model:

$$A = \frac{1 + \frac{1.5K_f}{h_{O_2}} + \frac{K_r}{h_{CO}}}{\frac{1.5K_f}{D_{O_2}} + \frac{K_r}{D_{CO}}} \tag{2.8a}$$

$$B = \frac{(K_f C^*_{O_2} - K_r C^*_{CO}) / N_0}{\frac{1.5K_f}{D_{O_2}} + \frac{K_r}{D_{CO}}} \tag{2.8b}$$

and the growth can be expressed in the same form as Eq.(2.2) with a linear and parabolic regime. Note that these equations reduce to the Deal Grove silicon result if $D_{CO}= \infty$ and/or $K_r=0$. In thermal oxidation the flow of oxidant to the oxide surface is rarely a rate-limiting step so that $h >> K_f$, K_r, or both. During oxidation, $C^*_{O_2} >> C^*_{CO}$,

So we can rewrite Eqs. (2.8) as:

$$B / A = \frac{(K_f C^*_{O_2} - K_r C^*_{CO_x}) / N_0}{1 + \frac{1.5K_f}{h_{O_2}} + \frac{K_r}{h_{CO_x}}} \approx \frac{C^*_{O_2}}{N_0} K_f \tag{2.9a}$$

$$B = \frac{(K_f C^*_{O_2} - K_r C^*_{CO}) / N_0}{\frac{1.5K_f}{D_{O_2}} + \frac{K_r}{D_{CO}}} \tag{2.9b}$$

The implications of these equations are described below.

(1) In the linear growth regime, the interface reaction will be the rate-controlling step,

$$B / A \approx \frac{C^*_{O_2}}{N_0} K_f \tag{2.10}$$

(2) In the parabolic growth regime, diffusion could be the rate-controlling step. If oxygen diffusion is the rate controlling step, or $\frac{K_f}{D_{O_2}} >> \frac{K_r}{D_{CO}}$,

$$B \approx \frac{C^*_{O_2}}{1.5 N_0} D_{O_2} \tag{2.11}$$

In this case, the activation energy of the parabolic rate constant will be the same as that for oxidation of Si. If the CO out-diffusion is the rate controlling step, or $\frac{K_f}{D_{O_2}} << \frac{K_r}{D_{CO}}$ the parabolic rate constant will be:

$$B \approx \frac{C^*_{O_2} K_f}{N_0 K_r} D_{CO} \tag{2.12}$$

The same method may also be applied to the wet oxidation of Si where the out-diffusion of H_2 should be strictly considered,

$$Si + 2H_2O \longleftrightarrow SiO_2 + 2H_2$$

However, the simple Deal Grove model is correct for wet oxidation of Si, since H_2 diffusion is not a rate-limiting-step.

Experimental procedure

SiC samples used for the experiment were ~5mm x 5mm, cut from a double-side polished (0001)/(000$\bar{1}$) oriented (research grade, n type, on axis), and (11$\bar{2}$0) oriented (research grade, n type, on axis) wafers, supplied by CREE Inc. Samples were cleaned by acetone, methanol and 5% HF solution in successive steps. Immediately after this cleaning, the

samples were loaded into the oxidation furnace. A Lindberg high temperature furnace was used for oxidation between 950°C and 1150°C for different oxidation times. Dry oxidation was performed at atmospheric pressure keeping the oxygen flow rate at 1 liter/min. $^{4}He^{+}$ ions of 1.8 MeV energy generated by the 2MeV Van de Graaf accelerator at our laboratory were used to perform Rutherford Backscattering (RBS) / channeling experiments. The oxide thickness was calculated from the RBS spectra by finding the total areal density of oxygen atoms in the film. Analysis of the Si and O peaks confirmed that the oxide was stoichiometric SiO_2. The thickness of the oxide films was also measured by spectroscopic ellipsometry as a complimentary technique. The M-2000DI, J.A. Woolam and Co. Spectroscopic ellipsometer (190-900nm source, at 65º, 70 º and 75º incidence, using SiO_2/SiC model for data analysis) was used for this purpose. The results of the RBS and ellipsometry agreed well within the limits of experimental errors (Fig.2.2).

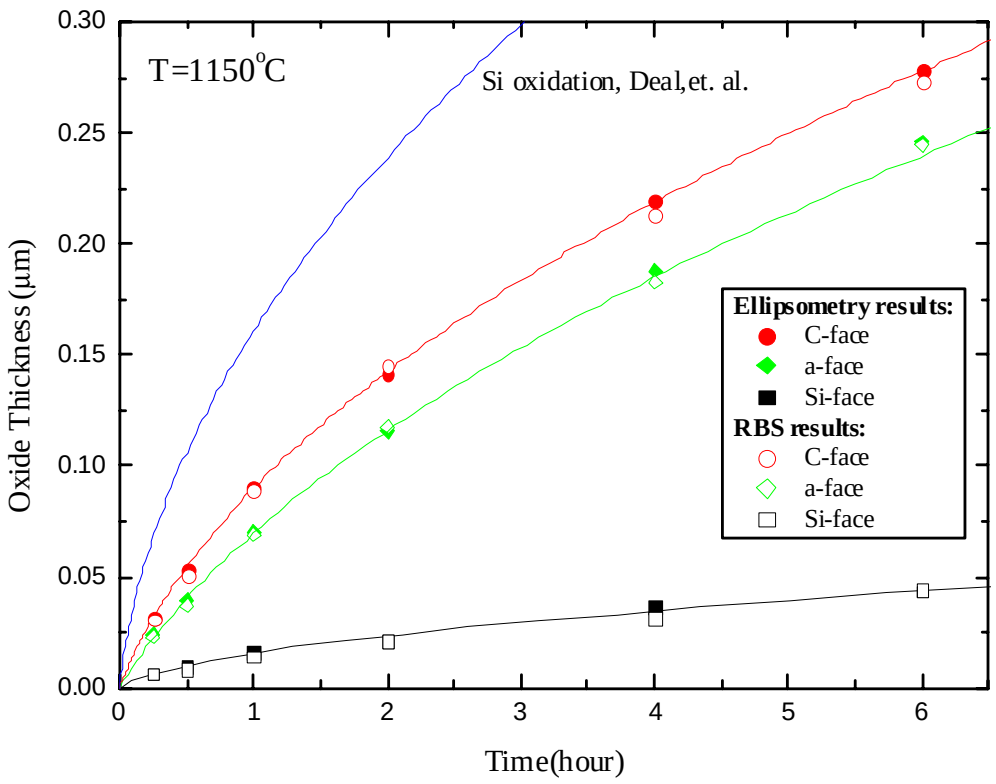

FIG. 2. 2 Oxide thickness as a function of time for dry thermal oxidation of the $(000\bar{1})$ C-, $(11\bar{2}0)$ a- and (0001) Si-terminated faces of 4H-SiC at 1150°C. The solid symbols indicate ellipsometer results and the opened symbols indicate RBS results.

Results and Discussion

Figures 2.3, 2.4 and 2.5 show the oxidation growth kinetics of the $(000\bar{1})$ C face, $(11\bar{2}0)$ a face and the (0001) Si face respectively, as a function of oxidation temperature. There is a large variation in the oxidation rate among the three different faces with the $(000\bar{1})$ C face oxidizing much faster than the slowest (0001) Si face. Oxidation of the $(11\bar{2}0)$ a- face shows intermediate behavior. The growth data is fit to our modified Deal Grove model. The values of τ are set to zero, because the native oxide thickness of is only about 2Å for all of the C-, a- and Si faces as measured by Medium Energy Ion Scattering.[14] Compared to the C-face and a-face, the Si-face data is difficult to fit because of the very slow oxidation rate and thin oxides. Table 2.1 and Table 2.2 show the parabolic rate constant B and linear rate constant B/A, respectively.

The linear rate constants B/A show the apparent activation energy of 1.29eV, 1.20eV and 1.34eV for the $(000\,\bar{1})$ C-face, $(11\,\bar{2}\,0)$ a-face and (0001) Si-faces, respectively (Fig. 2.6). The activation energies for the interface reaction are almost equal for these three faces. The pre-exponential factors for the C-, Si- and a-faces are different. It is well known[15] that the linear oxidation rate of Si is also dependent on crystal orientation. In the region of growth where the Deal Grove model is accurate, $\frac{(B/A)_{111}}{(B/A)_{100}}$ =1.68 for Si, and the activation energies for these linear rate constants are equal.

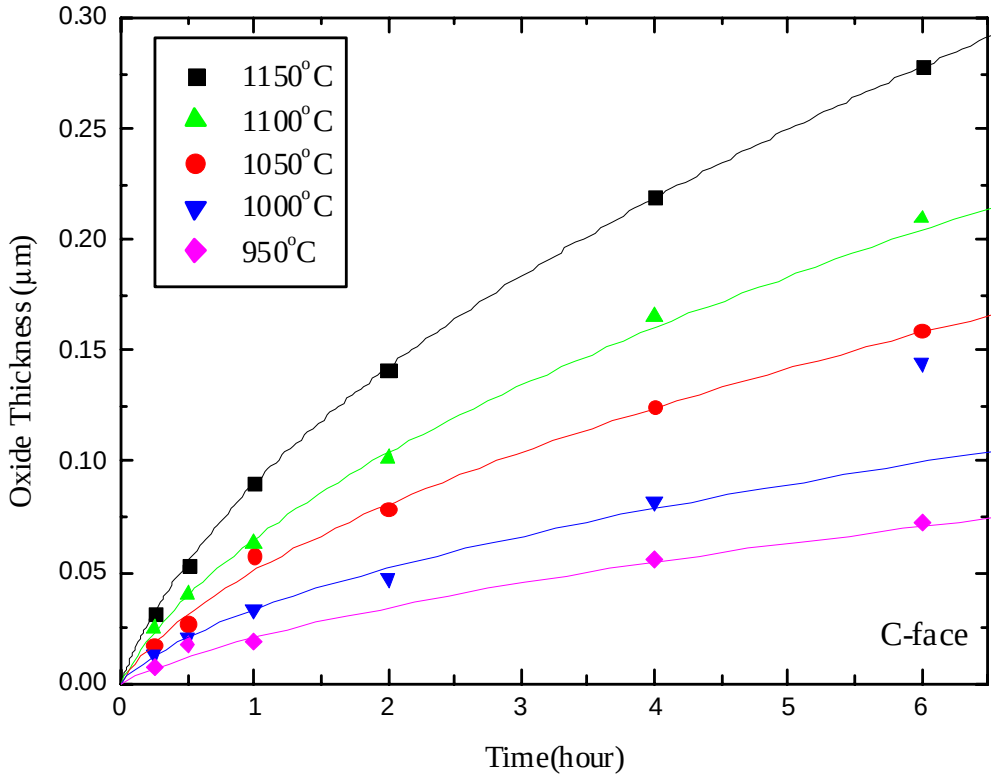

FIG. 2. 3 Oxide thickness as a function of time and temperature for dry thermal oxidation of the (000$\bar{1}$) C-terminated face of 4H-SiC. Solid lines indicate fits by Eq. (2.2).

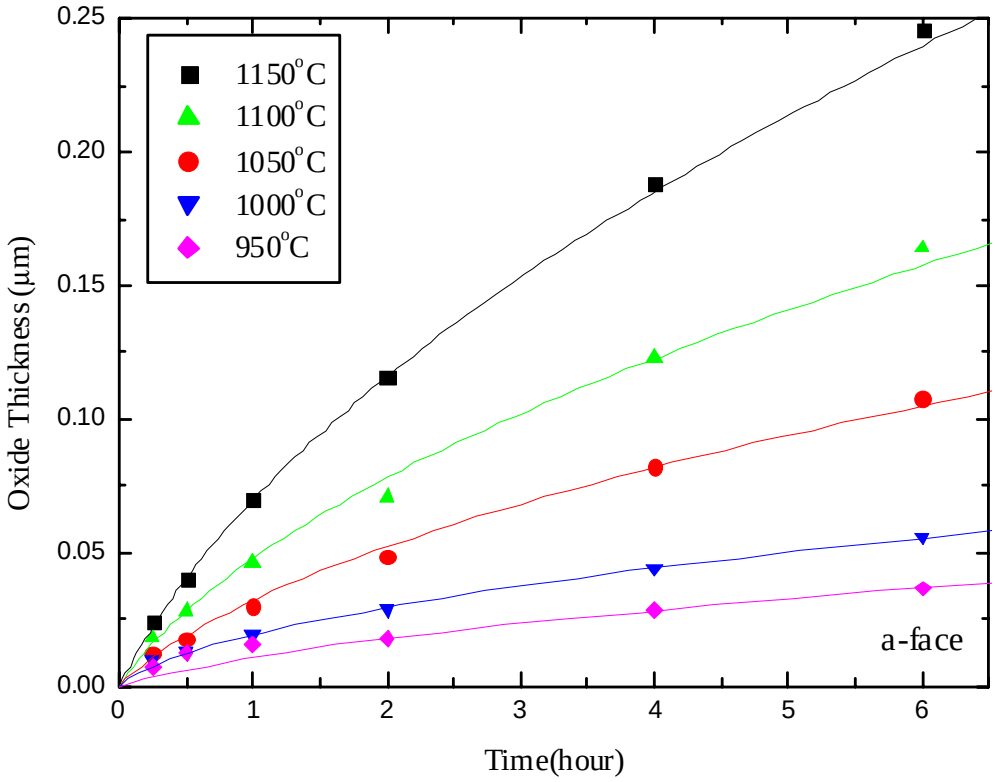

FIG. 2. 4 Oxide thickness as a function of time and temperature for dry thermal oxidation of the $(11\bar{2}0)$ a-face of 4H-SiC. Solid lines indicate fits by Eq. (2.2).

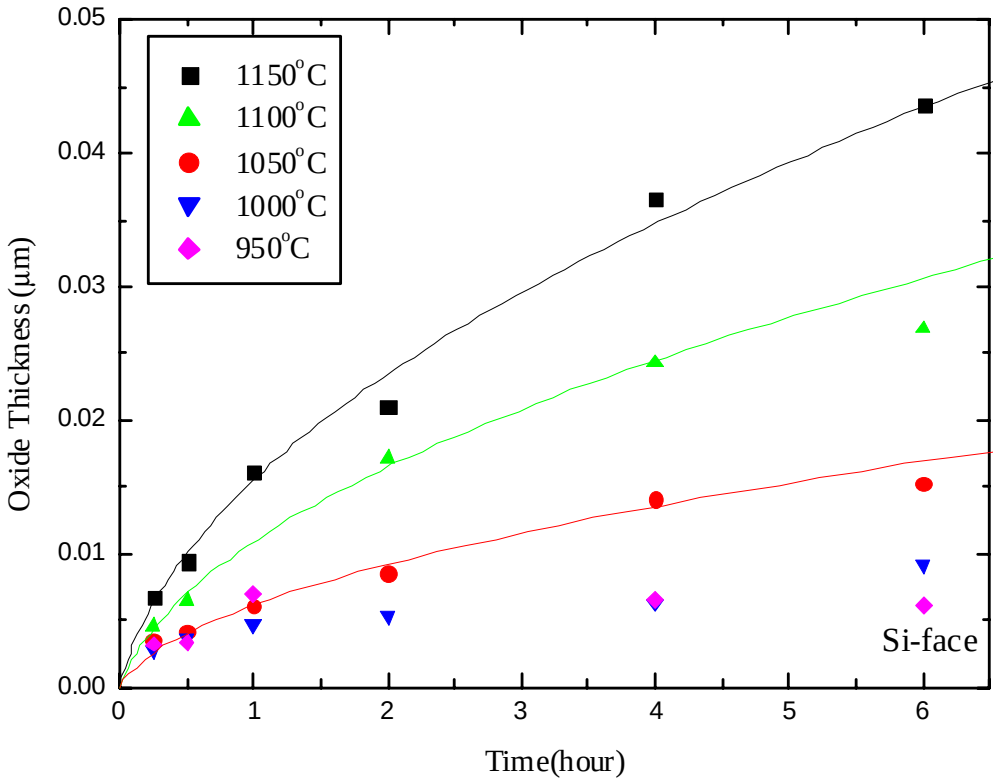

FIG. 2. 5 Oxide thickness as a function of time and temperature for dry thermal oxidation of the (0001) Si-terminated face of 4H-SiC. Solid lines indicate fits by Eq. (2.2)

Table 2. 1 Parabolic rate constant B

Temperature(°C)	1150	1100	1050	1000	950
C-face(μm^2/h)	0.018	0.010	0.0059	0.0022	0.0014
a-face(μm^2/h)	0.016	0.0064	0.0028	0.00065	0.00037
Si-face(μm^2/h)	0.00038	0.00019	0.000056	-	-

Table 2. 2 Linear rate constant B/A

Temperature(°C)	1150	1100	1050	1000	950
C-face(μm/h)	0.16	0.11	0.089	0.067	0.029
a-face(μm/h)	0.10	0.074	0.051	0.044	0.015
Si-face(μm/h)	0.042	0.029	0.018	-	-

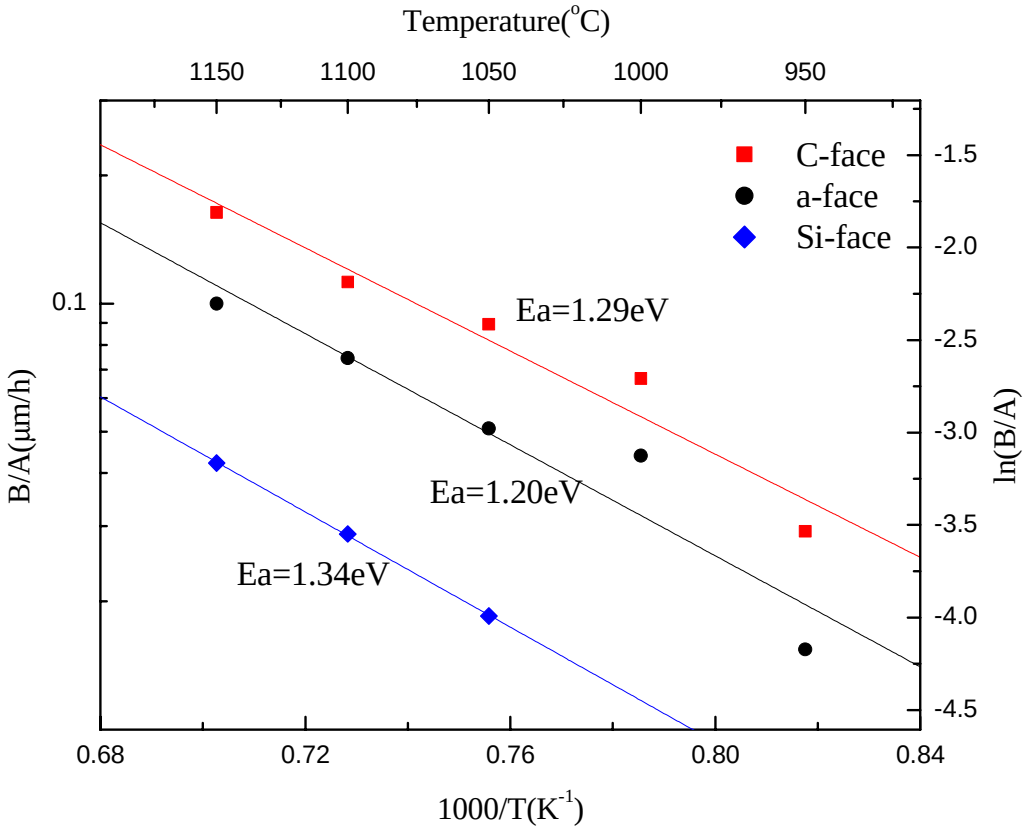

FIG. 2. 6 Arrhenius plots for the Deal Grove linear rate constant B/A . Activation energies were found to be 1.29 eV, 1.20eV and 1.34 eV for the $(000\bar{1})$ C-, the $(11\bar{2}0)$ a- and (0001) Si-faces,respectively.

The magnitude of the pre-exponential factor of the linear rate constant is attributed to the different areal density of atoms and mechanical stress effects present at the interface, but the interface chemical reaction is the same on the both surfaces.[15] This suggests an explanation of the SiC data. Table 2.3 shows the carbon and silicon areal density of the first layer for the different surfaces. The ratio of carbon areal density between the C-face and a-face is 1.64, close to our experimental result of $\frac{(B/A)_{000\bar{1}}}{(B/A)_{11\bar{2}0}}$ ~1.60. Since the oxidation rate on the Si-face, which has 100% Si atoms, is very slow compared to the other faces, we believe that the reaction rate is mainly proportional to the carbon areal density. Referring to Eq. (2.9a), this implies that K_f depends sensitively on the SiC crystal surface.

Table 2. 3 Areal density of the first layer for the different faces

	C-face	$(11\bar{2}0)$ face	Si-face
C areal density (10^{15} atoms/cm^2)	1.21	0.74	0
Si areal density (10^{15} atoms/cm^2)	0	0.74	1.21
Ratio of B/A to $B/A_{(000\bar{1})}$ at 1100°C	1	0.66	0.26

This interpretation is consistent with earlier results of Song and Smith for the etch rate of SiC, achieved at relatively low oxygen pressure.[16] It is well known that O_2 etches Si at low oxygen pressure. If O_2 etches SiC, the etch rate is also dependent on the crystal orientation. The work of Song and Smith shows that the etch rate of the C-face in the low partial pressure of O_2 is about 6 times larger than that of the Si-face. During the etching,

there is no diffusion. The etch rate is determined simply by the chemical reaction rate, and the etching data confirm the strong anisotropy in the interface chemical reaction rate.

Figure 2.7 shows B via 1/T for the $(000\bar{1})$, $(11\bar{2}0)$ and (0001) faces. It can be seen that for the $(000\bar{1})$ face, E_a is ~1.99eV, very close to the activation energy of oxygen diffusivity D_{O_2} in SiO_2.[17] This is a strong indication that the oxidation rate is limited by oxygen in-diffusion on the $(000\bar{1})$ C-face.

In the present work, the SiC samples were oxidized at 1 atm oxygen pressure. Recently, Trimalle, *et. al.*[18] have shown that the oxidation of the C-face of 6H-SiC is limited by the interface reaction when the oxygen pressure is below 0.1 atm, while the Si-face shows almost no pressure dependence. At this low oxygen pressure, the interface reaction is reduced and competes with the oxygen in-diffusion step for the C-face. For the a- and Si-face, the relatively low interface reaction rate is limiting even at 1 atm oxygen pressure. Thus, the results in Ref. 18 are consistent with the analysis presented here.

We find that the activation energies of B for the (0001) Si and $(11\bar{2}0)$ a- face are very different from that of C-face (1.99eV). Evidently, the oxidation rate-controlling step involves both oxygen diffusion and/or the interface reaction. In this case, Eq. (2.11) cannot be used to interpret the data. It is only valid when the oxygen in-diffusion step is the rate-controlling step. So Eq. (2.9b), which is a more general equation, must be used to interpret the data for the (0001) Si and $(11\bar{2}0)$ a- faces. In the denominator of Eq. (2.9b), neither of the two terms is obviously dominant.

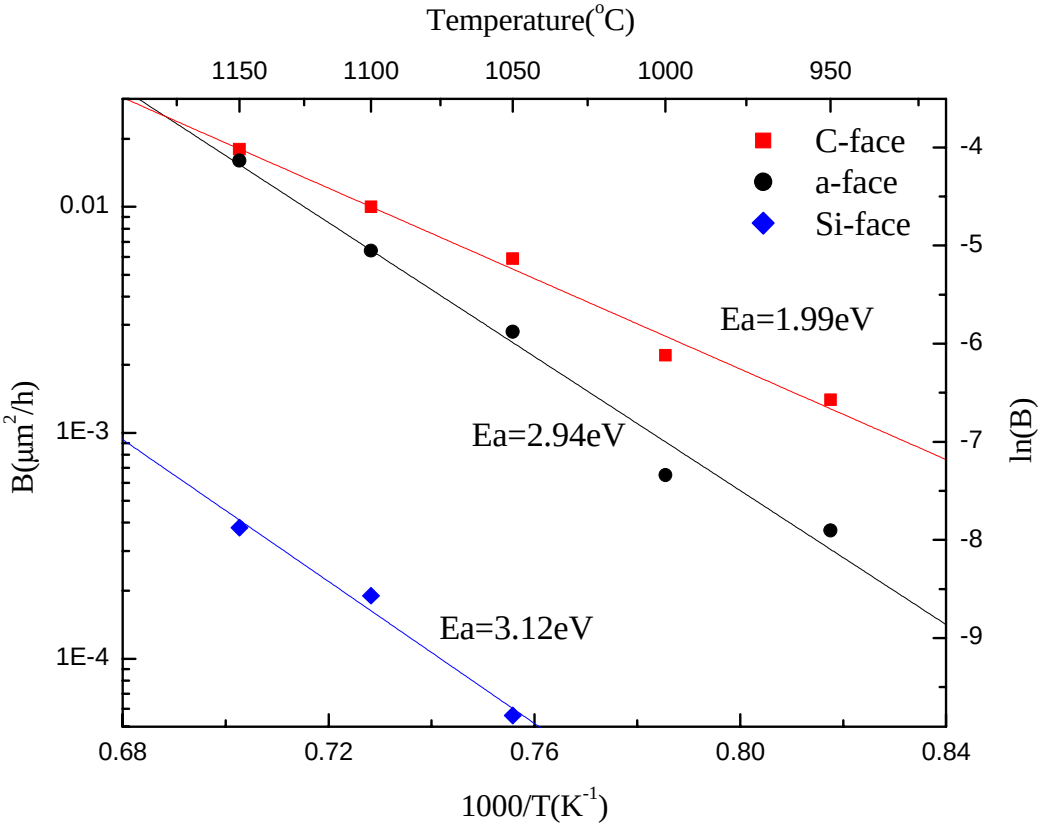

FIG. 2. 7 Arrhenius plots for the Deal Grove parabolic rate constant B. Activation energies were found to be 1.99 eV, 2.94eV and 3.12 eV for the (000$\bar{1}$) C-, the (11$\bar{2}$0) a- and (0001) Si-faces, respectively.

The activation energy for the B parameter for the a-face and Si-face are the same within error, and clearly different than the activation energy for the C-face. Since the data display Arrhenius behavior and the activation energy is significantly different than O_2 diffusion in SiO_2, we discuss the aspect of data in the terms of Eq. (2.12).

In the case where CO out-diffusion is the limiting step (Eq.(2.12)) the activation energy corresponds to the products of activation energies for K_f, K_r and D_{CO}. Unfortunately there is not sufficient information to separate there three quantities, nor are they known from the literature. However one may obtain some insight from the B/A analysis. As indicated in Eq. (2.9a) the B/A parameter is proportional to K_f. The measured values of B/A for the different faces indicated $K_f|_{a\text{-face}}$ has the same activation energy indicated as $K_f|_{Si\text{-face}}$, but has a significantly larger pre-exponential behavior. This was explained in the terms of the larger carbon density in the surface.

This is consistent with Eq. (2.12) and the observations. The B value for the Si-face and a-face yields the same activation energy, but the pre-exponential constant for the a-face is close to an order of magnitude greater than for the Si-face. This is in accord with the suggestion of Eq. (2.12), if we assume that K_r is not very different for the two surfaces.

Note that the oxidation temperature range could be very important for the oxidation rate limiting mechanism. As the temperature increases, the increase of the interface reactionrate may be significantly greater than that of the diffusion rate. This is confirmed by Zheng's results[2] where the oxygen in-diffusion becomes the rate limiting step for the Si-face at the higher the oxidation temperature range from 1200 °C to 1500 °C.

Based on the model described above and our experimental results, both K_f and K_r play an important role for the anisotropic oxidation behavior for SiC. The surface composition is an important factor: for the $(000\bar{1})$ C-face, the first layer is 100% C atoms, for the (0001) Si-face, the first layer is 100% Si atoms and for the $(11\bar{2}0)$ a-face, the first layer is 50% C atoms and 50% Si atoms. We infer that K_f is proportional to the carbon areal density. The interface chemistry may be described as follows: on the $(000\bar{1})$ C-face, there is a large driving force for C atoms in the first layer to easily break Si-C bond and form C-O, a very stable molecule. Following the first layer removal, the Si atoms in the second layer may react with O since there is only one Si-C bond connected to the third layer (C-layer). However, on the (0001) Si-face, it is more difficult to break Si-C bonds and form Si-O since there are three Si-C bonds connected to the second C layer. From the $(11\bar{2}0)$ a-face geometry, the situation is intermediate in the Si/C ratio.

Conclusions

A modified Deal Grove model for oxidation of SiC is established which takes into account CO out-diffusion. The oxidation behavior can be predicted fron this model. The oxide growth rate on the $(11\bar{2}0)$ a-face of 4H-SiC is measured accurately for the first time. Comparing the oxidation kinetics with the $(000\bar{1})$ C-face and the (0001) Si-face, the growth rate of this face is intermediate between the C- and the Si-4H-SiC faces. The interface reaction plays a key role in the oxidation anisotropy of SiC.

Acknowledgements

We wish to thank B. Rogers for ellipsometer measurements, A. B. Hmelo and W. Augustyniak for RBS measurements, and E. Garfunkel and T. Gustafsson for MEIS measurement. This work was supported by DARPA Contract N00014-02-1-0628 (John Zolper, Ingham Mack technical program monitors) and by ONR Grant N000140110616 (John Zolper, technical program monitor) and by NSF grant DMR-0218406 .

References

1 J.A. Castello and R. E. Tressler, J. Am. Ceram. Soc. **69**, 674 (1986).

2 Z. Zheng, R. E. Tressler, and K. E. Spear, J. Electrochem Soc. **137,** 850 (1990).

3 G. H. Schiroky, R. J. Price, and J. E. Sheehan, Rep. No. GA-A18696, GA Technologies Inc., San Diego, CA 1986.

4 T. Naushima, T. Goto, and T. Hirai, J. Am. Ceram. Soc. **72**, 1386 (1989).

5 R.C.A. Harris, J.Am.Ceram. Soc. **58,** 7 (1975)

6 E. Fitzer and R. Ebi, in *Silicon Carbide 197*3, edited by R. C. Marshall, J. W. Faust, Jr., and C. E. Ryan (University of South Carolina Press, Colum-bia, SC, 1974), p. 320.

7 D.M Mieskowski, T. E. Mitchell, and A. H. Heuer, J. Am. Ceram. Soc. **67,** C17 (1984)

8 W.W. Pultz, J. Phys. Chem. **71** ,4556 (1967)

9 N.S.Jacobson, J.Am.Ceram. Soc. **76,** 3 (1993)

10 K. L. Luthra, J. Am. Ceram. Soc, **74,** 1095 (1991)

11 K. Motzfeld, Acta Chem. Scand. **18,** 1596 (1964)

12 B.E. Deal and A.S. Grove, J. Appl. Phys. **36,** 3770 (1965)

13 If reaction (2.1) is a first-order reaction, $F = K_f C_{O_2}^{1.5} - K_r C_{CO}$ is more reasonable. However, this reaction may not be a first-order reaction. Otherwise,

oxidation behaviors should be same for the different crystal faces. In order to simplify the model, Eq. (2.6) is assumed to be correct.

[14] S. Dhar S. Dhar, Y. W. Song, L. C. Feldman, T. Issacs-Smith, C. C. Tin, J. R. Williams, G. Chung, N. Nishimura, D. Starodub, T. Gustafsson, and E. Garfunkel, Appl. Phys. Lett. **84,** 1498 (2004). (Chapter III of this thesis)

[15] E.A.Irene, H.Z.Massoud and E.Tierney J.Electrochem.Soc. **133,** 1253 (1986)

[16] Y. Song, F. W. Smith, Appl. Phys. Lett. **81,** 3061 (2002)

[17] F. J. Norton, Nature (London) **171**,701 (1961)

[18] I. Trimaille, 16th International Conference on Ion Beam Analysis, June 29-July 4, 2003, Albuquerque, NM, USA

Appendix

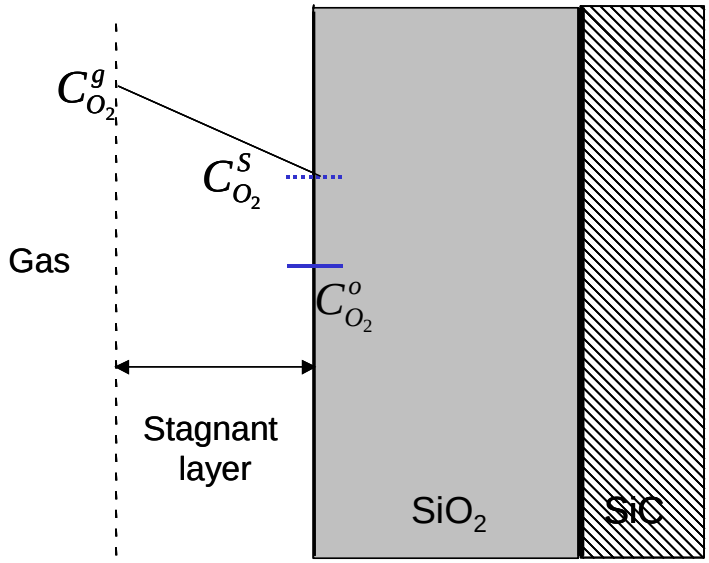

Fig. 2A.1 Relevant oxygen concentrations (described in appendix I A) for transport of O_2 molecules from the bulk of the gas to the oxide surface.

(A) Derivation of equation 2.3 (see Fig. 2A.1)

Flux of O_2 molecules from the gas atmosphere to the outer surface of the oxide is given by:

$$F_{O_2} = h^g{}_{O_2} (C^g_{O_2} - C^S_{O_2}) \qquad (1A.1)$$

where h^g is the gas-phase mass transport co-efficient, $C^g_{O_2}$ the O_2 concentration in the bulk of the gas and $C^S_{O_2}$ the O_2 concentration next to the oxide surface respectively.

Using the ideal gas law,

$C^g_{O_2} = \frac{P^g{}_{O_2}}{kT}$ and $C^S_{O_2} = \frac{P^S{}_{O_2}}{kT}$ where $P^g{}_{O_2}$ and $P^S{}_{O_2}$ are the partial pressures of O_2 in the bulk of the gas and next to the oxide surface respectively.

To write eqn. (1A.1) in terms of the concentrations in the oxide layer, Henry's law can be used. Henry's law states that in the absence of chemical reaction at the surface, concentration of O_2 in the solid is related to the partial pressure of the oxidant in gas by:

$$C^{O}_{O_2} = HP^{S}{}_{O_2} \qquad (1A.2)$$

where $C^{O}_{O_2}$ is the O_2 concentration at the outer surface of the oxide and H is Henry's constant. Also, defining

$$C^{*}_{O_2} = HP^{g}{}_{O_2} \qquad (1A.3)$$

where $C^{*}_{O_2}$ is the equilibrium O_2 concentration in the oxide which represents the concentration which would be in equilibrium with the partial pressure $P^{g}{}_{O_2}$ in the bulk of the gas.

Using (1A.2) and (1A.3) the equation (1A.1) can be expressed as

$$F_{O_2} = h_{O_2}(C^{*}_{O_2} - C^{O}_{O_2}) \qquad \text{(eq. 2.3 in text)}$$

where $h_{O_2} = \dfrac{h^{g}_{O_2}}{HkT}$ is the gas-phase-mass-transfer co-efficient *in terms of concentration in the solid.*

(B) Derivation of equation 2.8 (a) and 2.8 (b)

From eqn. (2.3) - (2.5) in the text we get under steady state

For O_2:

$$F_{O_2} = D_{O_2}\frac{C^{i}{}_{O_2} - C^{O}_{O_2}}{X_0} = h_{O_2}(C^{O}_{O_2} - C^{*}_{O_2}) \qquad (1A.4)$$

For CO:

$$F_{CO} = D_{CO}\frac{C^{i}{}_{CO} - C^{O}_{CO}}{X_0} = h_{CO}(C^{O}_{CO} - C^{*}_{CO}) \qquad (1A.5)$$

From (1A.4) we get

$$C_{O2}^{O} = C_{O_2}^{*} - \frac{F_{O_2}}{h_{O_2}} = \frac{X_o F_{O_2}}{D_{O_2}} + C^{i}{}_{O_2}$$

therefore,

$$C_{O2}^{i} = C_{O_2}^{*} - (\frac{1}{h_{O_2}} + \frac{X_o}{D_{O_2}})F_{O_2} \qquad \text{(1A.6)}$$

Similarly from (1A.5) we get

$$C_{co}^{i} = C_{co}^{*} + (\frac{1}{h_{co}} + \frac{X_o}{D_{co}})F_{co}$$

At the SiO_2/SiC interface

$$F = K_f C^{i}{}_{O_2} - K_r C^{i}{}_{CO} \qquad \text{(1A.7) (also eq. 2.6 in text)}$$

Using (1A.5) and (1A.6) in (1A.7)

$$F = K_f[C_{O_2}^{*} - (\frac{1}{h_{O_2}} + \frac{X_o}{D_{O_2}})F_{O_2}] - K_r[C_{co}^{*} + (\frac{1}{h_{co}} + \frac{X_o}{D_{co}})F_{co}] \qquad \text{(1A.8)}$$

For the steady-state condition, $F : F_{O_2} : F_{CO} = 1 : 1.5 : 1$

Thus eqn. (1A.8) can be re-written as:

$$F = \frac{K_f C_{O_2}^{*} - K_r C_{CO}^{*}}{(1 + \frac{1.5K_r}{h_{O_2}} + \frac{K_r}{h_{CO}}) + (\frac{1.5K_f}{D_{O_2}} + \frac{K_r}{D_{CO}})X_o} \qquad \text{(1A.9)}$$

The rate of SiO_2 growth is given by

$$\frac{dX_0}{dt} = \frac{F}{N_0} \qquad \text{(1A.10) (also eq. 2.7 in text)}$$

where N_0 is the number of oxidant molecules incorporated into a unit volume of the oxide layer.

Using eqns (1A.9) in eqn (1A.10) we get

$$\frac{dX_0}{dt} = \frac{K_f C^*_{O_2} - K_r C^*_{CO}}{(1 + \frac{1.5K_r}{h_{O_2}} + \frac{K_r}{h_{CO}}) + (\frac{1.5K_f}{D_{O_2}} + \frac{K_r}{D_{CO}})X_o} . (\frac{1}{N_0}) \qquad (1A.11)$$

Integrating we obtain

$$X_0^2 + \frac{1 + \frac{1.5K_f}{h_{O_2}} + \frac{K_r}{h_{CO}}}{\frac{1.5K_f}{D_{O_2}} + \frac{K_r}{D_{CO}}} X_0 = \frac{(K_f C^*_{O_2} - K_r C^*_{CO})/N_0}{\frac{1.5K_f}{D_{O_2}} + \frac{K_r}{D_{CO}}} (t - \tau) \qquad (1A.12)$$

This equation is of the form :

$$X^2 + AX = B(t + \tau) \qquad \text{(eq. 2.2 in text)}$$

where

$$A = \frac{1 + \frac{1.5K_f}{h_{O_2}} + \frac{K_r}{h_{CO}}}{\frac{1.5K_f}{D_{O_2}} + \frac{K_r}{D_{CO}}} \qquad \text{(eq. 2.8 (a) in text)}$$

$$B = \frac{(K_f C^*_{O_2} - K_r C^*_{CO})/N_0}{\frac{1.5K_f}{D_{O_2}} + \frac{K_r}{D_{CO}}} \qquad \text{(eq. 2.9 (b) in text)}$$

CHAPTER III

EFFECT OF NITRIC OXIDE ANNEALING ON THE INTERFACE TRAP DENSITY NEAR THE CONDUCTION BAND-EDGE OF 4H-SiC AT THE SiO_2/ $(11\bar{2}0)$ 4H-SiC INTERFACE

S. Dhar, [a)] Y. W. Song,[a)] L. C. Feldman,[a)], T. Isaacs-Smith,[b)] C. C. Tin,[b)] J. R. Williams,[b)]

G. Chung,[c)] T.Nishimura [d)], D.Starodub, [d)] T. Gustafsson, [d)] and E. Garfunkel[c)]

a) Dept. of Physics and Astronomy & Interdisciplinary Program in Materials Science
Vanderbilt University, Nashville, TN 37235, USA

b) Physics Department, Auburn University, Auburn, Alabama 36849

c) Dow Corning Inc., Tampa, Florida 33619

d) Dept. of Physics and Astronomy, Rutgers University, Piscataway, New Jersey 08854

e) Dept. of Chemistry, Rutgers University, Piscataway, New Jersey 08854

Published in Applied Physics Letters, March (2004)

Abstract

Interface state density measurements were performed on metal-oxide semiconductor capacitors fabricated by dry oxidation, with and without NO annealing, on the $(11\bar{2}0)$ crystal face of n-4H-SiC. Nitric oxide post-oxidation anneal results in a significant decrease of defect state density (D_{it}) near the conduction band edge of n-4H-SiC. Comparison with measurements on the conventional (0001) Si- terminated face shows a similar interface state density following passivation. Medium energy ion scattering (MEIS) provides a quantitative measure of nitrogen incorporation at the SiO_2/SiC interface.

Introduction

The 4H polytype of silicon carbide (4H-SiC) is one of the most promising materials for power electronics applications. Among the attractive properties of SiC is the ability to grow a thermal oxide leading to the development of SiC MOSFET (metal oxide semiconductor field effect transistor) technology similar to that of silicon. Although this oxide is similar to SiO_2 grown on Si[1], the SiO_2/SiC interface results in much poorer electronic properties than the SiO_2/Si interface. Until recently MOSFETs fabricated on the conventional (0001) Si- terminated face of 4H-SiC have typically shown very low inversion channel mobilites (μ_{inv}~0.1-25 cm^2/V-s). Such low mobilities were attributed to the high density of interface states present within the band gap of SiC. Moreover 4H-SiC MOSFETs show lower mobilities than 6H devices (μ_{inv}~25-100 cm^2/V-s), although the bulk mobility of 4H is higher than 6H (800cm^2/V-s, compared to 300 cm^2/V-s). This problem has been attributed to the presence of a high interface state density (D_{it}); a broad distribution lying approximately 2.9 eV above the valence band[2]. These states fall within the band gap of 4H-SiC (E_g=3.26 eV), but lie in the conduction band for 6H-SiC(E_g=3.02 eV). Thus the channel mobility is reduced in 4H-SiC by field termination, carrier trapping and Coulomb scattering associated with this high density of interface states.

Recent studies have reported an order of magnitude reduction of D_{it} on the (0001) Si terminated face near the conduction band edge of 4H-SiC by using a nitric oxide (NO) post oxidation anneal (POA)[3-6]. Intriguingly, reports by other groups have indicated improved device properties of MOS structures built on the $(11\bar{2}0)$ oriented 'a' face substrates using wet oxidation only[7-9] (i.e., without an NO passivation anneal) and

suggested an intrinsic low density of acceptor like interface states near the conduction band edge on the $(11\bar{2}0)$ surface[8]. Others have indicated good $(11\bar{2}0)$ properties after passivation of these interface states by hydrogen[9]. In this paper, we report the effects of the NO POA on the interface state density for dry oxides on $(11\bar{2}0)$ 4H-SiC. Our results indicate that dry oxidation of the $(11\bar{2}0)$ face results in comparable D_{it} to that of the (0001) Si face (~10^{13} $cm^{-2}eV^{-1}$) at ~0.2 eV below the conduction band. NO annealing results in a substantial improvement, reducing the value to ~10^{12} $cm^{-2}eV^{-1}$, which is comparable to the best values obtained for the Si face.

The main feature distinguishing the (0001) and $(11\bar{2}0)$ crystal faces is the polar structure. The first monolayer of the Si face is 100% Si, while that of the $(11\bar{2}0)$ a-face is 50% C and 50% Si. Thus, exploration of the a-face interface structure is important for explaining the basic physics of SiC oxidation. Furthermore, understanding the interface properties at these structurally different surfaces is important not only for fabricating devices utilizing wafers of different orientation, but it also plays a key role in the physics of UMOSFETs[10]. In the UMOSFET structure, the gate is 'U' shaped, resulting in the SiO_2/SiC interface lying along both the (0001) and $(11\bar{2}0)$ surfaces**.** Since the inversion channel formation takes place along the $(11\bar{2}0)$ /oxide interface, it is critical to realize high inversion layer mobility and low interface state density on this face.

Experimental procedure

$(11\bar{2}0)$ n-type 4H-SiC substrate wafers (N_d = $5x10^{18}$ cm^{-3}) supplied by CREE, Inc. were used to grow thin lightly doped n epi layers (5 μm, N_d~10^{16} cm^{-3}). After a standard RCA clean, the samples were oxidized at 1150°C in dry oxygen to yield an

oxide thickness of about 30 nm. For the sample subjected to the NO POA process, the temperature was ramped up to 1175 °C in flowing Ar, and the NO anneal was performed for 2 h. The NO POA process is completed by ramping down the temperature from 1150 °C to 900 °C at a ramp rate of 4°C/min in flowing Ar and unloading the samples under these conditions. A standard sample was made by annealing in Ar at the oxidation temperature for 30 min after oxidation, a common practice in SiC technology. Gate metallization was performed by sputtering Mo and Au in succession and colloidal Ag paste was used for a large area backside ohmic contact. Simultaneous hi-lo C-V (capacitance-voltage) measurements (high frequency-100kHz and quasistatic) were performed using Keithley 590,597and 230 C-V modules. These measurements were performed at room temperature, and the gate bias was swept from accumulation to depletion. Similar sets of samples were prepared on the (0001) oriented samples for comparison between these two crystal faces.

Medium Energy Ion Scattering (MEIS)[11] using 100 keV H^+ ions at normal incidence and 125^o scattering geometry was performed on the $(11\bar{2}0)$ 4H-SiC samples to determine nitrogen incorporation at the interface. Two sets of samples were made with and without NO annealing. Dry oxidation was performed at 1150°C to grow a ~40 nm oxide layer, followed by an NO anneal at 1175 °C for 2 h. The oxide layer was carefully etched with HF to thin the layer in order to preserve the interface resolution for MEIS analysis.

Results and Discussions

Interface state density profiles for the $SiO_2/(11\bar{2}0)$ 4H-SiC interface are shown in Fig. 3.1. The NO POA process resulted in an order of magnitude reduction in D_{it} close to the conduction band edge. At E_c-E= ~0.1eV, the density of defects traps is reduced from ~10^{13} $cm^{-2}eV^{-1}$ to ~ 10^{12} $cm^{-2}eV^{-1}$. Reduction of D_{it} also occurs further from the conduction band, but the effect is most pronounced near the conduction band edge. This reduction is similar to that observed for the nitric oxide anneal for the (0001) Si face MOS capacitors, as shown on the same plot. The results also show that the interface state density before passivation by NO for the $(11\bar{2}0)$ face is of the same order of magnitude as for the (0001) Si face, at least in the case of dry oxides. This is contrary to the observations made for wet oxides where the $(11\bar{2}0)$ interface was found to have a lower D_{it} in comparison to the (0001) Si face[7,8]. This could be due to the wet oxidation bringing about some in-situ passivation of traps during the wet oxidation process-a process that is associated with hydrogen. It should be noted that there exists a significant anisotropy in the oxidation kinetics among the different crystal faces of SiC [12,13], so it is likely that the interface chemistry is different for these two faces. However our observations indicate that the electrically active trap density behavior of dry oxides is similar for the two faces. Fig. 3.2 shows the high frequency and quasistatic C-V curves for as-oxidized and NO passivated $(11\bar{2}0)$ MOS capacitors.

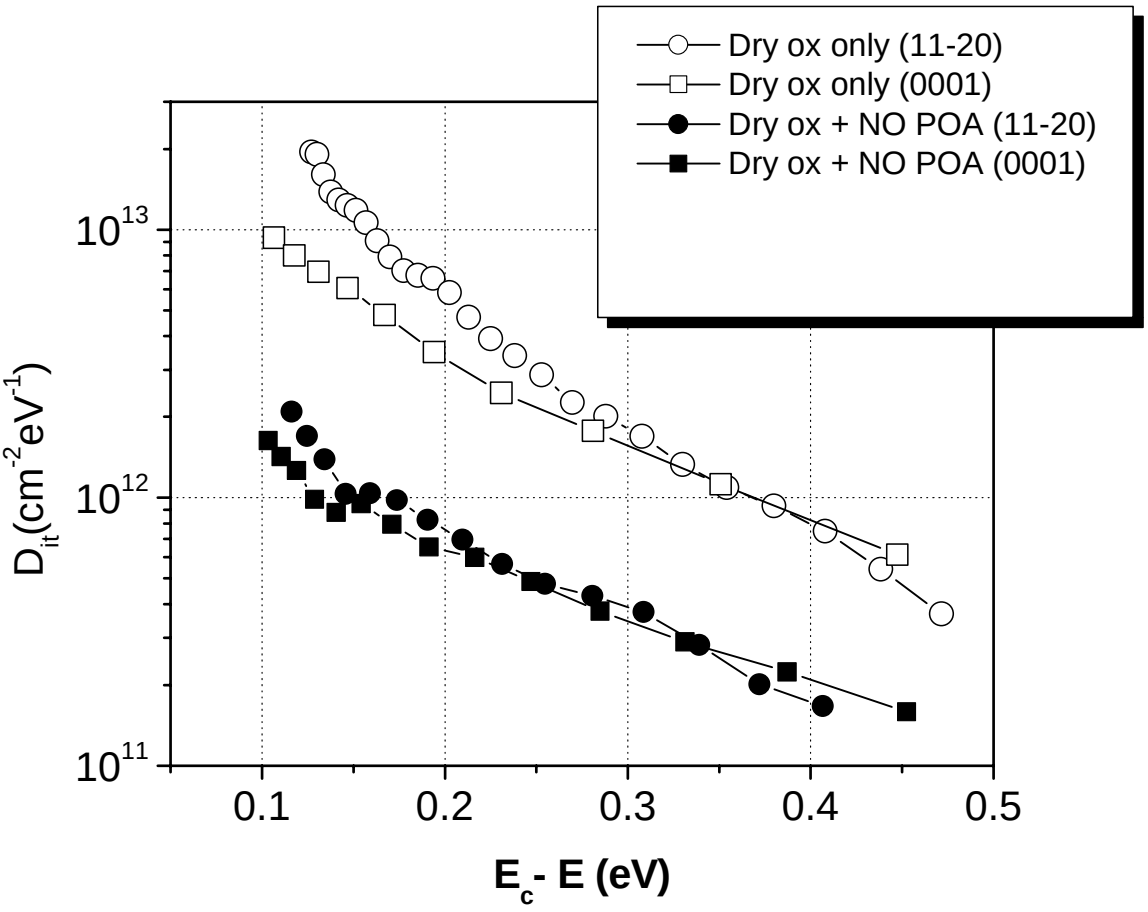

FIG. 3. 1. Interface state density profile $D_{it}(E)$ near E_c measured for $(11\bar{2}0)$ (circles) and (0001) (squares) with (solid symbols) and without (open symbols) NO post oxidation anneal The NO POA significantly reduces the D_{it} near the conduction band for both the orientations.

The nitridation process leads to a shift of the flat-band voltage towards less positive voltages. This can be attributed to the decrease in effective negative charge at the interface due to the NO anneal. Similar effect has been observed for the (0001) capacitors (not shown) in this work and in previous reports [3]. The nature of these traps could have a variety of sources. Previous studies indicate the possibility of carbon clusters, sub-oxides or oxycarbides at the interface, and Si and C dangling bonds have also been considered[3,5,8,14,15]. Furthermore, it has been suggested that the NO POA may not physically remove these defects but may instead shift the energies of these defects in the band gap, thereby removing their detrimental effects[5,16]. Earlier studies have also indicated that passivation depends only on the amount of nitrogen incorporated at the interface and is independent of anneal temperature and time [1, 3,5].

Fig.3.3 shows the MEIS spectrum of $(11\bar{2}0)$ sample oxidized and subjected to the NO POA process and a sample without the NO treatment. We observe incorporation of nitrogen at or near the interface from the MEIS measurement. It is possible that the NO anneal leads to the formation of a thin nitride at this interface. The areal density of N atoms was found to be 0.66 x 10^{15} atoms/cm^2 and 1.16 x 10^{15} atoms/cm^2 for the $(11\bar{2}0)$ and (0001) surfaces respectively (spectrum for (0001) not shown). These N atoms are distributed very close to the interface with a distribution that has a full width at half maxima of the order ~ 10 $\mathring{A}$, which is very close to the depth resolution limit of MEIS. In Table 3.1 the atomic areal densities of Si and C obtained from MEIS have been compared with theoretically calculated values for both (0001) and $(11\bar{2}0)$. The theoretical C density is found by calculating the contribution from the intrinsic surface

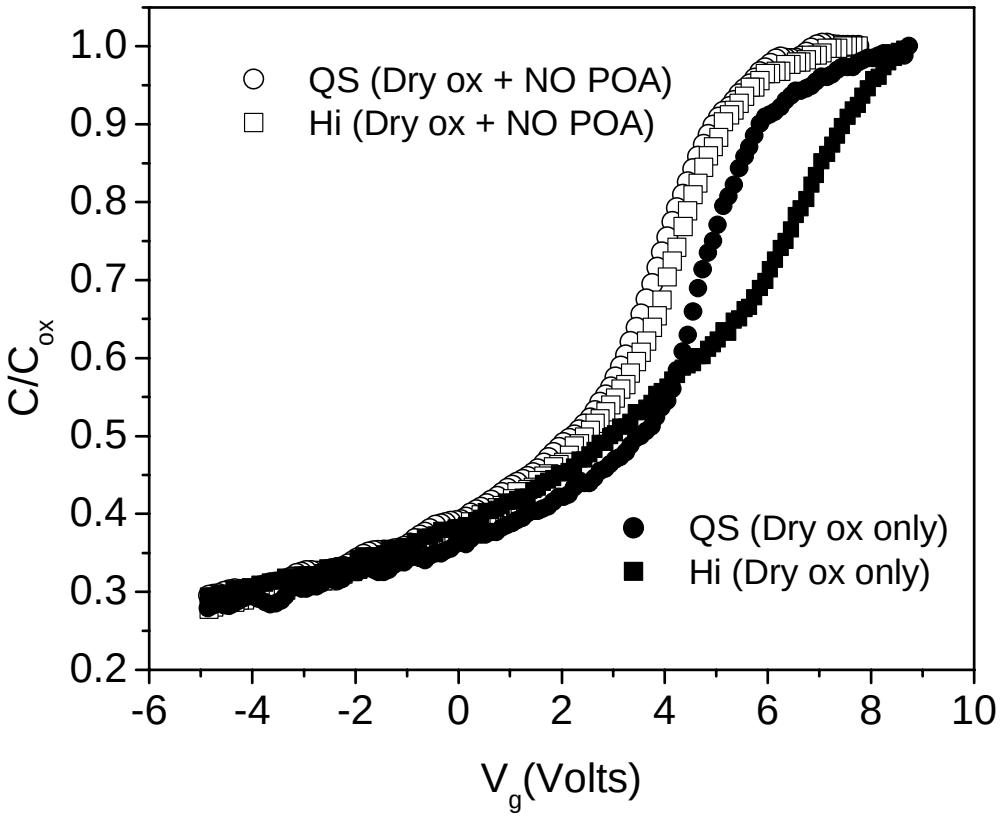

FIG. 3. 2 High frequency (squares) and quasistatic (circles) C-V curves for as-oxidized (solid symbols) and NO annealed (open symbols) $(11\bar{2}0)$ 4H-SiC capacitors .

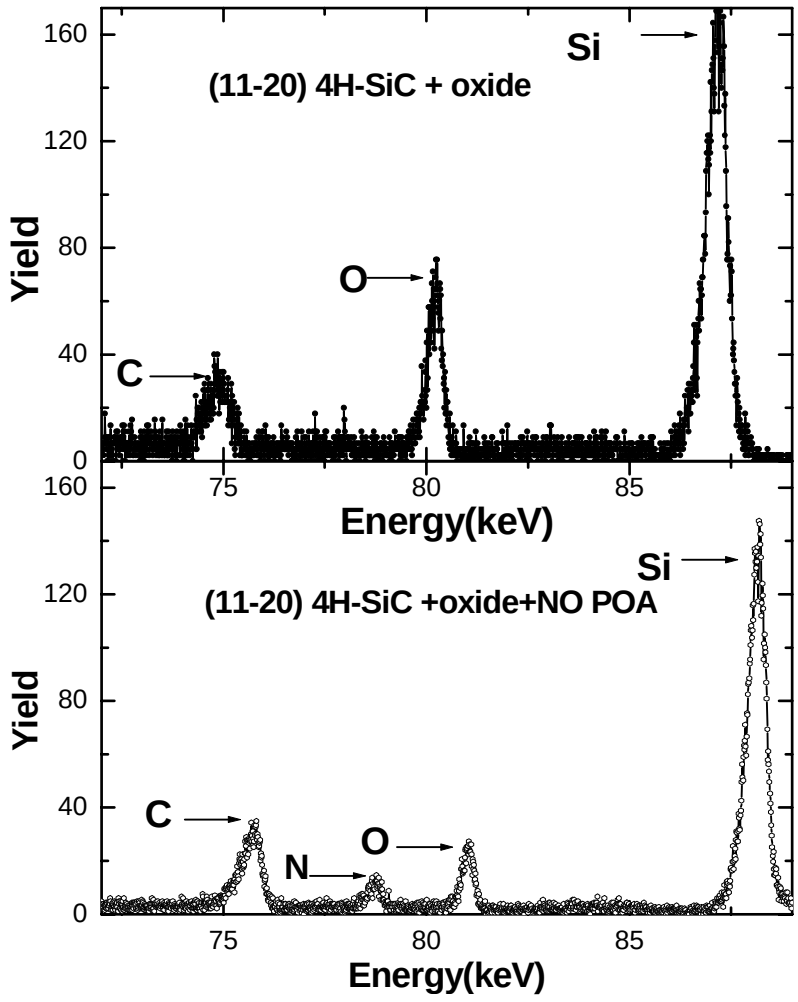

FIG. 3. 3 MEIS spectra of (11$\bar{2}$0) 4H-SiC: Sample as–oxidized at 1150 °C (top) compared to a sample that underwent a NO POA at 1175 °C for 2 h after oxidation (bottom). Nitrogen incorporation at or near the interface can be observed from the spectra. N atom areal density calculated to be 0.66 x10 ^{15} atoms/cm^2. Error has been estimated as 5% of the experimental values. The difference in amount of Oxygen in the two samples is due to different thickness resulting from etching of the oxide. The shift in the energy scale is due to small shifts in incident ion energy.

Table 3. 1 Areal densities of Si, O, C and N atoms obtained experimentally from MEIS. Theoretical values of the Si and C areal densities are shown for comparison. The C intensity for all samples is much higher than that expected from an ideal SiC crystal. This could correspond to either a reconstructed interface or interfacial carbon. The discrepancy between the theoretical and measured Si surface intensities could correspond to a thin sub-oxide at the interface.

Sample	**Oxide Thick--ness (A)**	**Si 10^{15} atoms cm $^{-2}$**	**O 10^{15} atoms cm $^{-2}$**	**C 10^{15} atoms cm $^{-2}$**	**N 10^{15} atoms cm^2**	**$Si_{intrinsic}$+ Si_{SiO2} (calcula --ted) 10^{15}at--oms cm^{-2}**	**$C_{intrinsic}$ (calcul-ated) 10^{15} atoms cm $^{-2}$**
$(11\bar{2}0)$ as-oxidized	≅ 6.7	3.77 ±0.19	3.01 ± 0.15	3.84 ± 0.19	-	1.6 + 1.51 = 3.11	2.7
$(11\bar{2}0)$ With NO	≅ 2.2	2.79 ± 0.14	0.97 ± 0.05	4.27 ± 0.21	0.66 ± 0.03	1.6 + 0.485 = 2.09	2.7
(0001) as-oxidized	≅ 9.7	4.24 0.21	4.36 0.22	3.39 0.17	-	2.9 + 2.18 = 5.08	2.4
(0001) With NO	≅ 7.4	3.96 0.2	3.33 0.17	3.58 0.18	1.16 ± 0.06	2.9 + 1.67 = 4.57	2.4

peak of C in $(11\bar{2}0)$ SiC[11,17]. The intrinsic surface peak is the intensity arising from the ion beam's interaction with the first monolayers of atoms. For Si, the sum of the intrinsic surface peak of Si and Si in a thin layer of stoichiometric SiO_2 has been calculated.

The carbon intensity for both faces is significantly greater than that expected for an ideal SiC crystal, for both the as-oxidized and NO passivated samples. This may be due to a severely reconstructed interface or, more likely interfacial carbon produced during the oxidation process. The difference between the calculated and measured values of carbon sets a limit on the amount of the excess interfacial carbon to approximately a monolayer of carbon. The measured Si surface intensity for the $(11\bar{2}0)$ face is somewhat higher than that expected for an ideal SiO_2/SiC. On the contrary, for the (0001) samples; the measured Si intensities were lower than the calculated theoretical values. This could be a preliminary indication of a thin layer of non-stoichiometric sub-oxide (i.e SiO) existing between the stoichiometric SiO_2 and the SiC substrate.

Conclusion

In conclusion, we have observed that the density of states on dry oxides near the conduction band edge at the SiO_2/$(11\bar{2}0)$ 4H-SiC interface decreases following a post-oxidation anneal in NO. We have observed nitrogen incorporation at the interface, - a key element in the passivation process. Moreover, the interface states on the (0001) Si face show a similar decrease upon NO POA. This suggests that the physical natures of defects contributing to the density of interface states near the conduction band on these two crystal faces are similar.

Acknowledgements

The authors thank J.A.Cooper (Purdue) and T.Hmelo, W.M.Augustyniak, S.Pantelides (Vanderbilt) for useful discussions. This work was supported by DARPA Contract N00014-02-1-0628 (John Zolper, Ingham Mack technical program monitors) and by ONR Grant N000140110616 (John Zolper, technical program monitor) and by NSF grant DMR-0218406 .

References

[1] K. McDonald, M. B. Huang, R. A. Weller, L. C. Feldman, J. R. Williams, F. C. Stedile, I. J. R. Baumvol, and C. Radtke, Appl. Phys. Lett. **76**, 568 (2000).

[2] R. Schorner, P. Friedrichs, D. Peters, and D. Stephani, IEEE Electron Device Lett. **20,** 241 (1999).

[3] G. Y. Chung, C. C. Tin, J. R. Williams, K. McDonald, M. DiVentra, S. T. Pantelides, L.C.Feldman, and R.A.Weller, Appl. Phys. Lett. **76,** 1713 (2000).

[4] G. Y. Chung, J. R. Williams, C. C.Tin, K. McDonald, D. Farmer, R. K. Chanana, S. T. Pantelides, O. W. Holland, and L. C. Feldman, Appl. Surf Sc. **184,** 399 (2001).

[5] K. McDonald, R. A. Weller, S. T. Pantelides, L. C. Feldman, G. Y. Chung, C. C.Tin, and J. R. Williams, J. Appl. Phys. **93** , 2719 (2003).

[6] K. McDonald, L. C. Feldman, R. A. Weller, G. Y. Chung, C. C. Tin, and J. R.Williams, J. Appl. Phys. **93,** 2257 (2003).

[7] H. Yano, T. Hirao, T. Kimoto, H. Matsunami, K. Asano, and Y. Sugawara, IEEE Electron Device Lett. **20**, 611 (1999).

[8] H. Yano, T. Hirao. T. Kimoto, and H. Matsunami , J. Appl. Phys. **78,** 374 (2001).

[9] J. Senzaki, K. Kojima, S. Harada, R. Kosugi, S. Suzuki, T. Suzuki, and K. Fukuda, IEEE Electron Device Lett. **23**, 13 (2002).

[10] J. A .Cooper, Jr. and A. Agarwal, Proceedings of the IEEE **90,** 956 (2002).

[11] T. Gustafsson, H. C. Lu, B. W. Busch, W. H. Schulte, and E. Garfunkel, Nucl. Instr. Meth. B **183,** 146 (2001).

[12] Z .Zheng, R. E. Tressler, and K. E. Spear, J. Electrochem. Soc. **137,** 2812 (1990).

[13] K. Chritiansen and R. Helbig, J. Appl. Phys. **79**, 3276 (1996).

[14] V. V. Afanas'ev. M. Bassler, G. Pensl, and M. Schulz, Phys.Stat. Sol A **162** 321 (1997).

[15] B. Hornetz, H-J. Michel, and J. Halbritter, J. Mater. Res. **9**, 3088 (1994).

[16] V. V. Afanas'ev, A. Stesmans, F. Ciobano, G. Pensl, K.Y.Cheong, and S.Dimitrijev, Appl. Phys. Lett. **82,** 568 (2003).

[17] L. C. Feldman, J. W. Mayer, and S. T. Picraux , Materials analysis by ion channeling, (Academic Press, London, 1982) p. 12. For SiC , the surface peak intensity was calculated using the values of ρ(C) and ρ(Si), the two dimensional vibrational amplitudes for carbon and silicon respectively at θ_D = 1200K (Debye temperature for 4H-SiC).

CHAPTER IV

INTERFACE TRAP PASSIVATION FOR SiO_2/ $(000\bar{1})$ C-TERMINATED 4H-SiC

S. Dhar, [a)] L. C. Feldman, [a)] S.Wang,[b)] T. Isaacs-Smith,[b)] and J. R. Williams[b)]

a) Dept. of Physics and Astronomy & Interdisciplinary Program in Materials Science
Vanderbilt University, Nashville, TN 37235, USA
b) Dept. of Physics, Auburn University, Auburn, Alabama 36849

Submitted to Journal of Applied Physics (December, 2004)

Abstract

Interface trap passivation at the SiO_2/carbon terminated $(000\bar{1})$ face of 4H-SiC utilizing nitridation and hydrogenation has been evaluated. The SiO_2/ SiC interface, created by dry thermal oxidation on the C-face, shows appreciably higher interface state density near the conduction band compared to the (0001) Si-face. A post-oxidation anneal in nitric oxide followed by a post-metallization anneal in hydrogen results in dramatic reduction of the trap density by over an order of magnitude near the conduction band. The electrical measurements have been correlated with the interfacial chemistry.

Introduction

High interface state densities (D_{it}) at the silicon dioxide (SiO_2)/ 4H-silicon carbide (4H-SiC) interface result in poor inversion channel mobilities in 4H-SiC metal-oxide-semiconductor field effect transistors (MOSFETs).[1,2] Much effort has been dedicated to the development of improved processing techniques that can be applied to lower the trap

densities. It is not entirely clear whether the interface states are intrinsic to the SiO_2/4H-SiC system or result from a non-optimized thermal oxidation process.[3] The interface state distribution is highest near the 4H-SiC conduction band-edge where D_{it} approaches values greater than 10^{13} $cm^{-2}eV^{-1}$. Physical defects that have been attributed to the high D_{it} are carbon clusters, Si or C dangling bonds at the interface and/or a non-stoichiometric sub-oxide very near the interface.[4-7] Among the different procedures employed for the reduction of D_{it}, nitridation using post-oxidation annealing in nitric oxide (NO) is an established process that results in a dramatic reduction of D_{it} to ~10^{12} $cm^{-2}eV^{-1}$ at ~0.2 eV below the conduction band edge.[8,9] Most of the reported work to date has been on the (0001) Si terminated face of 4H-SiC. In this article, we report results of trap passivation on the $(000\bar{1})$ C terminated face of 4H-SiC, exploring the possibility that the use of different crystal faces may result in improved interface quality. Recent studies indicate that devices fabricated on 'alternate' crystal orientations such as $(11\bar{2}0)$ and $(03\bar{3}8)$ could have improved interface properties; either intrinsic or as a result of post-oxidation treatments.[10,11] (In this article, for the sake of clarity we shall simply refer to the different crystal faces as C-face $(000\bar{1})$, a-face $(11\bar{2}0)$ and Si –face (0001))

The C-face of SiC is polar containing 100 % C atoms; the $(000\bar{1})$ plane being a basal plane in the hexagonal unit lattice. Historically, the lack of availability of high quality epitaxial layers on the C-face was a constraint for reliable device fabrication. This problem is now of less significance with the availability of electronic grade commercial epitaxial layers. The main advantage of using the C-face for MOS devices is the higher oxidation rate compared to Si-face (a factor of about 5 at 1150°C) that could potentially lead to a lower thermal budget for SiC MOS processing.[12] The different oxidation rates

suggests the possibility of different interfacial structure.[13] Previous work on this face for both the 4H and 6H polytypes suggest an inferior interface with higher interface state density.[5,14] Recently however, high mobility (μ_{max} ~ 111 cm^2 $V^{-1}s^{-1}$) has been reported in lateral MOSFETs fabricated on the C-face using hydrogen passivation.[15] Characterization of the SiO_2/C-4H-SiC interface is also important for possible development of new device structures employing new geometries. In the present work, interface state densities and passivation of interface traps using nitrogen and hydrogen for the C-face have been evaluated. Comparisons have been made to results obtained for the Si-face and 'a'-face. Our results indicate that the as-oxidized C-face contains a considerably higher trap density than the Si-face near the conduction band; however, nitric oxide and hydrogen processing results in comparable and low defect densities for all crystal faces.

Experimental procedure

Si, C (both 8° off axis) and a-face (on-axis) n-type 4H-SiC wafers with 10 μm epitaxial layers doped with nitrogen at ~$1x10^{16}$ cm^{-3} were used to fabricate MOS capacitors for D_{it} measurements. After a standard RCA cleaning process, samples underwent dry oxidation at 1150°C for different time durations depending on crystal orientation. All samples were loaded and unloaded at 900°C in Ar. Samples without any passivation treatment were held at the oxidation temperature (1150°C) in Ar for 30 min after oxidation. To study the effect of nitridation on the C-face, samples were subjected to NO POA at 1175°C for 2 h and 4 h. Some samples that underwent the NO POA at 1175°C for 2h were further subjected to a post-metallization anneal (PMA) in H_2 at 500°C for 1 h using Pt as a gate metal to evaluate the effects of hydrogen. Results

obtained recently show that PMA in H_2 using Pt as a gate metal of nitridated oxides leads to a further lowering of D_{it} near E_C by about a factor of 2 for Si and a-face 4H-SiC.[16] Field effect mobilities for MOSFETs fabricated by the same process increased for both faces, with the effect being more prominent on the a-face (μ_{max} ~ 100 cm^2 $V^{-1}s^{-1}$).[17] The presence of a catalytic metal like Pt is key to this process, as it leads to the dissociation of molecular hydrogen on the surface and subsequent H incorporation at the SiO_2/SiC interface. It should be noted that for 2h NO and 2h NO + Pt/H_2 samples, the a-face and C-face samples were processed together. The a-face samples could be used as control since the effects of nitridation and hydrogenation on the a-face have been established in previous work .[16-18]

The simultaneous hi-lo capacitance-voltage (CV) technique[19] (100 kHz, quasistatic) was used at room temperature to estimate D_{it} from 0.1 to 0.6 eV below the conduction band. The gate voltage was swept from accumulation to deep depletion under light-tight conditions. It should be noted that the uncertainty in absolute D_{it} measurements by the hi-lo C-V technique are highest close to the band-edge. Therefore, the goal was to determine the relative differences in D_{it} among a systematic set of samples, measured under identical conditions. Processing information for all capacitors and trap densities at E_c-E ~ 0.2 eV are summarized in Table 4.1. The amounts of nitrogen incorporation at the SiO_2/SiC interface listed in this table are from nuclear reaction analysis (NRA) and electron energy loss spectroscopy (EELS) measurements performed on samples fabricated with similar processing. Details of these measurements can be found elsewhere.[20] Briefly, the two analytical techniques yielded the same values for the areal density of nitrogen, while the EELS demonstrated that the N was located in a thin

layer (≤ 1 nm) within ~1 nm of the oxide/semiconductor interface.

Table 4. 1 Processing summary for 4H-SiC MOS capacitors. D_{it} at E_c-E≈ 0.2 eV and N content at the interface for each sample are also shown.

Crystal face	Oxide thickness (nm)	Gate metal	Passivation treatment	D_{it} at E_c-E ≈ 0.2 eV (cm^{-2} eV^{-1})	Interfacial N areal density (10^{15}atoms cm^{-2})
C	57	Mo/Au	None	1.6×10^{13}	-
a	59	Al	None	5.8×10^{12}	-
Si	47	Mo/Au	None	1.6×10^{12}	-
C	40	Mo/Au	NO POA 1175°C, 2 h	9.1×10^{11}	1.0 ± 0.2
C	51	Al	NO POA 1175°C, 4 h	8.0×10^{11}	1.0 ± 0.2
a	28	Mo/Au	NO POA 1175°C, 2 h	5.4×10^{11}	~1.0 ± 0.2
Si	57	Mo/Au	Same as above	4.3×10^{11}	0.35 ±0.13
C	40	Pt	NO POA 1175°C, 2 h + H_2 PMA 500 °C, 1 h	6.8×10^{11}	1.0 ± 0.2
a	28	Pt	Same as above	4.2×10^{11}	~1.0 ± 0.2
Si	53	Pt	Same as above	3.3×10^{11}	0.35 ±0.13

Results and Discussion

Intrinsic interface state density for SiO_2/C-face 4H-SiC

Typical unpassivated trap densities for the three faces are shown in Fig. 4.1 (a). The C-face is found to have the highest D_{it} close to the conduction band-edge - an

observation consistent with earlier reports.[5,14] The higher D_{it} is reflected in the much larger dispersion between high frequency (CH) and quasistatic (CQ) capacitance curves shown in Fig 4.1 (b). The large difference in flat-band voltage for the Si-face (V_{FB}: 1.5 V) and the C-face (V_{FB}: 15.3 V) arises from the difference in the negative effective charge ($N_{eff\ Si\text{-}face} \sim 2.\ 6 \times 10^{11}\ cm^{-2}$ and $N_{eff\ C\text{-}face} \sim 5.4 \times 10^{12}\ cm^{-2}$). The effective charge is a sum of the fixed oxide charge and mobile ions (both positive), oxide trapped charge (positive or negative) and interface charge trapped at flatband (negative). The large negative effective charge suggests a much higher density of deep traps or oxide traps (near interface or border traps) that appear as a fixed charge in these measurements. The 'bump' marked 'A' in the high frequency CV curve of Fig. 4.1(b) is consistent with features attributed by Fukuda et. al.[14] to slower, deep states for the C-face.

In an earlier report, the higher trap density for the C-face was attributed to the presence of greater excess carbon at the interface resulting from a higher surface C density of this face.[5] The different surface structure and higher oxidation rate could also result in a structurally different sub-oxide (or oxy-carbide) layer. Physical analysis of the interface by several techniques such as surface enhanced Raman spectroscopy (SERS),[21] and electron energy loss spectroscopy (EELS)[20] suggest a higher interfacial carbon content on the C-face compared to the Si-face. The presence of a different carbon containing sub-oxide on the C-face has also been detected by XPS.[13] This indicates that the as-grown interfaces may be significantly different for the C-face than the Si-face due to possible inclusion of 'free' carbon and carbon containing sub-oxides. Both these possibilities, i.e. higher interfacial carbon and/or different sub-oxide could result in the higher D_{it} observed for the C-face.

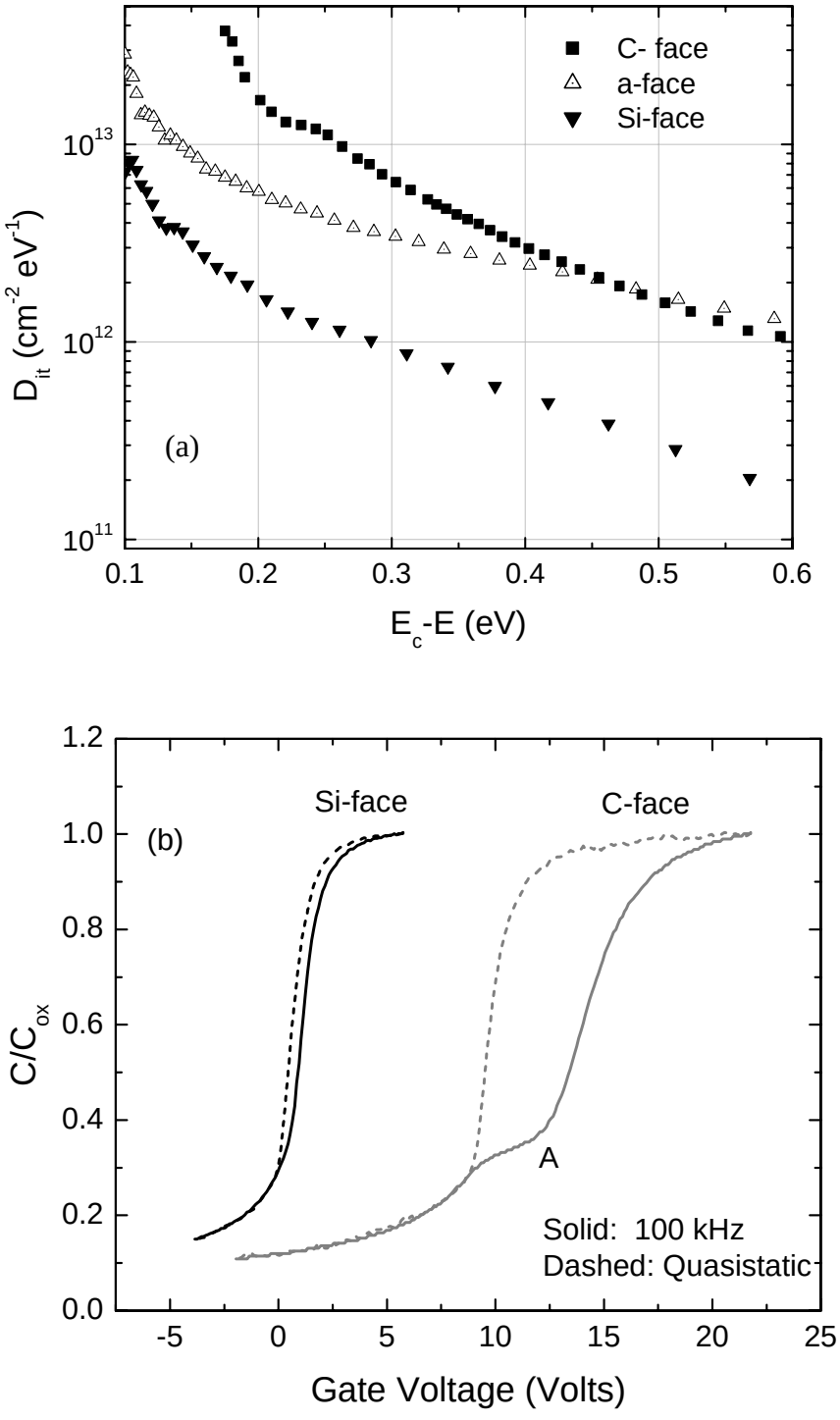

Fig. 4. 1 (a) Interface state densities for unpassivated oxides on the Si-face, a-face and C- face of 4H-SiC showing the highest trap density on the C-face (b) Comparison of hi-lo CV characteristics for the Si and C-faces. The point 'A' corresponds to the observed 'bumps' as described in the text and in ref. 14.

Effect of nitridation using NO POA

The results of NO passivation shown in Fig. 4.2 clearly show a dramatic reduction of D_{it} (~10^{13} cm^{-2} eV^{-1} to ~10^{12} cm^{-2} eV^{-1} at E_C-E ~0.2 eV) for the C-face, analogous to the other faces. The significant reduction of effective negative charge can be observed from the shift in V_{FB} before and after the NO POA [Fig. 3 (b)]. However, D_{it} after NO passivation is higher for the C-face compared to the other faces, especially for states deeper than E_C-E > 0.3 eV.

The NO POA results in interfacial nitrogen incorporation with a profile having a FWHM of < 2 nm.[20] It should be noted that the N passivated interface is also a 'new' interface created due to the extra oxide growth that takes place during NO anneal.[22,23] For the Si-face, it has been shown that the D_{it} reduction is dependent only on the amount of interfacial N, and not on the NO anneal time or temperature.[24] In a similar manner, C-face samples annealed for 2h and 4h with comparable N content [Table 4.1] essentially yield the same trap density, i.e. the D_{it} reduction does not depend on the anneal time at 1175°C but only on the interfacial N content. The 2h and 4h anneal samples have the same N content due to the saturation of N incorporation with anneal time at 1175°C. A saturation regime in the NO nitridation kinetics is observed on all faces, although for any anneal time, the N content on C-face is comparable to the a-face and a factor of ~3 greater than Si-face.[20,23] On the Si-face, D_{it} saturates at a minimum level after a critical amount of N incorporation (~2.5 x10^{14} N cm^{-2})[24] well before the N saturation (~ 1 x 10^{15} atoms cm^{-2}).

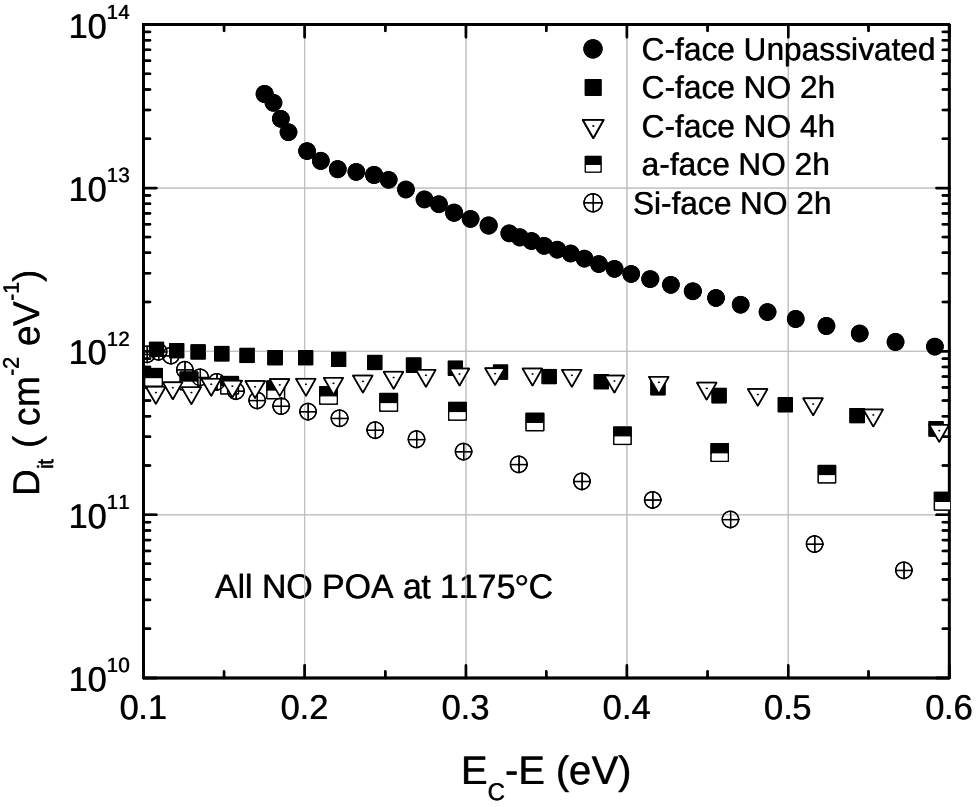

Fig. 4. 2 Interface state densities for NO passivated SiO_2/4H-SiC (Si-face, a-face and C-face) compared to the unpassivated C-face profile. Processing details for these samples can be found in Table 4.1.

Thus, it is unlikely that greater incorporation of nitrogen on the C-face (possibly by higher temperature NO anneal) would lead to any further reduction of D_{it}. The higher D_{it} (and Q_{eff}) observed in nitridated interfaces on the C-face compared to the Si-face could then arise from the following possibilities:

(i) *The presence of defects particular to the C-face not susceptible to passivation by nitrogen.* A structurally different interface on the C-face as described earlier suggests this possibility. These defects may require the use of a passivating agent other than nitrogen.

(ii) *The shifting of trap energy levels close to the conduction band to deeper levels as a result of nitrogen passivation*. In a 'cluster' defect model of the interface, the energy levels of traps are determined by the size of clusters with larger clusters close to the conduction band. Such clusters may be small collections of carbon atoms, SiO regions or other interface structures. It has been suggested that nitrogen passivation reduces the size of these clusters sequentially and lowers the trap energy in the band gap.[24] The final distribution of the defect states with energy is a result of the competition between N up-take and oxidation rate. In accordance with this model, we can assume that the significantly higher D_{it} of unpassivated C-face (compared to the unpassivated Si-face) is due to presence of more clusters on this face. Nitrogen passivation would shift traps close to the conduction band to deeper energy levels by changing cluster size. This would lead to a preferential reduction of traps near the conduction band-edge relative to traps deeper in the gap, giving rise to the difference in shape of D_{it} profile between NO passivated Si-face and C-face samples. After NO passivation, the trap density is comparable to the Si-face near E_c, but is much higher than the Si-face deeper in the gap [Fig. 4.2]. Thus qualitatively, the N passivation results on the C-face are consistent with the 'cluster' passivation model. It should be borne in mind that the arguments are valid for any interfacial cluster defects where the defect energy levels are determined by the size of the defects. Carbon clusters are a strong candidate, but not the only possibility.

(iii) *Higher 'extra' oxide growth rate during NO anneals.* Oxidation during NO POA could generate additional defects, resulting in a competition between trap passivation and generation. This competition could be a more serious problem for the C-face due to its higher oxidation rate, even though more N is incorporated. The trap densities of NO passivated a- face are intermediate to the other faces for states with energy E_c-E ≥ 0.3 eV [Fig.4.2] consistent with this possibility, since the oxidation rate of this face is intermediate compared to the other two faces.

(iv) *The presence of higher 'unused' nitrogen at the interface.* As mentioned earlier, interfacial N incorporation in $SiO_2/(000\bar{1})$ 4H-SiC is a factor of ~2 greater than the (0001) face. So there is a possibility that this leads to the presence of unwanted N at the interface resulting in a higher D_{it}. However, passivation of the SiO_2/(0001) 4H-SiC interface using ammonia results in much higher concentrations of N at the interface, but a comparable D_{it}[25], suggesting that this possibility is not a dominant factor.

All of the factors mentioned above could contribute in different degrees for the D_{it} in nitridated oxides. Thus, further reduction of D_{it} may only be possible by the use a different passivation treatment after the NO POA. In the following section, the effect of hydrogen on the $SiO_2(N)/(000\bar{1})$ 4H-SiC has been evaluated.

Passivation of nitridated interface using hydrogen

To study the effect of hydrogen, capacitors passivated with NO (1175°C, 2h) and metallized with Pt were used for post-metallization anneals (PMA) in pure H_2 at 500°C

for 1 h. The D_{it} profiles and CV characteristics are shown in Figs. 4.3(a) and 4.3(b), respectively. Comparison to 'NO only' passivation reveals an average reduction factor of ~20% for D_{it} in the energy range 0.1 eV $\leq E_c$-E $\leq$ 0.6 eV. Also shown are the D_{it} profiles on the Si-face and a-face following the same NO/H_2 anneal. The sequential anneal process gives us the lowest D_{it} in this energy range on all the three faces. Due to the smaller magnitude of the reduction, the D_{it} profiles in Fig. 4.3(a) have been obtained by averaging over ~15 capacitors. However, the D_{it} data alone does not reveal the overall effect of H. A significant reduction in effective negative charge (Δ N_{eff}) also occurs leading to a big shift in flat-band voltage ($\Delta V_{FB} \approx 3.5$ V) as shown in Fig.3 (b). (It should be noted that a $\Delta V_{FB} \approx 0.7$ V is expected due to the work function difference between Mo and Pt.) The reduction of N_{eff} could be due to the decrease of negative charge in traps at the interface and/or an increase in positive charge related to hydrogen.[26] On the Si-face, the Pt/H_2 process incorporates ~ 10^{14} atoms/cm^2 of hydrogen within ~ 3.5 nm of the interface as measured by SIMS and NRA.[27] The total H (^{2}H) content in the oxide has been measured the ^{2}H (^{3}He,p) ^{4}He nuclear reaction (Table 4.2). Comparison of ΔN_{eff} and H content in the oxide between the Si and C faces shows that, although the H concentrations for the two faces are similar, ΔN_{eff} is greater on the C-face. This suggests that the main contribution to ΔN_{eff} is the passivation of deep interface states by hydrogen for the C-face, rather than the introduction of positive oxide charge - although the latter

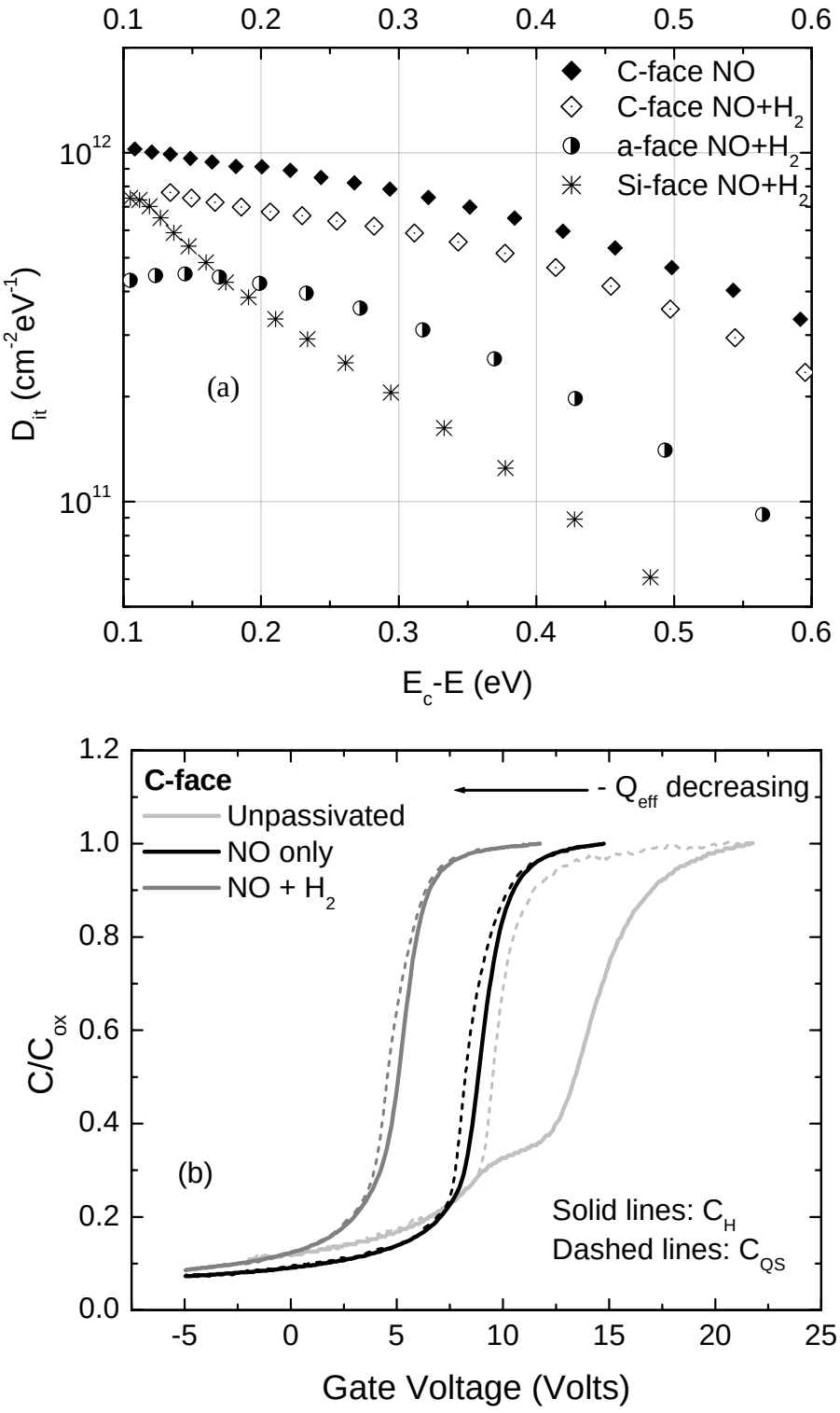

Fig. 4. 3 (a) Lowest interface state densities obtained for the three faces using sequential anneals in NO and H_2. The 'NO only' C-face sample is shown for comparison. Processing details for these samples can be found in Table I. (b) Comparison for the CV characteristics for unpassivated, 'NO only' and NO + H_2 C-face samples. The shift in flat-band voltage to les spositive voltages is due to reduction in negative effective charge.

Table 4. 2 Decrease of effective negative charge and H areal densities in the oxide (and at the interface) for (0001) Si and $(000\bar{1})$ C samples. The H areal densities were measured using NRA as described in the text.

Face	ΔN_{eff} (cm^{-2})	H areal density (atoms cm^{-2})
(0001) Si	6.3×10^{11}	$(3.66 \pm 0.1) \times 10^{14}$
$(000\bar{1})$ C	2.5×10^{12}	$(3.21 \pm 0.3) \times 10^{14}$

possibility may not be completely ruled out. Trap densities for the entire band gap need to be determined in order to have a complete picture of the H passivation process.

Summary and conclusions

The interface state density of SiO_2/4H-SiC is considerably higher near the semiconductor conduction band edge for dry thermal oxides on C-face 4H-SiC compared to the Si-face and a-face orientations. Passivation of the interface using nitrogen in conjunction with hydrogen results in substantial reduction of the interface state density, improvement analogous to the other faces. However, the lowest interface state densities on the C-face were higher than those measured for Si-face and a-face following similar passivation procedures.

Acknowledgements

The authors wish to acknowledge financial support from DARPA via Contract No. N00014-02-1-0628 (Ingham Mack and John Zolper, technical managers). We are

pleased to acknowledge useful discussions with S. Pantelides (Vanderbilt university), J. A. Copper (Purdue university) and L. M. Porter (Carnegie Mellon university).

References

[1] R. Schorner, P. Friedrichs, D. Peters, and D. Stephani, IEEE Electron Device Lett. **20,** 241 (1999).

[2] N. S. Saks, S. S. Mani, and A. K. Agarwal, Appl. Phys. Lett **76,** 2250 (2000).

[3] V. V. Afanas' ev, F. Ciobanu, S. Dimitrijev, G. Pensl, and A. Stesmans, J. Phys. Condens. Matter **16,** 1839 (2004).

[4] J. L. Cantin, H. J. Von Bardeleben, Y. Shishkin, Y. Ke, R. P. Devaty, and W. J. Choyke, Phys Rev Lett **92,** 15502 (2004).

[5] V. V. Afanas' ev, M. Bassler, G. Pensl, and M. Schulz, Phys. Status Solidi a **162,** 321 (1997).

[6] G. G. Jernigan, R. E. Stahlbush, M. K. Das, J. A. Cooper Jr, and L. A. Lipkin, Appl. Phys. Lett. **74,** 1448 (1999).

[7] R. Buczko, S. J. Pennycook, and S. T. Pantelides, Phys. Rev. Lett. **84,** 943 (2000).

[8] H. Li, S. Dimitrijev, H. B. Harrison, and D. Sweatmean, Appl. Phys. Lett. **70,** 2028 (1997).

[9] G. Y. Chung, C. C. Tin, J. R. Williams, K. McDonald, M. D. Ventra, S. T. Pantilides, L. C. Feldman, and R. A. Weller, Appl. Phys. Lett. **76,** 1713 (2000).

[10] H. Yano, T. Kimoto, and H. Matsunami, Appl. Phys. Lett. **81,** 301 (2002).

[11] H. Yano, T. Hirao, T. Kimoto, H. Matsunami, and H. Shiomi, Appl. Phys. Lett. **81,** 4772 (2002).

[12] Y. Song, S. Dhar, L. C. Feldman, G. Chung, and J. R. Williams, J. Appl. Phys., **95,** 4953 (2004).

[13] C. Virojanadara and L. I. Johansson, J. Phys. Condens. Matter **16,** 1783 (2004).

[14] K. Fukuda, W. J. Cho, K. Arai, S. Suzuki, J. Senzaki, and T. Tanaka, Appl. Phys. Lett. **77,** 866 (2000).

[15] K. Fukuda, M. Kato, K. Kojima, and J. Senzaki, Appl. Phys.Lett. **84,** 2088 (2004).

[16] J. R. Williams, T. Isaacs-Smith, S. Wang, C. Ahyi, R. M. Lawless, C. C. Tin, S. Dhar, A. Franceschetti, S. T. Pantelides, L. C. Feldman, G. Chung, and M. Chisholm, in *Fundamentals of Novel Oxide/Semiconductor Interfaces*, proceedings of the 2003 MRS Fall Meeting, Boston, MA, edited by C.R. Abernathy, E. Gusev, D. Schlom and S. Stemmer (MRS, Warrendale, PA, 2003), p. 371

[17] S. S. Wang, T. Isaacs-Smith, C. Ahyi, J.R. Williams, S. Dhar, S.T. Pantelides, L.C. Feldman and G.Y. Chung, *35th IEEE Semiconductor Interface Specialists Conference***,** December 9-11, 2004, San Diego, CA, in preparation.

[18] S. Dhar, Y. W. Song, L. C. Feldman, T. Issacs-Smith, C. C. Tin, J. R. Williams, G. Chung, N. Nishimura, D. Starodub, T. Gustafsson, and E. Garfunkel, Appl. Phys. Lett. **84,** 1498 (2004).

[19] E. H. Nicollian and J. R. Brews, *MOS (Metal Oxide Semiconductor) Physics and Technology*, (John Wiley & Sons, New York, 1982).

[20] K.-C. Chang, Y. Cao, L.M. Porter, J. Bentley, S. Dhar, L. C. Feldman and J. R. Williams, *High resolution elemental profiles of the silicon sioxide/4H-silicon carbide interface***,** submitted to J. Appl. Phys., October, 2004.

[21] W. Lu, L. C. Feldman, Y. W. Song, S. Dhar, W. E. Collins, W. C. Mitchell and J. R. Williams, Appl. Phys. Lett**., 85,** 3495 (2004).

[22] K. McDonald, L. C. Feldman, R. A. Weller, G. Y. Chung, C. C. Tin, and J. R. Williams, J. Appl. Phys. **93,** 2257 (2003).

[23] S. Dhar, L. C. Feldman K. C. Chang, Y. Cao, L. M. Porter, J. Bentley and J.R. Williams, to be published in J. of Appl. Phys. (March 2005) (also chapter V of this thesis)

[24] K. McDonald, R. A. Weller, S. T. Pantelides, L. C. Feldman, G. Y. Chung, C. C. Tin, and J. R. Williams, J. Appl. Phys. **93,** 2719 (2003).

[25] G. Chung, C. C. Tin, J. R. Williams, K. McDonald, M. D. Ventra, R. K. Chanana, S. T. Pantelides, L. C. Feldman, and R. A. Weller, Appl. Phys. Lett. **77,** 3601 (2000).

[26] G. Pensl, M. Bassler, F. Ciobanu, V. Afanas' ev, H. Yano, T. Kimoto, and H. Matsunami, in *Silicon Carbide - Materials, Processing and Devices*, proceedings of the 2000 MRS Fall Meeting, Boston, MA, edited by A.K. Agarwal, J.A. Cooper, Jr., E. Janzen, M. Skowronski, (MRS, Warrendale, PA, 2001), p.H3.2.1

[27] Chapter VI of this thesis.

CHAPTER V

NITRIDATION ANISOTROPY IN SiO_2/4H-SiC

S. Dhar [a)], L. C. Feldman [a)], K. -C. Chang,[b)] Y. Cao,[b)] L. M. Porter,[b)] J. Bentley,[c)] and J.R. Williams[d)]

a) Dept. of Physics and Astronomy & Interdisciplinary Program in Materials Science Vanderbilt University, Nashville, TN 37235, USA

b) Dept. of Materials Science and Engineering, Carnegie Mellon University, Pittsburgh, Pennsylvania 15213, USA

c) Metals and Ceramics Division, Oak Ridge National Laboratory, PO Box 2008, Oak Ridge, TN 37831-6064, USA

d) Dept. of Physics, Auburn University, Auburn, Alabama 36849, USA

Accepted for publication in Journal of Applied Physics (March 2005)

Abstract

Nitrogen incorporation at the SiO_2/SiC interface due to annealing in NO is measured and shown to be a strong function of crystal face. The annealing process involves two major solid-state chemical reactions: nitrogen up-take at the interface and N loss associated with second-order oxidation. An ad hoc kinetics model explains the experimental observations of anisotropy and nitrogen saturation.

Introduction

Thermally grown silicon dioxide (SiO_2) layers on silicon carbide are of great importance for metal-oxide-semiconductor (MOS) power electronics. A large interface trap density (D_{it}) at the SiO_2/SiC interface near the conduction band-edge of 4H-SiC has been the limiting factor for obtaining high inversion-channel mobilities in 4H-SiC MOSFETs.[1,2] These electrically active traps could be a result of excess C[3,4] at or near the interface resulting from the oxidation process, C clusters,[4-7] C dangling bonds[8] and/or non-stoichiometric interfacial suboxides.[9-11] Nitridation by post-oxidation annealing in nitric oxide (NO) is an extremely effective process for reducing trap density near the conduction band and increasing channel mobility.[12,13] Although the detailed chemical structure of the nitrided interface is not yet well understood, previous studies indicate that incorporation of nitrogen atoms at or near the interface is vital for trap passivation.[14] The role of nitrogen could be in the passivation of interfacial defects like carbon clusters or sub-oxides as suggested in various reports.[14,15] Interfacial Si-N and Si-O-N bonds have been observed by x-ray photoelectron spectroscopy (XPS).[15,16] Recent electron paramagnetic resonance (EPR) studies on porous 4H-SiC show a decrease in the EPR line related to carbon-clusters following nitridation, which indicates that the presence of C-N bonds should not be ruled out.[17] Interestingly, the incorporation of N is a strong function of the crystal face. In this paper we report measurements of this nitrogen-uptake anisotropy and describe a model to explain these observations.

Most electrical and physical characterization of nitrided oxides has been performed on the (0001) Si-terminated surface of 4H-SiC. The dramatic reduction of D_{it} by post-oxidation annealing in nitric oxide is also observed at interfaces formed on

different crystal surfaces such as the $(11\bar{2}0)$ and $(000\bar{1})$ faces.[18,19] The $(000\bar{1})$ C and (0001) Si faces are polar faces containing 100% C atoms and 100% Si atoms respectively; the $(000\bar{1})$ and (0001) planes being basal planes in the hexagonal lattice. The $(11\bar{2}0)$ a-face is a non-polar face comprised of 50% C and 50% Si atoms. In this article, for clarity and simplicity we will refer to the different crystal faces as C-face $(000\bar{1})$, a-face $(11\bar{2}0)$ and Si-face (0001). Anisotropy in the oxidation kinetics among these faces is well known.[20,21] In the temperature range for most MOS processing (1000°C-1200° C) the oxidation rates for the different surfaces are as follows: C-face > a-face > Si-face. Utilization of the 'fast-oxidizing' crystal faces for device fabrication could potentially lead to a lower thermal budget for MOS processing. Development of new device structures employing these faces may also be possible. In all cases the nitridation process will be required for adequate electronic properties.

The defect density, D_{it} (near E_c) at the SiO_2/4H-SiC interface created by dry oxidation is a function of crystal face and follows the order: $(D_{it})_C > (D_{it})_a > (D_{it})_{Si}$.[19] Post-oxidation annealing in nitric oxide results in comparable and lower trap densities for all these crystal faces. Thus, understanding the nitridation kinetics and oxide composition of SiO_2(N)/ SiC for the different crystal faces is important for developing reliable fabrication processes. In this article, we compare the kinetics of interfacial-nitrogen incorporation by NO post-oxidation anneals at 1175°C among the Si, 'a' and C crystal faces. We have observed anisotropy in nitridation; the nitridation of the C- and a-faces is approximately three times greater than that of the Si-face. A kinetics model has been developed for nitridation by NO that is based on a proposed mechanism involving competition between interfacial nitrogen accumulation and removal.

Experimental procedure

Samples used for this work were Si, C, (both 8° off axis) and a-face (on-axis) n-type 4H-SiC wafers with ~10-μm-thick epitaxial layers doped with ~1 x 10^{16} cm^{-3} nitrogen. Dry oxidation was performed at 1150°C for different durations depending on the crystal face, to grow oxide layers of ~30 nm (Si-face and a-face) and ~37 nm (C-face) thickness. The samples were then annealed in a static atmosphere (100 Torr) of ^{15}NO (98%) at 1175°C for 0.5-6 h. All oxide thickness measurements before and after the NO passivation anneals were performed using spectroscopic ellipsometry.

The total ^{15}N content (areal density) in the SiO_2/SiC structures was measured by nuclear reaction analysis (NRA) using the $^{15}N(p,\alpha)^{12}C$ reaction at E_p=1 MeV and alpha particle detection at 180°. A Si reference sample containing 2.4 x 10^{16} atoms/cm^2 of ^{15}N (measured by Rutherford backscattering spectrometry (RBS)) was used to calculate the ^{15}N areal densities. It should be noted that due to the broad resonance of the $^{15}N(p,\alpha)^{12}C$ reaction, the change in reaction cross section due to energy loss in the oxides (30-70 nm) was considered negligible.

High-resolution nitrogen profiles were obtained from SiO_2/4H-SiC interfaces by electron energy-loss spectroscopy (EELS) performed in the scanning transmission electron microscopy (STEM) mode. The total nitrogen was measured by EELS for comparison with NRA. For these analyses, Si-face and C-face samples were annealed at 1175°C for 2h in flowing ^{14}NO (350 sccm) at 1 atm. The oxide thickness was approximately 50 nm for both the C-face and Si-face samples. It should be noted that for standard MOS fabrication, flowing-gas (1 atm) ^{14}NO anneals were used instead of the static ^{15}NO anneals, used for the NRA samples.

Cross-sectional TEM specimens were prepared by standard dimpling plus ion-beam milling techniques. The EELS analyses were conducted with a Philips CM 200 (field emission gun at 200 kV) equipped with a Gatan imaging filter (GIF model 678, Gatan Inc., Pleasonton, CA) and a high-angle annular dark-field (HAADF) detector. Tens of regions in both C-face and Si-face TEM samples were analyzed. The experimental details of the EELS analyses are reported elsewhere.[22]

Results and discussion

Nitridation anisotropy

The ^{15}N content measured by NRA in SiO_2/4H-SiC after a 2h anneal at 1175°C in 100 Torr ^{15}NO for the three crystal faces is shown in Fig. 5.1. The data shown are the average of two samples per crystal face. The nitrogen content of the Si- face: $(1.62 \pm 0.1) \times 10^{14}$ cm^{-2} is a factor of ~3 less than that of the C-face: $(4.8 \pm 0.2) \times 10^{14}$ cm^{-2}. Within the limits of experimental error, the C-face has ~10% higher nitrogen content than the a-face. As mentioned before, the oxidation rates among these crystal faces follow the trend: C-face $\geq$ a-face > Si-face. Thus, the nitrogen incorporation resulting from post-oxidation anneals in NO appears to follow the same trend as the oxidation rate.

The ^{15}N (p,α) ^{12}C reaction is an effective way to measure the 'total' nitrogen incorporation in the sample but it has relatively poor depth resolution. As a result, this method cannot determine the spatial distribution of the nitrogen although it is quite sensitive to total N content. High-resolution N profiles obtained by EELS, showed the spatial location of nitrogen in the SiO_2(N)/4H-SiC structures as entirely interfacial. A typical EELS intensity profile for nitrogen obtained from a C-face sample is shown in

Fig. 5.2(a). The profile clearly shows the presence of N only in the interfacial region with no accumulation in the bulk of the oxide or in the SiC. Fig. 5.2(b) is a nitrogen intensity profile obtained from a Si-face sample. Note that the nitrogen intensity in the Si-face sample is lower than the C-face sample. Within the spatial resolution (~ 1.2 nm) of the technique, the location of N for both Si- and C-face samples was estimated to be within 1 nm of the interface. Further details of the EELS analyses can be found in Ref. [22]. The N areal density determined by EELS for the C-face ($(1.0 \pm 0.2) \times 10^{15}$ cm^{-2}) is a factor of ~3 greater than that for the Si-face ($(0.35 \pm 0.13) \times 10^{15}$ cm^{-2}). Thus, the nitridation anisotropy in SiO_2/SiC is confirmed by observations from two independent techniques i.e. NRA and EELS.

Nitrogen areal densities obtained by NRA and EELS are compared in Table 5.1. The apparent difference of a factor ~2 in N_N between the EELS and NRA samples is due to the difference in annealing pressure, i.e. 100 Torr static ^{15}NO anneal for NRA samples as compared to flowing ^{14}NO (1 atm) anneal for EELS samples. This difference in N content between the samples annealed in 100 Torr and flowing gas (1 atm) illustrates the weak dependence of nitridation rate on NO partial pressure, as reported in an earlier work on the Si-face.[23] In that work, a difference factor of 2.2 ± 0.2 was found from calibration by secondary ion mass spectrometry (SIMS) and NRA between the flowing gas (1 atm) and 100 Torr samples. Also shown in Table 5.1 are values obtained by taking this normalization factor into consideration, illustrating that the NRA and EELS results agree closely within the limits of experimental error.

Nitrogen incorporation, as a function of ^{15}NO annealing time at 1175°C and 100 Torr is shown in Fig. 5.3. Although the N elemental profiles were obtained only for Si- and C-

face samples annealed for 2h, previous data on similar Si-face samples show that N incorporation is entirely interfacial for the entire time range (0.5 h- 6h).[23] All three faces initially show a rapid accumulation of N at the interface before reaching an approximately constant level. Such a 'steady-state' condition can be achieved only due to saturation of the number of available reaction sites and/or the influence of competing processes that remove N from the interface.

At high temperature, NO decomposes by the reaction 2 NO→ N_2 + O_2.[24,25] Nitrogen removal, observed previously on the Si-face, was associated with oxidation related to the O_2 partial pressure.[23] The 'extra-oxide' growth during the NO anneals caused by O_2 is shown in Fig. 5.4 for all three faces. The oxidation kinetics are linear on all three faces and also exhibit the expected growth-rate anisotropy. Attributing oxidation as the source of N loss suggests a higher nitrogen removal rate for a crystal face that oxidizes faster. To confirm this, nitrided samples (1175°C, 2h, 100 Torr ^{15}NO) were subjected to a further oxidation ('re-oxidation') at 1000°C and 1100°C for 15 min in flowing O_2. The nitrogen lost due to the 're-oxidation' is shown in Fig. 5.5. The 'nitrogen retainment ratio' in Fig. 5.5 is the fraction of initial nitrogen content retained in the sample after 're-oxidation'. It can be clearly seen that the nitrogen removal rate on the different faces indeed scales with the oxidation rates.

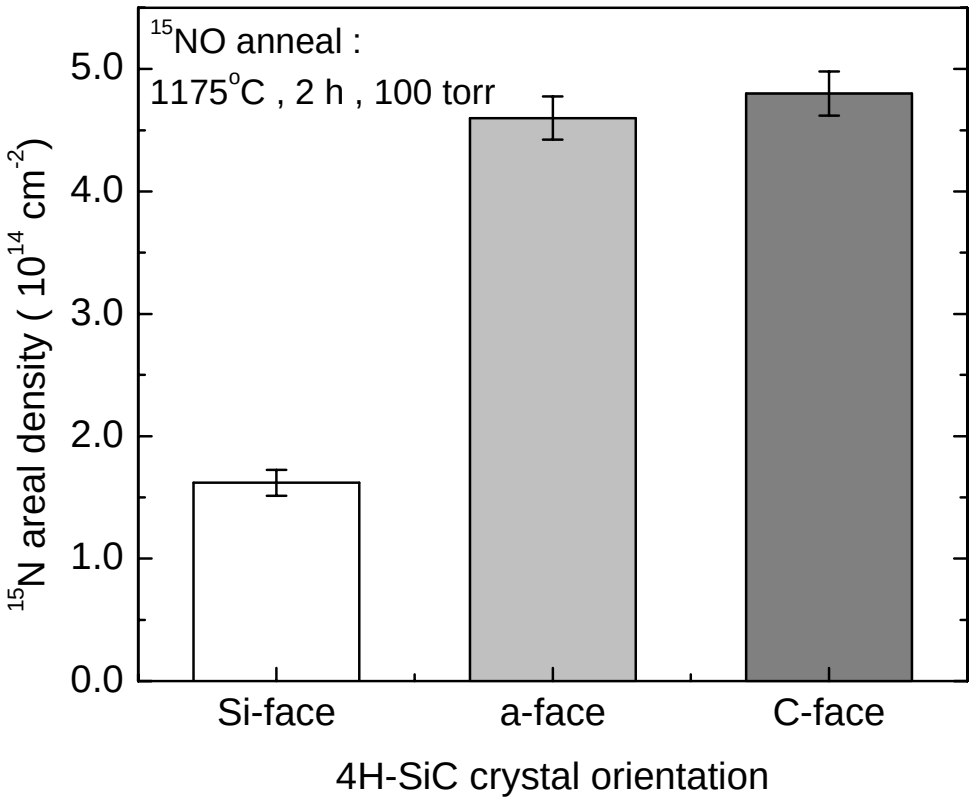

FIG. 5. 1 ^{15}N content in SiO_2/4H-SiC after annealing at 1175 °C in 100 torr ^{15}NO for Si-, a- and C –faces illustrating the nitridation anisotropy. The data are the average nitrogen contents from two samples per crystal face and error bars represent the error in counting statistics only.

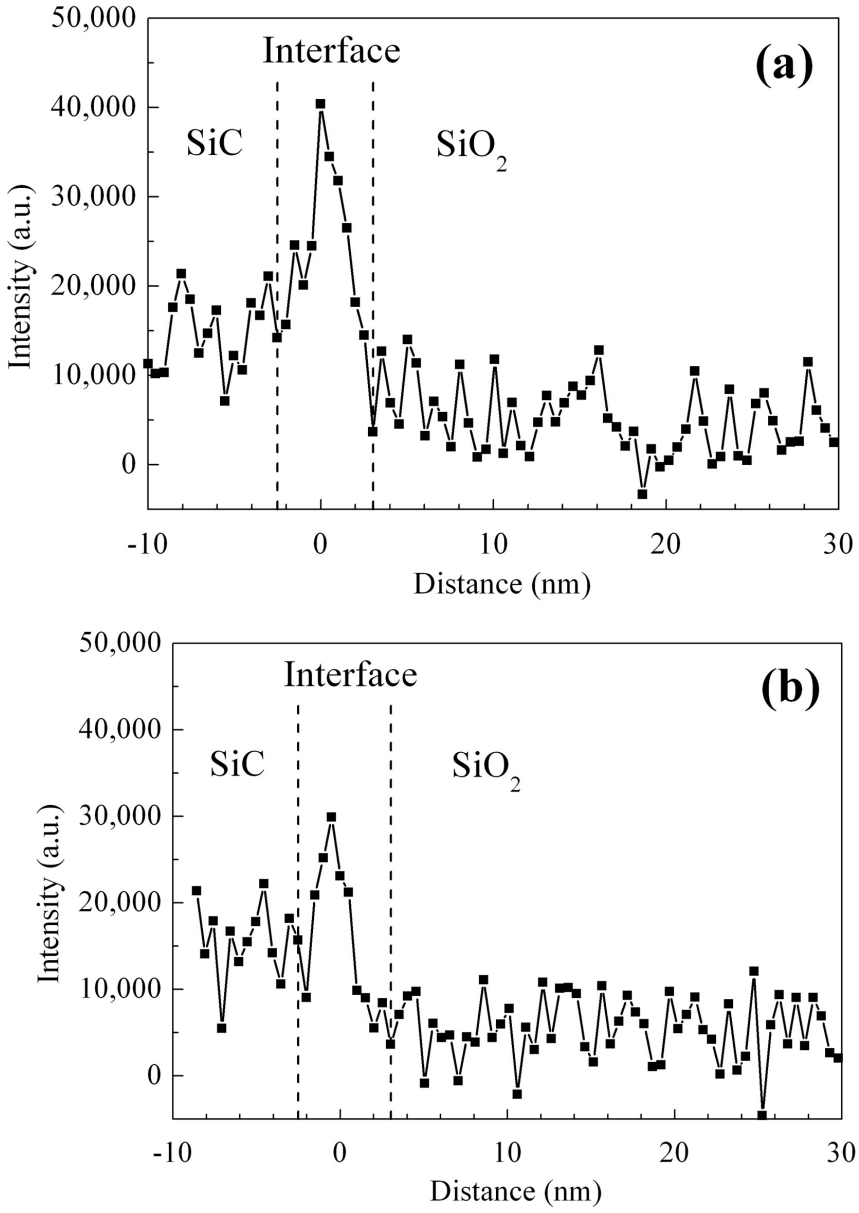

FIG. 5. 2 (a) Nitrogen intensity profile obtained by EELS, near the interface of a NO-annealed C-face sample showing that N is detected only at the interface. Note that the positive values of N intensity for positions outside the interface region are artifacts resulting from inadequate background fitting of the raw EELS spectra. Careful inspection of individual spectra revealed that N is detectable only within the interface region. (Ref. 22) (b) The nitrogen intensity profile obtained near the interface of a NO-annealed Si-face sample.

Table 5. 1 Comparison of nitrogen areal density measurements from EELS and NRA (for anneals at 1175°C for 2 h)

SiC surface	N RA (static gas, 100 Torr ^{15}NO) (atoms cm^{-2})	NRA-SIMS Calibration (flowing gas, 1 atm ^{14}NO) (atoms cm^{-2})	EELS (flowing gas, 1 atm ^{14}NO) (atoms cm^{-2})
C-face	$(0.48 \pm 0.02) \times 10^{15}$	$(1.06 \pm 0.04) \times 10^{15}$	$(1.0 \pm 0.2) \times 10^{15}$
Si-face	$(0.16 \pm 0.01) \times 10^{15}$	$(0.35 \pm 0.02) \times 10^{15}$	$(0.35 \pm 0.13) \times 10^{15}$

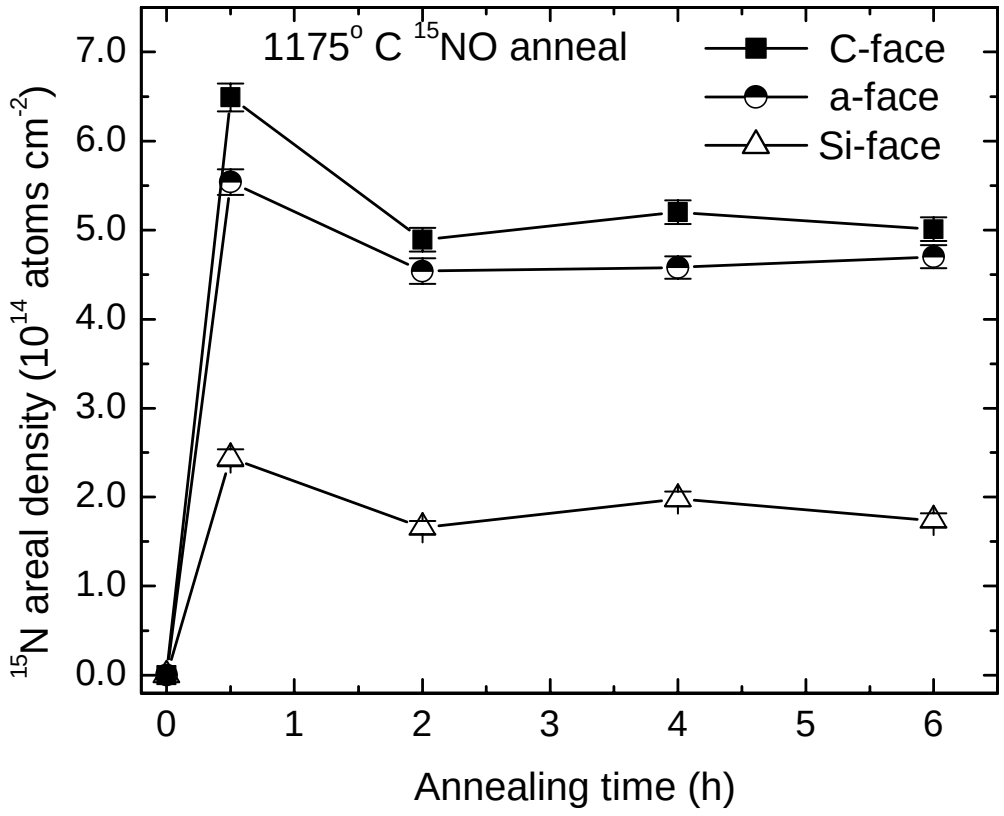

FIG. 5. 3 Nitridation kinetics for SiO_2/4H-SiC interfaces formed on the C-, a- and Si-faces of 4H-SiC. All samples were annealed at 1175°C, in 100 Torr ^{15}NO. The error bars represent the statistical error in the NRA measurements. The solid lines are for guidance of the eye only.

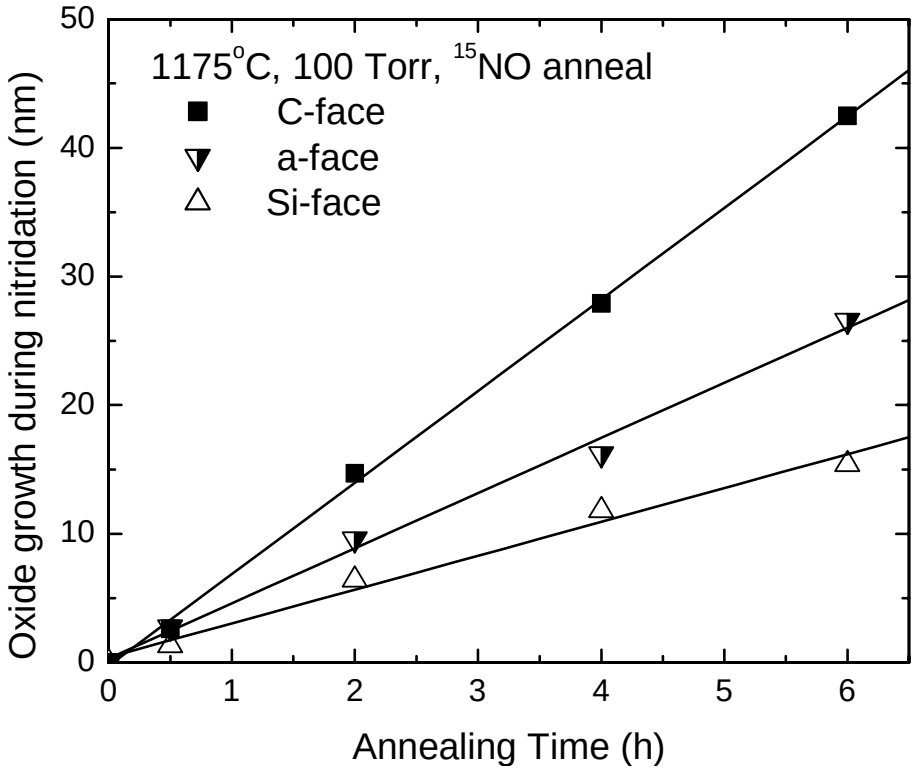

FIG. 5. 4 'Extra' oxide growth during 1175°C, 100 Torr ^{15}NO post-oxidation anneals of SiO_2 layers on Si-, a- and C-face 4H-SiC. The data are shown for the same samples as in Fig. 5.3.

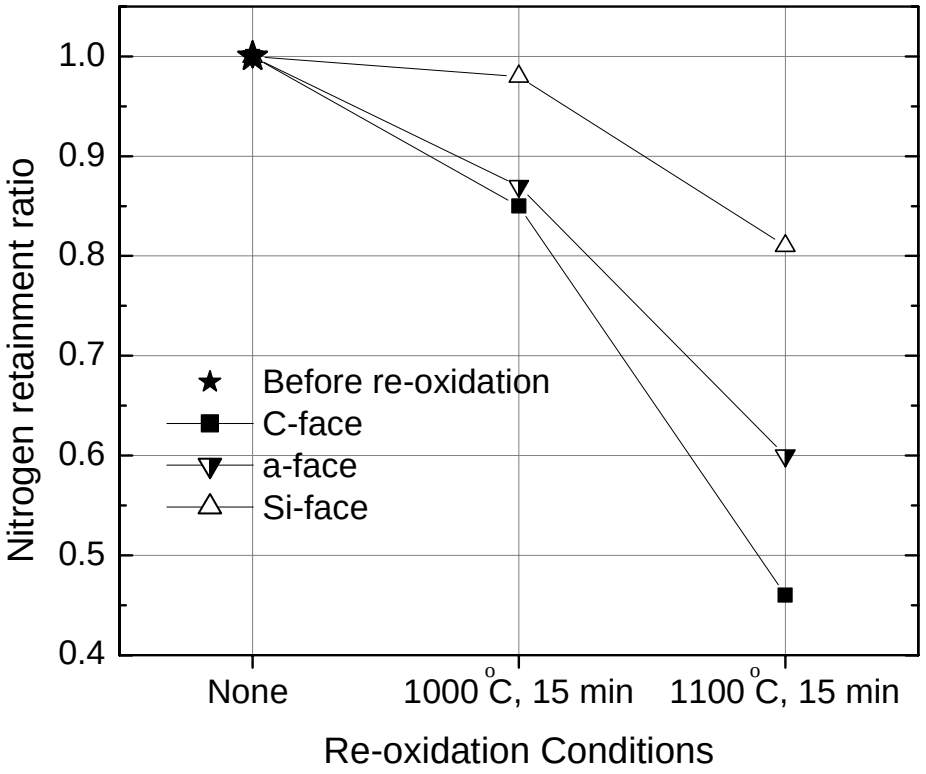

FIG. 5. 5 Effect of re-oxidation on interfacial nitrogen for the C-, a- and Si-faces of 4H-SiC. Nitrogen removal due to oxidation scales with the oxidation rate for each crystal face. The 'nitrogen retainment ratio' is the fraction of initial nitrogen content retained in the sample after 're-oxidation'.

NO nitridation kinetics model

Nitridation of the SiO_2/SiC interface via post-oxidation annealing in NO is governed by two overall interfacial reactions:

(i) Nitrogen enrichment by NO gas.

(ii) Nitrogen removal associated with the O_2 formed by the decomposition of NO gas at high temperatures.

Thus, a simple nitridation kinetics model can be constructed using the following rate equation:

$$\frac{dA_N(t)}{dt} = k_+ C_{NO}(t) - k_- C_{O_2}(t) A_N(t) \qquad (5.1)$$

where $A_N(t)$ is the nitrogen content at the interface as a function of time [atoms cm^{-2}]; $C_{NO}(t)$ and $C_{O_2}(t)$ are the concentration of NO and O_2 at the gas/solid interface, respectively.[atoms cm^{-3}]; and k_+ and k_- are the interfacial N incorporation and removal rates respectively ([k_+]: cm s^{-1} , [k_-]: cm^3 s^{-1}) .

Case I : Flowing gas anneals

The equilibrium gas composition on the sample surface has been determined by Mc Donald et. al. at various annealing temperatures for 1 atm and 100 Torr.[23,26] For flowing gas (1 atm) anneals, the concentrations of NO and O_2 remain almost constant in the relatively short time that these gases are in the furnace tube. The differential equation 5.1 then reduces to:

$$\frac{dA_N(t)}{dt} = K_+ - K_- A_N(t) \qquad (5.2)$$

where $K_+ = k_+ C_{NO}^0$ and $K_- = k_- C_O^0$ are the nitrogen incorporation and removal rate constants at 1 atm and include the constant partial pressures of the gases. C_{NO}^0 and C_O^0 are the constant NO and O gas concentrations. ([K_+]: cm^{-2} s^{-1} , [K_-]: s^{-1})

Eq. 5.2 is a linear first order differential equation with the following solution:

$$A_N(t) = \frac{K_+}{K_-}(1 - e^{-K_- t}) \tag{5.3}$$

Following the procedure described in the appendix the parameters K_+ and K_- has been determined as:

$K_{-Si-face} = 0.96\,h^{-1}$;

$K_{-C-face} = 2.14\,h^{-1}$ (5.4)

and

$K_{+Si-face} = 1.02 \times 10^{15}$ atoms cm^{-2} h^{-1} ;

$K_{+C-face} = 2.71 \times 10^{15}$ atoms cm^{-2} h^{-1} (5.5)

Nitridation equation for 1175 ℃, flowing NO (1 atm) as a function of crystal face:

Using Eqs. 5.4 and 5.5 in Eq. 5.3, we obtain expressions for the interfacial N content (atoms cm^{-2}) as a function of time t (h) for the different crystal faces as:

$A_N(t)_{Si-face} = 1.06 \times 10^{15}.(1 - e^{-0.96t})$

$A_N(t)_{C-face} = 1.27 \times 10^{15}.(1 - e^{-2.14t})$ (5.6)

From Eq. 5.6 we can see that the model predicts a higher N saturation value, i.e K_+/K_- for the C-face than the Si-face as evident from the above expressions. The expressions

are plotted in Fig. 5.6 and the experimental values are included for comparison. The model correctly predicts a higher N content for the C-face than for the Si-face for 2h-annealed samples (EELS data). For the C-face, agreement between the model and the experimental values is satisfactory (± 20 %) within the limits of experimental and calculation errors. However, for the Si-face, the value predicted by the model is a factor of ~3 greater than the experimental value, suggesting that the simplistic model does not describe the nitridation kinetics of the Si-face quantitatively. The disagreement could be the saturation of available N bonding sites on the Si-face before the oxidation-limited saturation regime is reached. This argument suggests the presence of different interfacial N reaction layers arising from the presence of different sub-oxides (possibly carbon containing) on the two faces.

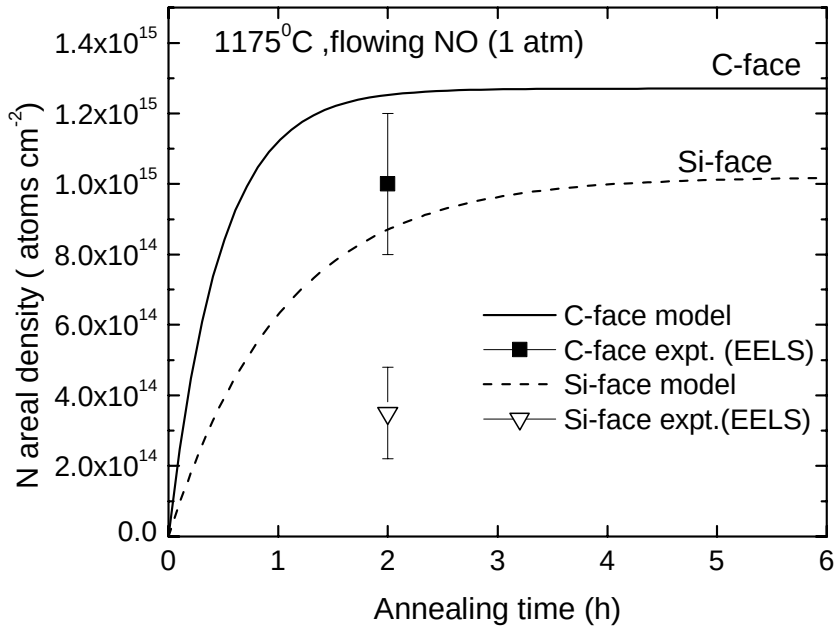

FIG. 5. 6 Nitridation kinetics for the C-face (solid line) and Si-face (dotted line) for flowing-gas (1 atm) NO-anneals at 1175°C simulated with the proposed model (Eq. 5.6) proposed in the text. Experimental data obtained by EELS are shown for comparison.

Case II: Static anneal at 100 Torr

For 1175°C anneals at a static pressure of 100 Torr, the NO decomposition occurs relatively quickly in the time frame of the passivation anneal. From the equilibrium gas composition analysis in Ref. 23, the concentrations of NO and O_2 in the system as a function of time can be empirically written as:

$$C_{NO}(t) = C^{*}_{NO}\, e^{-\alpha t} + C^{'}_{NO} \tag{5.7}$$

$$C_{O_2}(t) = C^{*}_{O_2}\, (1 - e^{-\beta t}) \tag{5.8}$$

where α , β, C^{*}_{NO}, $C^{*}_{O_2}$ and $C^{'}_{NO}$ are constants that depend on annealing temperature and pressure.

Equations 5.7 and 5.8 can be used in eq. 5.1 to obtain a nitridation rate equation:

$$\frac{dA_N}{dt} = D + E\, e^{-\alpha t} - B\, (1 - e^{-\beta t}).A_N \tag{5.9}$$

where D, E, B, α and β are all positive constants.

Values of α and β at 1175°C have been estimated from Ref. 23 to be 2.17 h^{-1}. The value of B has been estimated by a similar analysis to that for the flowing-gas case. Values of all parameters used are listed in Table II. With the use of E and D as 'fitting' parameters, Eq. 5.9 can be numerically solved and qualitatively fit to the experimental data as shown in Fig. 5.7. The model predicts the shape of the experimental nitridation curve fairly accurately. Unlike the flowing gas case, the model predicts a decrease in N content after a maximum N incorporation is attained. This is due to the changes in gas composition in the system, i.e., increase and decrease of the partial pressures of O_2 and NO, respectively.

Table 5. 2 Model parameters used in Eq. 5.9 (Fig. 5.7) α, β and B are calculated values, and E and D are fitting parameters.

Face	α (h^{-1})	β (h^{-1})	E (cm^{-2} h^{-1})	B (h^{-1})	D (cm^{-2} h^{-1})
C	2.17	2.17	2.0×10^{15}	0.54	2.1×10^{14}
Si	2.17	2.17	0.48×10^{15}	0.24	0.5×10^{14}

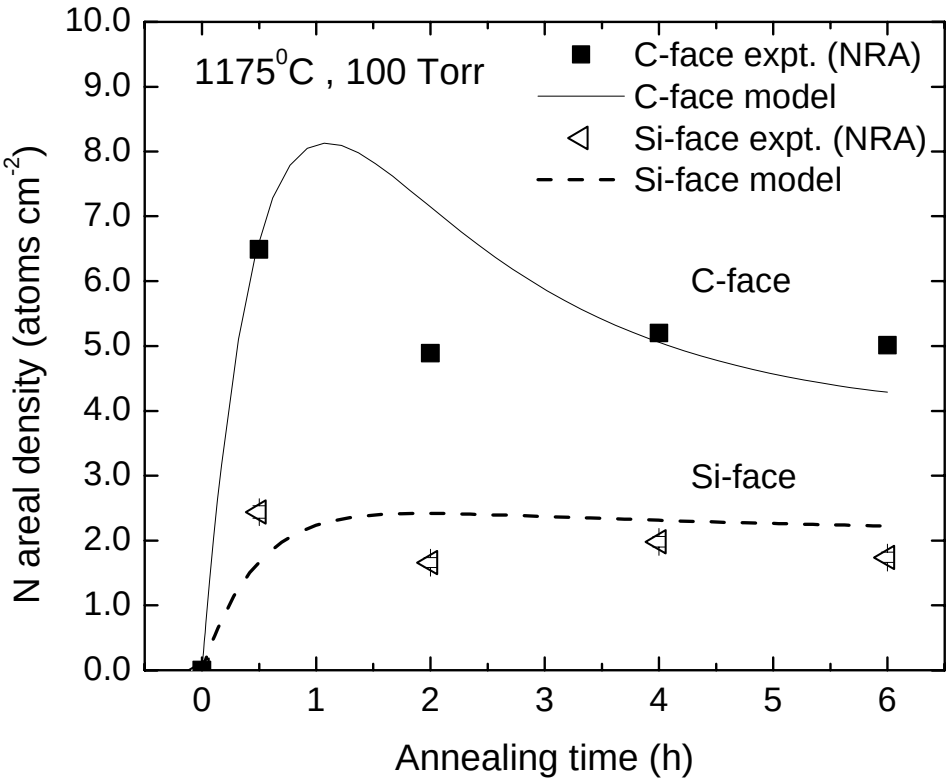

FIG. 5. 7 Nitridation kinetics for the C-face (solid line) and Si-face (dotted line) for 100 Torr static NO anneals at 1175°C qualitatively fitted to experimental data by using the proposed model (Eq. 5.9). The required model parameters are listed in Table 5.2.

It should be noted that the model does not consider the diffusion of gaseous components through the oxide to the interface. The mechanism is bound to play a role since the oxide thickness keeps increasing with time. Thus, experimentally, the N content for samples annealed in a flowing ambient will not saturate for long times but will decrease once the diffusion starts playing a dominant role.

Summary and conclusions

Anisotropy in nitridation rates have been observed for the first time at SiO_2/4H-SiC interfaces. Nitridation kinetics among the $(000\bar{1})$ C-face, $(11\bar{2}0)$ a-face and (0001) Si-face follow the same trend as in their oxidation rates: C-face ≥ a-face > Si-face. Interfacial N incorporation by post-oxidation annealing in NO occurs by the interplay of two processes – N enrichment by NO and a competing O_2 related N removal process. An ad hoc model based on these two mechanisms has been proposed to explain the experimental nitridation kinetics.

Acknowledgements

The authors wish to acknowledge financial support from DARPA via Contract No. N00014-02-1-0628 (Ingham Mack and John Zolper, technical managers). Research at the ORNL SHaRE User Center was supported by the Division of Materials Sciences and Engineering, Office of Basic Energy Sciences, U.S. Department of Energy, under contract DE-AC05-00OR22725 with UT-Battelle, LLC.

References

[1] R. Schorner, P. Friedrichs, D. Peters, and D. Stephani, IEEE Electron Device Lett. **20,** 241 (1999).

[2] N. S. Saks, S. S. Mani, and A. K. Agarwal, Appl. Phys. Lett **76,** 2250 (2000).

[3] K.-C. Chang, N. T. Nuhfer, L. M. Porter, and Q. Wahab, Appl. Phys. Lett. **77,** 2186 (2000).

[4] K.-C. Chang, J. Bentley, and L. M. Porter, J. Elec. Mater. **32,** 464 (2003).

[5] V. V. Afanasev, M. Bassler, G. Pensl, and M. Schulz, Phys. Status Solidi a **162,** 321 (1997).

[6] M. Bassler, G. Pensl, and V. Afanas' ev, Diamond Relat. Mat**6,** 1472 (1997).

[7] W. Lu, L. C. Feldman, Y. Song, S. Dhar, W. E. Collins, W. C. Mitchel, and J. R. Williams, Appl. Phys. Lett. **85,** 3495 (2004).

[8] J. L. Cantin, H. J. V. Bardeleben, Y. Shishkin, Y. Ke, R. P. Devaty, and W. J. Choyke, Phys. Rev. Lett. **92,** 15502 (2004).

[9] G. G. Jernigan, R. E. Stahlbush, M. K. Das, J. A. Cooper Jr, and L. A. Lipkin, Appl. Phys. Lett. **74,** 1448 (1999).

[10] R. Buczko, S. J. Pennycook, and S. T. Pantelides, Phys. Rev. Lett. **84,** 943 (2000).

[11] C. Virojanadara and L. I. Johansson, J. Phys. Condens. Matter **16,** 1783 (2004).

[12] H.-F. Li, S. Dimitrijev, H. B. Harrison, and D. Sweatman, Appl. Phys. Lett. **70,** 2028 (1997).

[13] G. Y. Chung, C. C. Tin, J. R. Williams, K. McDonald, M. D. Ventra, S. T. Pantilides, L. C. Feldman, and R. A. Weller, Appl. Phys. Lett. **76,** 1713 (2000).

[14] K. McDonald, R. A. Weller, S. T. Pantelides, L. C. Feldman, G. Y. Chung, C. C. Tin, and J. R. Williams, J. Appl. Phys. **93,** 2719 (2003).

[15] P.Jamet, S. Dimitrijev, and P. Tanner, J. Appl. Phys. **90,** 5058 (2001).

[16] C. Virojanadara and L. I. Johansson, J. Phys. Condens. Matter **16,** 3435 (2004).

[17] H. J. v. Bardeleben, J. L. Cantin, I. C. Vickridge, Y. W. Song, S. Dhar, L. C. Feldman, J. R. Williams, L. Ke, Y. Shishkin, R. P. Devaty, and W. J. Choyke, *Proceedings of the European Conference of Silicon Carbide and Related Materials, Bologna, Italy, 2004.*

[18] S. Dhar, Y. W. Song, L. C. Feldman, T. Issacs-Smith, C. C. Tin, J. R. Williams, G. Chung, N. Nishimura, D. Starodub, T. Gustafsson, and E. Garfunkel, Appl. Phys. Lett. **84,** 1498 (2004).

[19] S. Dhar, L. C. Feldman, T. Isaacs-Smith, S. Wang, and J. R. Williams, submitted to J. Appl. Phys., November, 2004.

[20] I. C. Vickridge, I. Trimaille, J.-J. Ganem, S. Rigo, C. Radtke, I. J. R. Baumvol, and F. C. Stedile, Phys. Rev. Lett. **89,** 256102-1 (2002).

[21] Y. Song, S. Dhar, L. C. Feldman, G. Chung, and J. R. Williams, J. Appl. Phys. **95,** 4953 (2004).

[22] K.-C. Chang, Y. Cao, L. M. Porter, J. Bentley, S. Dhar, L. C. Feldman, and J. R. Williams, submitted to J. Appl. Phys., October 2004.

[23] K. McDonald, L. C. Feldman, R. A. Weller, G. Y. Chung, C. C. Tin, and J. R. Williams, J. Appl. Phys. **93,** 2257 (2003).

[24] N. M. Laurendeau, Combust. Sci. Technol. **11,** 89 (1975).

[25] R. J. Wu and C. T. Yeh, Int. J. Chem. Kinet. **28,** 89 (1996).

[26] K. McDonald, Ph.D. dissertation, Vanderbilt University (2001).

Appendix

Estimation of model parameters K_- and K_+ for flowing gas (1 atm) case

Loss parameter K_-:

Assuming the oxidation-induced nitrogen loss to be a first order kinetic process, N loss by re-oxidation in flowing O_2 in Fig. 5.5 (a) can be described by:

$$\frac{dA_N(t)}{dt} = -K_-(T)A_N(t) \tag{5A.1}$$

where $K_-(T)$ represents the value of K_- at any temperature T. The above differential equation has the well-known solution:

$$\frac{A_N(t)}{A_N^0} = e^{-K_- t}$$

where A_N^0 is the initial amount of nitrogen present before the re-oxidation anneal Therefore at any temperature, (dropping the symbol T)

$$K_{\_} = -\frac{1}{t}.\ln\frac{A_N(t)}{A_N^0} \tag{5A.2}$$

From the data in Fig. 5.5 with t = 15 min (900 s) and the 'nitrogen retainment ratio' $\frac{A_N(15\,\text{min})}{A_N^0}$ we can obtain the value of $K_{\_}$ at temperatures of 1000°C and 1100°C in units of time^{-1}. Assuming $K_{\_}$ follows an Arrhenius relationship with temperature, $\ln K_{\_}$ is plotted as a function of $1/T$ for the Si- and C-faces as shown in Fig. 5A.1. The Arrhenius plots can be extrapolated to determine the value of $K_{\_}$ at 1175°C for a pure (100%) O_2

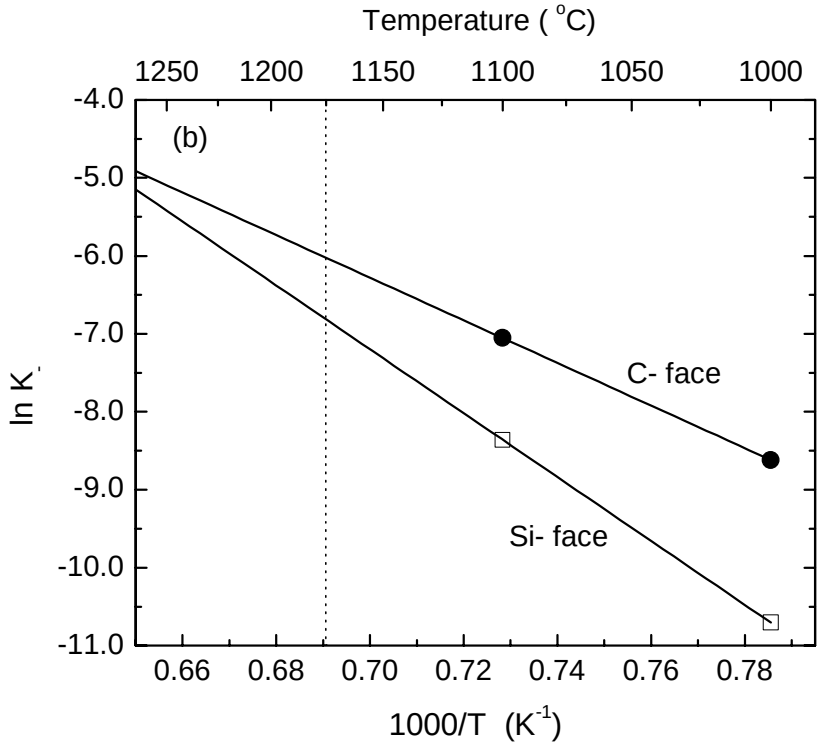

FIG. 5A.1 Arrhenius plot for the oxidation-induced N-loss parameter $K_{\_}$ as described in appendix.

environment. During the flowing NO anneals at 1175°C, the partial pressure of O_2 at any instant is approximately ~25 %.[23] Taking this factor into consideration, we obtain:

$K_{-Si-face} = 0.96\,\mathrm{h}^{-1}$ and

$$K_{-C-face} = 2.14\,\mathrm{h}^{-1} \qquad \text{(5A.3)}$$

Estimation of parameter K_+***:***

Using the slope through zero for increasing part of the ^{15}N (1175°C, 100 Torr) uptake curve (Fig. 5.3) we can estimate the value of K_+**.** Considering a factor of 2.2 (obtained by calibration between the NRA and EELS samples as described in the earlier section) for normalization between 100 Torr static anneals and the flowing gas anneals:

$K_{+Si-face} = 1.02 \times 10^{15}$ atoms cm^{-2} h^{-1} and

$$K_{+C-face} = 2.71 \times 10^{15} \text{ atoms cm}^{-2} \text{ h}^{-1} \qquad \text{(5A.4)}$$

CHAPTER VI

HYDROGEN INCORPORATION AT THE SiO_2/SiC INTERFACE

S. Dhar, [a)] L. C. Feldman, [a)] S.Wang,[b)] T. Isaacs-Smith,[b)] and J. R. Williams[b)]

a) Dept. of Physics and Astronomy & Interdisciplinary Program in Materials Science
Vanderbilt University, Nashville, TN 37235, USA
b) Dept. of Physics, Auburn University, Auburn, Alabama 36849

Abstract

Post metallization annealing of 4H-SiC MOS devices in hydrogen results in the reduction of trap density at the SiO_2/4H-SiC interface. Hydrogen incorporation in 4H-SiC metal – oxide- semiconductor (MOS) structures has been studied by Nuclear reaction analysis (NRA) and Secondary ion mass spectrometry (SIMS) techniques. We find that the presence of a catalytic metal layer like Pt during post-metallization results in a higher interfacial hydrogenation rate. Correlating the physical and electrical measurements suggests that reduction of trap density depends on hydrogen incorporation at the interface. The amount of near-interfacial hydrogen is at least two orders of magnitude higher than the reduction of traps, suggesting the limited availability of hydrogen susceptible defects at the interface. Kinetic studies of hydrogen uptake and desorption indicate the presence of thermally stable H-bonds at the SiO_2/SiC interface.

Introduction

High defect densities at the SiO_2/4H- SiC interface located energetically near the conduction band-edge of 4H-SiC cause degradation of inversion channel mobility in 4H-

SiC metal-oxide-field-effect transistors (MOSFETs).[1,2] The physical nature of these defects have been attributed to a variety of sources such as carbon clusters, sub-oxides and/or Si/C dangling bonds; either intrinsic to the SiO_2/SiC system or a result of thermal oxidation.[3-6] Passivation of these defects by utilizing efficient processing is critical for achieving higher inversion layer mobilities and reliable device operation. Significant reduction of interface trap density (D_{it}) – from > 10^{13} cm^{-2} eV^{-1} to ~10^{12} cm^{-2} eV^{-1} near the conduction band-edge can be achieved using post-oxidation annealing in NO.[7,8] However, device optimization requires still further reduction.

Additional post-metallization annealing of NO passivated samples in hydrogen using Pt as the gate metal, result in a further reduction of trap densities.[9] The trap density for samples annealed sequentially in NO and H_2 is typically about 20% lower near the conduction band edge compared to samples annealed only in NO. Trap passivation is also observed deeper in the band gap ($E - E_v$ = 1.6 to 2.6eV).[10] Although the hydrogen passivation effect is smaller than the NO effect, the overall improvement in channel mobility is significant.

Maximum field effect mobilities for MOSFETs fabricated on the (0001) Si-face and $(11\bar{2}0)$ a-face by sequential anneals in NO and H_2 are higher by 25-30% (Si-face) and 40-50% (a-face) compared to mobilities for 'NO only' devices.[10] These results motivate further studies of hydrogen passivation in SiO_2 /SiC from a standpoint of SiC MOSFET development. In this article, we focus on the hydrogenation of nitridated SiO_2 layers (NO passivated) grown on the (0001) Si-face of 4H-SiC. We report measurements of hydrogen incorporation at the SiO_2/4H-SiC interface using post-metallization annealing in hydrogen and correlate these measurements to interface trap passivation. We

find that the presence of a catalytic gate metal like Pt results in at least two orders of magnitude higher hydrogen incorporation at the SiO_2/4H-SiC interface. The interfacial hydrogen concentration is significantly higher than the trap density reduction possibly due to the limited availability of hydrogen susceptible defects at the interface. A kinetic study of the hydrogen uptake and thermal desorption also suggests the presence of thermally stable hydrogen in the oxide and at the interface.

Experimental procedure

Samples used for this work were 5 mm x 5mm pieces cut from n-type (0001) Si-face 4H-SiC wafers with ~10 um epitaxial layers having a nitrogen dopant concentration of ~10^{16} cm^{-3}. Dry oxidation was performed at 1150° C for 4 h followed by a post-oxidation anneal in NO at 1175°C for 2 h (unless otherwise mentioned) to yield oxides of thickness ~45–50 nm. MOS capacitors were formed by sputter deposition of Pt or Mo as the gate metal. The samples were then annealed in pure hydrogen at temperatures from 500° C - 700° C for 1 h. Simultaneous hi-lo capacitance-voltage (CV) technique[11,12] at room temperature was used to make interface state density measurements.

Physical characterization was performed using nuclear reaction analysis (NRA) and secondary ion mass spectrometry (SIMS). The samples were prepared in a similar manner as the MOS capacitors, the only difference being the use of deuterium (D) as the annealing ambient instead of hydrogen. Non-metallized control samples also underwent the D anneals. Use of D is advantageous as it is relatively easier to detect than H by most materials analysis tools. No major difference in chemical activity is expected between hydrogen and deuterium to first order.

Nuclear reaction analysis (NRA) was performed using the ^{2}H (^{3}He,p) ^{4}He reaction at E_{3He} = 700 keV to measure the total deuterium content. Emitted protons were detected using an annular solid-state detector at ~180°. A ~10 μm Al foil was placed in front of the detector to stop the backscattered ^{3}He. A reference Si sample implanted with 5 x 10^{15} D atoms cm^{-2} was used for the quantitative analysis. The poor depth resolution does not enable us to determine the D concentration profile, but allows us to determine the total D content accurately.

Secondary ion mass spectrometry (SIMS) was used for D depth profiling for comparison with NRA experiments. A 2.0 keV Cs+ primary ion beam at 60° incidence was used for the analysis in negative ion mode for detection of D. Elemental profiles of Si, C, O, N and ^{1}H were also obtained.

Results and discussion

Effect of hydrogen on the trap density near conduction band-edge

Interface trap density is shown in Fig. 6.1 for dry oxides with post-metallization anneal in H_2 (without NO treatment) at 500°C for 1h using Pt as the gate metal. Comparison with unpassivated dry oxides reveals a factor of ~ 2 reduction in D_{it} at E_C-E~ 0.1 eV. This effect is relatively small compared to NO passivation wherein the trap density reduction is almost an order of magnitude near the conduction band-edge. Typical trap densities in samples passivated by NO using post-oxidation anneal 1175°C

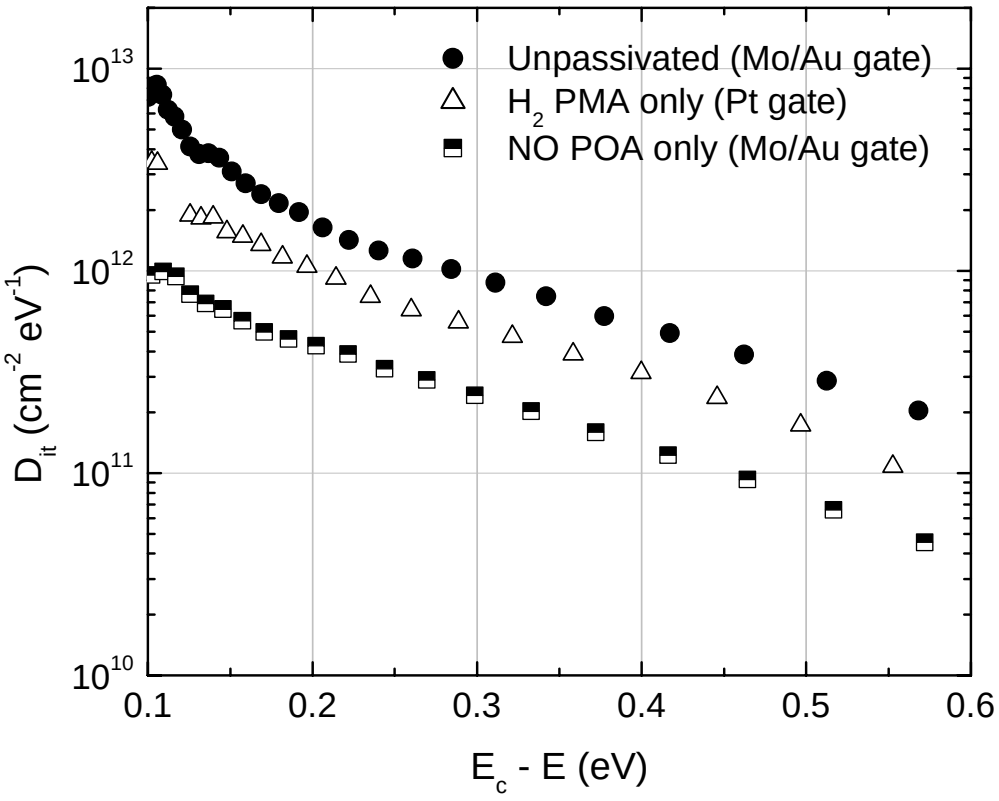

FIG. 6. 1 Interface state densities near the conduction band-edge of 4H-SiC for unpassivated , H annealed and NO annealed MOS capacitors illustrate the effectiveness of NO compared to H for reducing D_{it}. NO post-oxidation anneals were carried out at 1175°C for 2 h in flowing NO. The H_2 anneals were carried out at 500°C for 1 h after metallization with Pt. The oxide thickness ranged from 40-45 nm.

for 2 h is also shown in Fig.6.1. The magnitude of hydrogenation induced improvement of the SiO_2/4H-SiC observed in our experiments is comparable to previous reports employing post-oxidation anneals in hydrogen and/or oxidation in the presence of hydrogen (i.e., wet or pyrogenic).[13-15] It is however important to note that the hydrogenation process in the present work differs in two aspects –presence of a Pt layer (as gate metal) during annealing and relatively lower temperatures anneal (500 °C).

Hydrogen is well-known for the passivation of dangling bonds (P_b-center) at the SiO_2/Si interface.[16] Post-metallization annealing in a hydrogen containing ambient like forming gas at 400°C - 500°C is most commonly employed in Si MOS technology for the reduction of interface states (from ~10^{12} cm^{-2} eV^{-1} to ≤ 10^{11} $cm^{-2}eV^{-1}$ at midgap) for dry oxides thermally grown on Si. The relative ineffectiveness of hydrogen for passivating defects at the SiO_2/SiC interface could be because- (i) majority of interfacial defects are not susceptible to hydrogen or (ii) thermodynamically unstable processing conditions for H incorporation and H-defect bond formation. The rationale behind using Pt as the gate metal is derived from the second reason. Pt is well known for its surface catalytic properties in dissociating H_2 and to getter H. In fact, efficient catalytic gate SiC gas sensors have been built using Pt as the gate metal.[17] Thus, using Pt as the gate metal may favor the hydrogen incorporation into SiO_2 and lead to subsequent defect passivation. In the following section, we discuss experiments that quantify these processes.

Effect of a metal over-layer for hydrogen (deuterium) uptake

Interface trap density measurements for NO passivated capacitors having Pt and Mo as gate metals that underwent annealing in H_2 under identical conditions (500°C for 1

h) are shown in Fig. 6.2. Trap density in the Pt/H_2 samples at around 0.1 eV below the conduction band-edge are about 30% lower than the 'NO only' sample. On the contrary, the D_{it} profile of the Mo/H_2 sample is almost identical to the 'NO only' sample; suggesting that the effectiveness of hydrogen passivation strongly depends on the type of metal present on the sample surface.

Hydrogen (deuterium) concentrations in samples prepared similarly were measured using NRA and SIMS in an effort to correlate hydrogen incorporation with the electrical measurements. Measurements were made with the metal intact and after etching the metal with a H_2SO_4 + HNO_3 (3:1) solution to determine the D incorporation in the SiO_2/SiC (oxide, interface and possibly in the SiC) structure. Results from three sets of samples having (i) Pt over-layer (ii) Mo over-layer and (iii) no metal; that underwent identical deuterium anneals at 500°C for 1h are summarized Table 6.1. All values have been corrected for 'ion-induced D desorption' from the samples as described in the following section. The total deuterium (D) content in the entire MOS structure for both Pt and Mo samples was ~ 10^{15} atoms/cm^2; but the D content in the underlying oxide (metal etched) for the Mo sample was very close to the detection limit of NRA (~ 1 x 10^{13} atoms cm^{-2}). On the other hand, the areal density of D in the oxide underlying Pt was determined to be 3.28 x 10^{14} atoms cm^{-2} - almost two orders of magnitude higher than the Mo sample. (No trace of D could be detected in the sample after etching the SiO_2 completely, indicating less than 10^{13} atoms cm^{-2} of D in the SiC.) For the sample without a metal over-layer, no D was detected within the sensitivity of NRA. Utilizing the higher sensitivity of SIMS technique, the amount of D in this sample was determined to be approximately 1 x 10^{12} atoms cm^{-2}, below the detection limits of NRA. These results

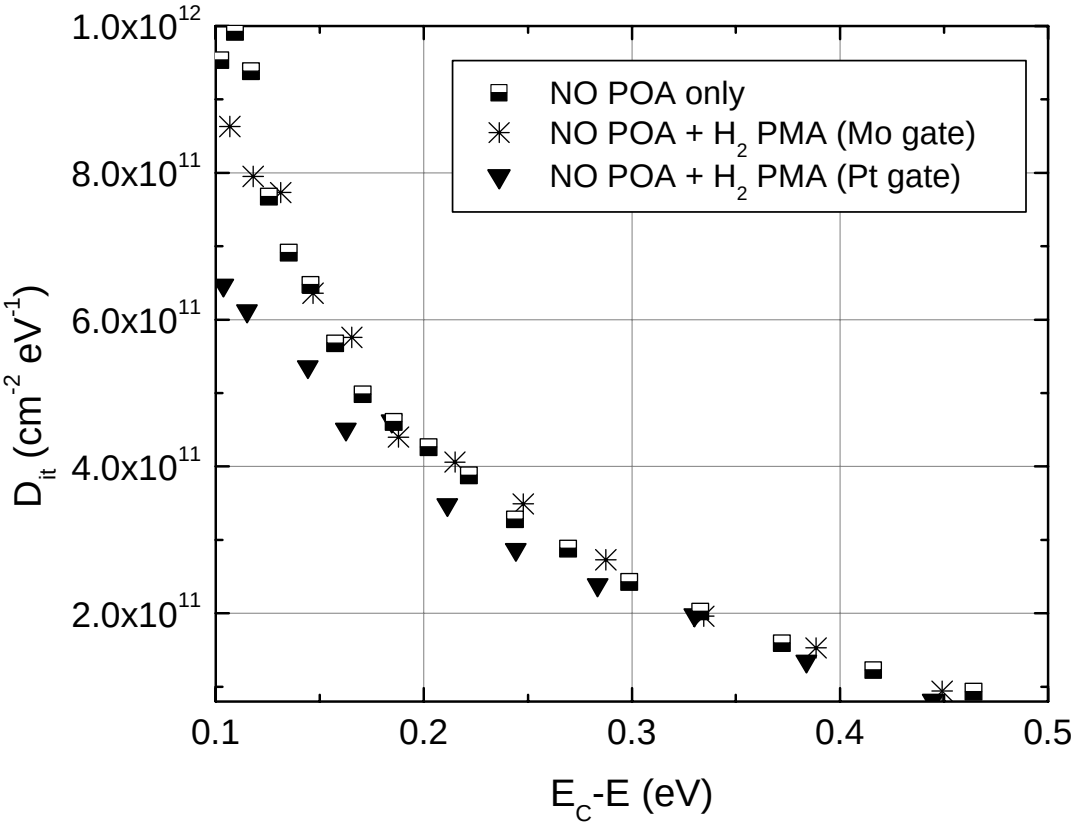

FIG. 6. 2 Interface state densities near the conduction band-edge of 4H-SiC for NO passivated samples that further underwent H_2 annealing with Mo and Pt over-layers. At $E_c - E \approx 0.1$ eV, D_{it} for the Pt/H_2 is about 30% lower than the 'NO only' reference sample. D_{it} of the Mo/H_2 sample is almost equal to the 'NO only' case.

Table 6. 1 Comparison of D areal density measurements from NRA and SIMS. All D anneals were carried out in flowing D_2 at 500°C for 1h. Thickness of Pt and SiO_2 layers were ~60 nm and 45-50 nm respectively.

SiO_2 over-layer	**NRA metal/SiO_2/ SiC ^{2}H atoms/cm^2**	**SIMS metal/SiO_2/ SiC ^{2}H atoms/cm^2**	**NRA SiO_2/SiC(metal etched) ^{2}H atoms/cm^2**	**SIMS SiO_2/SiC(metal etched) ^{2}H atoms/cm^2**	**NRA Near interface ^{2}H atoms/cm^2**	**SIMS Near interface ^{2}H atoms/cm^2**
Pt	1.50×10^{15}	2.4×10^{15}	3.28×10^{14}	3.2×10^{14}	1.66×10^{14} *	2.5×10^{14} **
Mo	1.04×10^{15}	-	$\sim 1.0 \times 10^{13}$	-	-	-
None	-	-	< sensitivity of NRA	1.0×10^{12}	-	8.0×10^{11}

* Oxide etched to ~3.0 nm

** FWHM of ^{2}H distribution ~3.5 nm

clearly indicate the effectiveness of the Pt layer in the hydrogen up-take kinetics. Macroscopically, a mechanism for the hydrogen incorporation could involve the following steps:

(1) Dissociation of H_2 molecules into atomic H on the surface of Pt aided by the catalytic property of Pt.

(2) Subsequent diffusion of atomic H into SiO_2, with the H enriched metal acting as a diffusion source.

(3) Passivation reaction at the interface with H susceptible defects.

For the Mo coated sample, a possible reason for relatively low hydrogen concentrations in the oxide could be the formation of a Mo-H compound that renders the H immobile for diffusion into the oxide.

Ion induced D desorption

Previous studies have shown that H and D can undergo desorption from thin films under the influence of the probing beam during ion beam analysis.[18,19] In the MeV energy range, incident ions lose energy in the solid mainly by inelastic electronic collisions, which result in electronic excitations. These excited electrons can produce H(D) bond breaking, resulting in loss of D atoms from the sample. In some cases, mobile hydrogen atoms may re-combine to form the more stable H_2. As shown previously by Adel *et al.*,[19],desorption by this process gives rise to similar non-linear behavior of hydrogen loss with dose as shown for our data in Fig. 6.3.

This hydrogen loss effect was also observed in the present work for $Pt/SiO_2/SiC$ and SiO_2/SiC samples, with the effect being comparatively smaller for the Pt coated samples. Thus, values obtained by NRA need to be corrected to avoid under-estimation

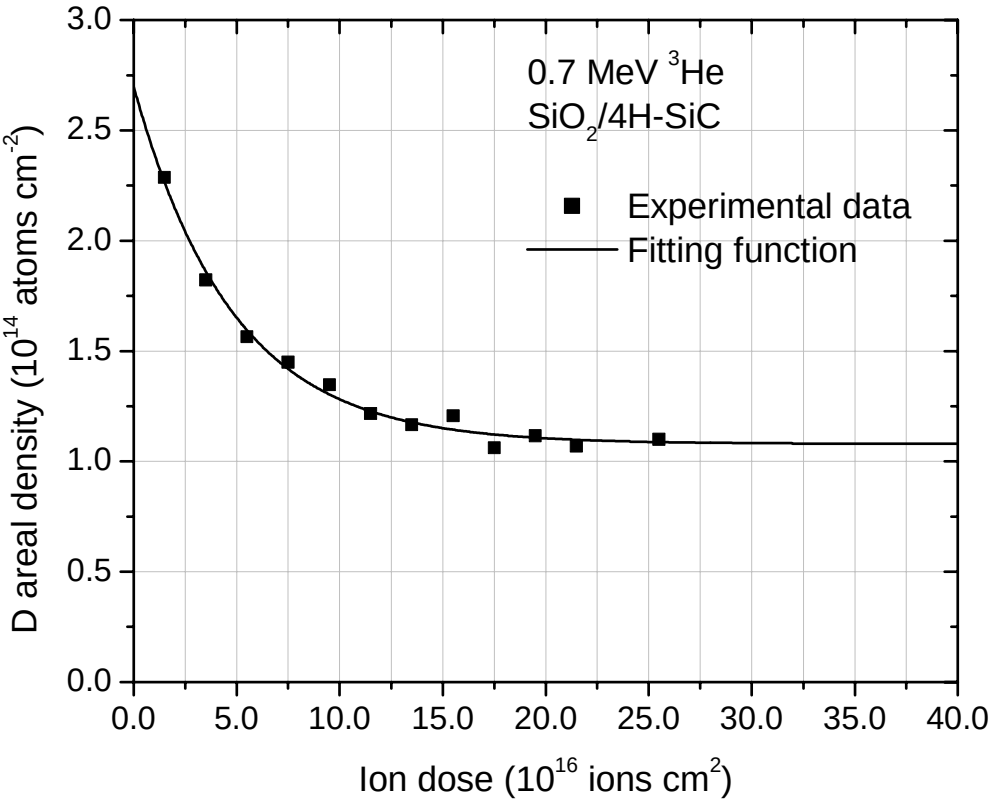

FIG. 6. 3 D loss from SiO_2/4H-SiC as a function of 0.7 MeV ^{3}He ion beam dose during NRA measurements. This curve has been used to obtain correction factors for the NRA measurements as described in the text.

of the 'true' D content. The measured D content in a SiO_2/SiC (no Pt) sample has been plotted as a function of ion dose as shown in Fig 6.3. An initial decay followed by a saturation regime is a characteristic of ion-induced D loss. The data has been fitted with the function:

$$y = y_0 + y_1 e^{-\frac{q}{q_1}} \tag{6.1}$$

where y is the experimental D content and q is the ion dose, y_0, y_1 and q_1 are fitting constants. This equation is an approximation to the form shown in ref. 19 where the loss mechanism is based on second-order kinetics associated with the release of H and the formation of H_2. Extrapolating this curve to zero allows us to determine the areal density at zero dose or the 'true' D areal density in the sample. (The typical dose required for detecting $\sim 10^{14}$ atoms cm^{-2} is around 10^{16} cm^{-2}.) Using this value, correction factors as a function of dose can be obtained (not shown). All NRA areal density values reported in this article have been corrected for ion induced desorption.

Deuterium incorporation at the SiO_2/SiC interface

Nuclear reaction analysis via ^2H (^3He,p) ^4He is an effective way to measure the total deuterium incorporation non-destructively, but suffers from poor depth resolution. SIMS, which has superior depth resolution, was used to obtain complete concentration profiles of deuterium as a function of depth. Comparison of SIMS results with NRA is summarized in Table 6.1. The SIMS samples comprised the following: (a) Reference SiO_2/4H-SiC sample, no D anneal (b) SiO_2/4H-SiC; D anneal at 500°C for 1h with no metal over-layer (c) Pt/SiO_2/4H-SiC, same D anneal as (b) and (d) Same as (c) but Pt

etched before SIMS measurement. All samples underwent NO post-oxidation anneals under conditions previously described in the experimental section. Elemental profiles of sample (a) and (b) are shown in Fig 6.4. No D was detected in sample (a) as expected; profiling of ^{1}H revealed the presence of approximately 2.3 x 10^{13} atoms cm^{-2} of ^{1}H in the SiO_2/SiC near-interfacial region. A part of this H corresponds to the inherent hydrogen at the SiO_2/SiC interface - unintentionally incorporated during processing, possibly from minute amounts of water vapor present during oxidation or from the gate metal. It should be noted that interface defect passivation by such 'intrinsic' hydrogen is always a possibility and the 'unpassivated' D_{it} data (Fig. 6.1) includes its effects. Previous studies by Afanas'ev et. al.[20] have shown that desorption of this intrinsic H by means of UV light results in an equal increase of interface positive and negative charge. This, in conjunction with a reversible depassivation-passivation behavior, suggested the presence of ~1.5 x 10^{12} cm^{-2} P_b-like amphoteric dangling bond centers at the SiO_2/4H-SiC interface. In the present work, we set aside 'intrinsic H passivation' and concentrate only on the H incorporation by intentional H treatments during processing.

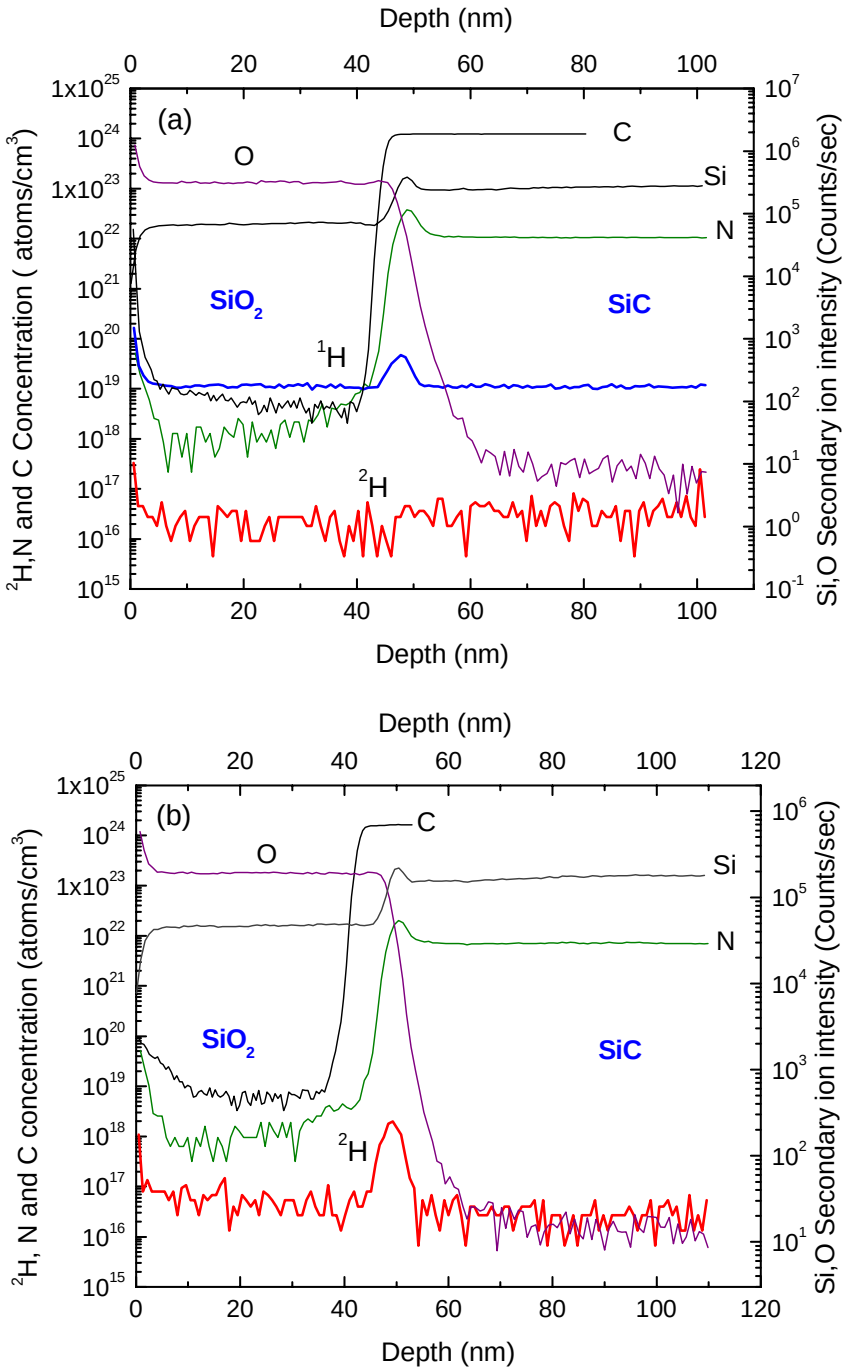

FIG. 6. 4 Elemental depth profiles obtained from SIMS for SiO_2(N)/4H-SiC samples (a) Reference sample, no D anneal. (b) D anneal at 500°C for 1 h, without any metal over-layer. The concentrations plotted for ^{1}H, ^{2}H, N and C are accurate in the oxide only. For Si and O, counts/sec has been plotted as a function of depth. N was detected as molecular SiN. The high N concentration in the SiC is an artifact due to interference of the $^{28}Si^{14}N$ signal with $^{29}Si^{13}C$.

For sample (b), which underwent D anneal without a metal over-layer (see Fig. 6.4 (b)), interfacial D can be quantified as 8.0 x 10^{11} atoms cm^{-2}. In the case of SiO_2/Si, as reported by Wilde *et al.*,[21] annealing a 41.5 nm oxide layer at 400°C for 40 min in 260 mbar H_2 results in the incorporation of (2.6 ± 0.4) x 10^{14} atoms cm^{-2} at the near-interfacial region. This is more than two orders of magnitude higher than H incorporation at the SiO_2/SiC interface, the oxide thickness and anneals conditions being similar. The difference in interfacial hydrogenation kinetics strongly suggests different nature of interfacial reactions at the two interfaces.

Depth profiles of deuterium of samples (c) and (d) are shown in Figs. 6.5 (a) and 6.5 (b). In the entire Pt/SiO_2/SiC structure, accumulation of D is observed at the two interfaces - Pt/SiO_2 and SiO_2/SiC. This 'bimodal' profile was also confirmed by NRA (results not shown), performed by oxide (or metal) etch steps in between each measurement to obtain a 'continuous' D concentration profile. Such a distribution is consistent with a mechanism suggested above where D diffusion through the Pt layer is much faster than diffusion through the oxide, which in turn is much faster than diffusion into SiC. SIMS profile for the sample with Pt etched (i.e sample (d)) shows almost 80% (2.5 x 10^{14} atoms cm^{-2}) of the D in the oxide at the SiO_2/SiC interface, a distribution having a full width at half maxima (FWHM) of ~3.5 nm within the depth resolution of SIMS. The same distribution looks much wider for the Pt coated sample (Fig. 6.5 (a)) as a result of poorer depth resolution due to greater samples thickness. Also, D accumulation at the Pt/SiO_2 interface is not clearly visible in Fig. 6.5 (b), possibly due to the inaccuracy of the SIMS technique very near the sample surface and/or location of most of the D on the 'Pt side' of the interface. The amount of near-interfacial D greatly

exceeds the observed reduction in trap density (Figs. 6.1 and 6.2), as in the case of the SiO_2/Si interface.[21] This could be due to the presence of H reaction sites in the near interfacial oxide region in the form oxygen deficient defects (sub-oxide) as suggested for Si/SiO_2.[22]

Deutrium uptake in the oxide and interface as a function of annealing temperature

To study the kinetics of D uptake, NRA was performed on samples with similar oxide thickness (45-50 nm), and Pt over-layers (~120 nm) that were annealed in flowing D for 1h at temperatures ranging from 300°C-500°C. (Thicker Pt layers were used for these experiments solely to make the samples dimensionally comparable to MOSFETs fabricated by similar processing, reported elsewhere.[10]) Areal density of D in the oxide for 500°C anneal was ~ 10% lower than that reported in the last section, suggesting that the D uptake is independent of the thickness of Pt for 60-120 nm. The D incorporation in the oxide is strongly dependent on annealing temperature - the D content keeps increasing with increase in temperature as shown in Fig. 6.6 (a). It is important to note that the data in Fig. 6.6 (a) represents the sum of the D in the bulk of the oxide and at the SiO_2/SiC interface. From an Arrhenius analysis of this data (see appendix (I)), an

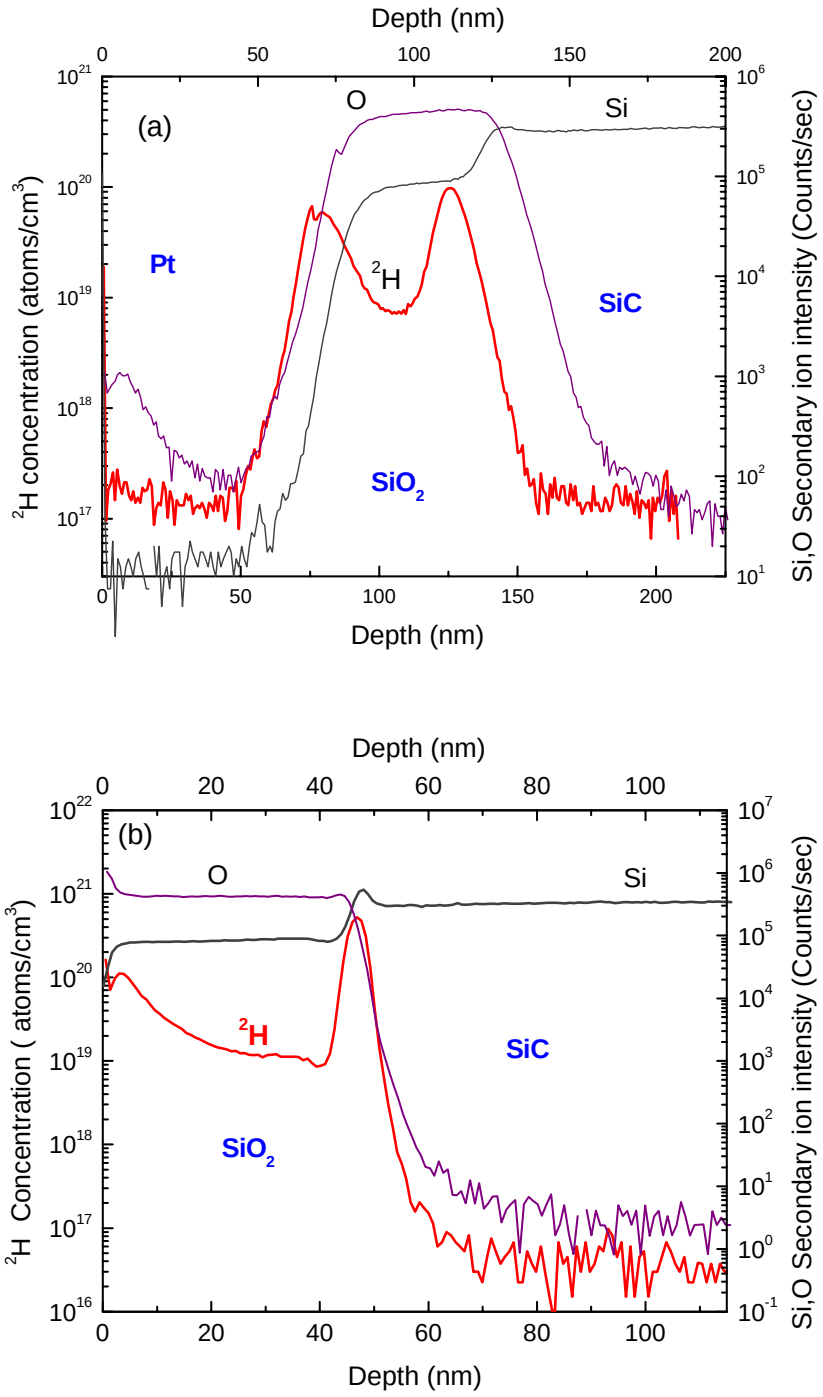

FIG. 6. 5 Elemental depth profiles obtained from SIMS for Pt/SiO_2(N)/4H-SiC samples annealed in D at 500°C for 1h (a) with Pt layer intact (b) Pt layer etched. The concentrations plotted for ^{2}H, N and C are accurate in the oxide only. For Si and O, counts/sec has been plotted as a function of depth.

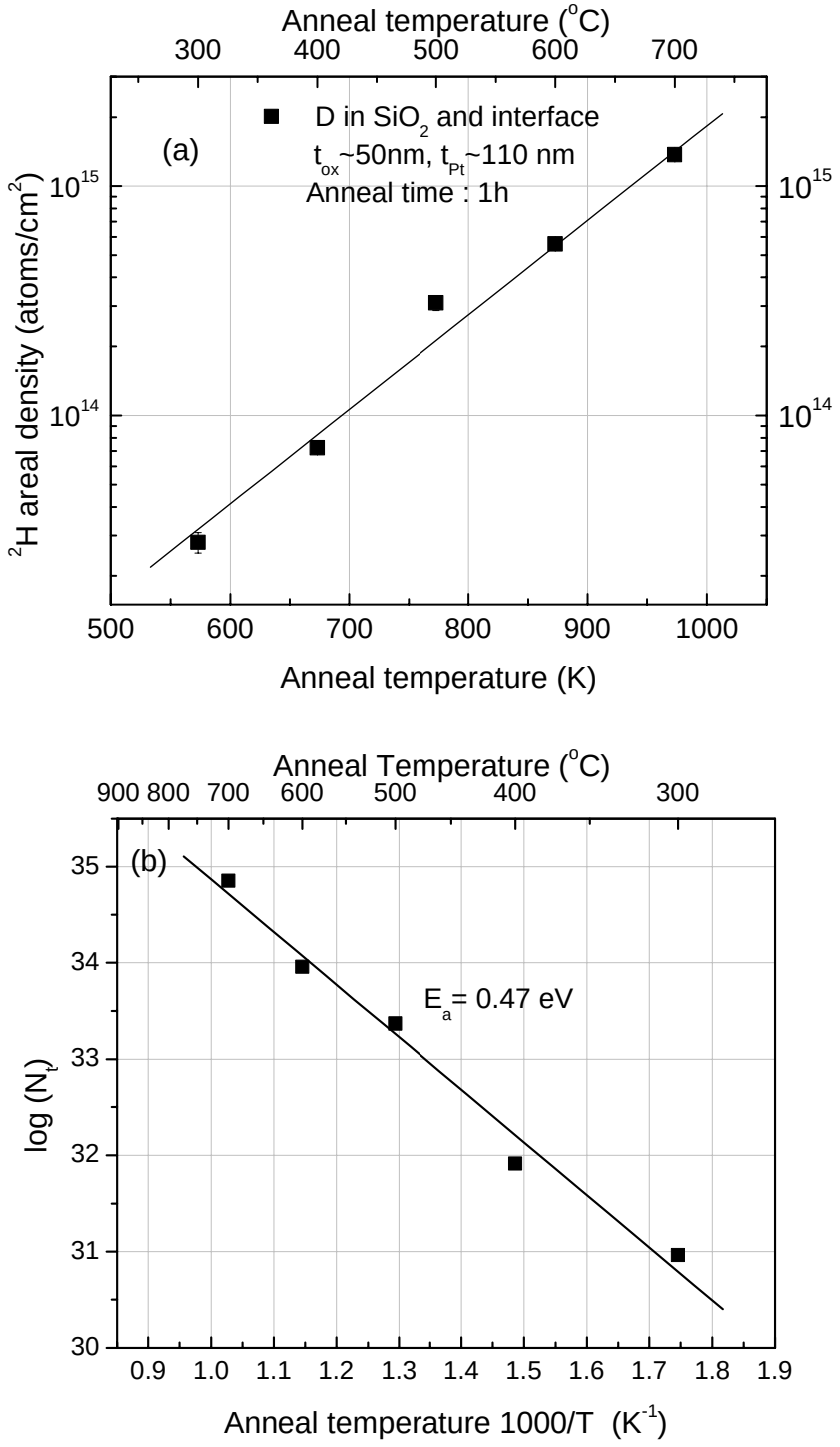

FIG. 6. 6 (a) D uptake kinetics in the temperature range 300°C-700°C for 1h PMA in presence of Pt. The D areal density reperesents the sum of the D incorporated into the bulk of the oxide and at the SiO_2/SiC interface. The straight line is only a guide to the eye. (b) Arrhenius plot of the same data following the procedure described in appendix (I). The effective activation energy for deuterium uptake into the oxide is estimated to be 0.47 eV.

apparent activation energy of 0.47 eV is determined for D uptake in the oxide as shown in Fig. 6.6(b). This is the Pt induced reduced effective activation barrier for D uptake into the oxide. Near-interfacial D content on the same samples was measured after etching the oxides to 1.4-3.0 nm. Assuming the D concentration to be constant close to the interface, the near-interfacial D concentration (atoms cm^{-3}) was estimated as a function of annealing temperature, as shown in Fig. 6.7. The interfacial D concentration increases with annealing temperature, in stark contrast with post-oxidation annealing of the SiO_2/Si interface, where the H uptake is suppressed above 430°C due to the desorption of H from the interface.[21]However, although the amount of interfacial D(H) increases with temperatures; higher temperatures may not be advantageous for device processing as samples annealed in H at 600°C have the same trap density compared to the samples annealed at 500°C (data not shown). Furthermore, the quality of the Pt as the gate metal degrades at anneal temperatures greater than 600°C - possibly due to the reaction of the Pt with the underlying SiO_2; considerably reducing device yield.

Thermal stability of D in SiO_2/SiC

To evaluate the thermal stability of the D incorporated into the SiO_2/SiC structure, oxides deuterated by 500°C, 1h D anneals were further annealed in an inert atmosphere of flowing Ar from 500°C-900°C for 15 min. The Pt over-layer was etched before the Ar anneal. NRA measurements were made before and after the Ar anneal to determine the amount of D desorbed. The fraction of D remaining (N/N_0) after desorption has been plotted as a function of desorption anneal temperature in Fig. 6.8 (a). Broadly, two

thermal desorption regimes were observed in the range 500°C to 900°C. The first occurs in a relatively narrow temperature range from around 500°C to 600°C and results in the

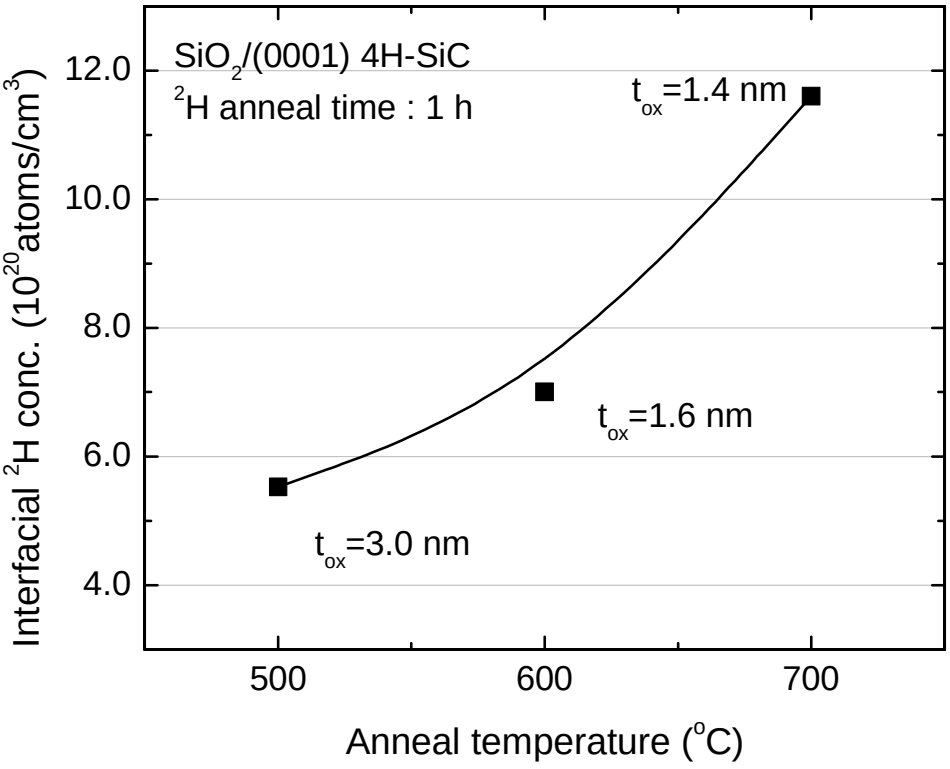

FIG. 6. 7 Near interfacial D concentrations as a function of anneal temperature. The solid line is a guide to the eye only. All samples had a Pt over-layer during the D anneals. Initial oxides of thickness 45-50 nm were etched down to the thickness shown in the figure. The near-interfacial D concentrations (atoms cm^{-3}) were calculated from the areal densities (atoms cm^{-2}) measured by NRA assuming the uniform concentrations close to the interface.

desorption of about 90% of the entire D in SiO_2/SiC. The second desorption occurs at 900°C, where the concentration of D in the sample gets close to the detection limit of NRA. No measurable desorption was observed in the range 650°C-900°C. A similar result reported in a previous work on deposited SiO_x (N,H) films was attributed to the presence of two major classes of Si-H bonding, one more stable than the other depending on the bonding configuration and environment (different nearest neighbors).[23] This hints at the presence of similar kinds of H-bonding in SiO_2/SiC, although more experiments need to be perfomed to understand the detailed H chemistry at the interface and in the bulk of the oxide. Furthermore, using NRA, it is difficult to distinguish between bulk-oxide D and near-interfacial D in the desorbed species. However, from the previous SIMS and NRA data (Table 6.1), we know that majority of the D resides at the interface for 500°C up-take anneals - suggesting that majority of the desorbed species is also near-interfacial D. Using a first order desorption kinetics model for the first desorption temperature range 550°C-600°C as described in the appendix (II), an activation energy of ~2.1 eV for desorption has been determined. The Arrhenius plot of the relevant parameters (see appendix) is shown in Fig. 6. 8(b). The higher activation energy for desorption compared to uptake suggests thermally stable D bonds in the oxide (and interface). It is worth mentioning that the activation energy for dissociation of H-passivated P_b defects at the Si/SiO_2 interface is 2.83 ± 0.02 eV, as determined by Stesmans.[24] It is important to note that the activation energies reported here (both uptake and desorption) are 'effective activation energies' of the processes. However, the nature of H bonds in the oxide and at the interface could have diverse configurations, leading to

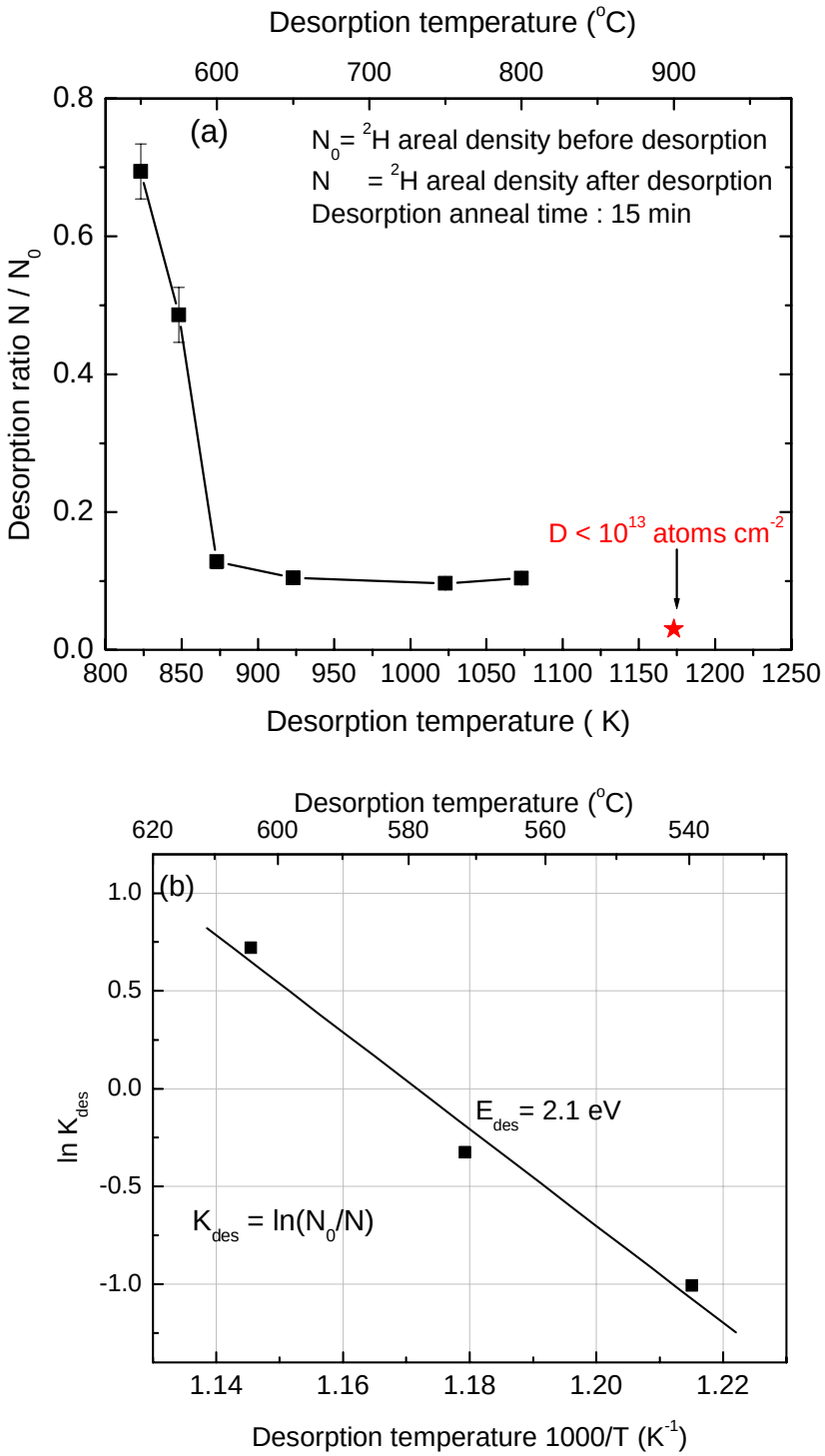

FIG. 6. 8 (a) Kinetics of D thermal desorption from SiO_2 and SiO_2/SiC interface (~80% of the D is near-interfacial) in the temperature range 500°C to 900°C. The vertical axis represents the fraction of D remaining in the sample after desorption anneal. The desorption kinetics has two regimes- from ~500°C to 600°C; and temperatures greater than 900°C respectively. (b) Arrhenius analysis of the data in the temperature range 550°C to 600°C (see appendix II) . The effective activation energy for D desoprtion is estimated to be 2.1 eV.

multiple activation energies. Investigations are therefore necessary to understand the chemical nature of H and understand the vital role of hydrogen in passivating electrically active defects at the SiO_2/SiC interface. Such studies can lead to optimized processing for development of efficient and reliable SiC MOS devices.

Summary and conclusions

Hydrogen incorporated at the SiO_2(N)/4H-SiC interface via post-metallization annealing of 4H-SiC MOS capacitors results in about 20% reduction of interface trap density near the conduction band-edge. Employing Pt as the gate metal results in significantly higher incorporation of H and subsequent lowering of trap densities. Kinetics of hydrogen uptake in the presence of Pt are found to be monotonically increasing with anneal temperature in the range 300°C-700°C. Comparison of effective activation energies of uptake with desorption suggests that hydrogenation at 500°C in the presence of Pt is a kinetically favorable process for H uptake for the SiO_2/SiC system.

Acknowledgements

The authors thank J.A.Cooper (Purdue University) and T.Hmelo, W.M.Augustyniak, S.Pantelides (Vanderbilt University) for useful discussions. We would also like to acknowledge Evans East, East Windsor, NJ, for the SIMS experiments. This work was supported by DARPA under Contract No. N00014-02-1-0628 (Ingham Mack and John Zolper, technical managers).

References

[1] R. Schorner, P. Friedrichs, D. Peters, and D. Stephani, IEEE Electron Device Lett. **20,** 241-244 (1999).

[2] N. S. Saks, S. S. Mani, and A. K. Agarwal, Appl. Phys. Lett **76,** 2250 (2000).

[3] V. V. Afanasev, M. Bassler, G. Pensl, and M. Schulz, Phys. Status Solidi a **162,** 321 (1997).

[4] V. V. Afanas' ev, F. Ciobanu, S. Dimitrijev, G. Pensl, and A. Stesmans, Journal of Physics Condensed Matter **16,** 1839-1856 (2004).

[5] R. Buczko, S. J. Pennycook, and S. T. Pantelides, Phys. Rev. Lett. **84,** 943 (2000).

[6] J. L. Cantin, H. J. V. Bardeleben, Y. Shishkin, Y. Ke, R. P. Devaty, and W. J. Choyke, Phys Rev Lett **92,** 15502 (2004).

[7] H.-F. Li, S. Dimitrijev, H. B. Harrison, and D. Sweatman, Appl. Phys. Lett. **70,** 2028 (1997).

[8] G. Y. Chung, C. C. Tin, J. R. Williams, K. McDonald, M. D. Ventra, S. T. Pantilides, L. C. Feldman, and R. A. Weller, Appl. Phys. Lett. **76,** 1713 (2000).

[9] J. R. Williams, T. Isaacs-Smith, S. Wang, C. Ahyi, R. M. Lawless, C. C. Tin, S. Dhar, A. Franceschetti, S. T. Pantelides, L. C. Feldman, G. Chung, and M. Chisholm, in *Mater Res Soc Symp Proc*, 2003, p. 371. (results also shown in chapter IV)

[10] S. Wang, T. Isaacs-Smith, C. Ahyi, J. R. Williams, S. Dhar, S. T. Pantelides, L. C. Feldman, and G. Y. Chung, 35th IEEE Semiconductor Interface Specialists Conference, December 9-11, 2004, San Diego, CA, in preparation.

[11] E. H. Nicollian and J. R. Brews, *MOS (Metal Oxide Semiconductor) Physics and Technology*, (John Wiley & Sons, New York, 1982).

[12] J. A. Cooper, Phys. Stat. Sol. (A) 162 (1997) 305.

[13] K. Fukuda, S. Suzuki, T. Tanaka, and K. Arai, Appl. Phys. Lett. 76(12) (2000) 1585.

[14] K. Fukuda, W. J. Cho, K. Arai, S. Suzuki, J. Senzaki, and T. Tanaka, Appl. Phys. Lett. **77,** 866 (2000).

[15] J. Senzaki, K. Kojima, S. Harada, R. Kosugi, S. Senzaki, T. Suzuki, and K. Fukuda, IEEE Elect. Dev. Lett. 23(1) (2002) 13.

[16] K. L. Brower, Phys. Rev. B **38,** 9657.

[17] P. Tobias, B. Golding, and R. N. Ghosh, IEEE Sensors J. **3,** 543 (2003).

[18] F. Corni, A. Monelli, G. Ottaviani, R.Tonini, G. Queirolo, and L. Zanotti, J. of Non-Cryst. Solids **216,** 71 (1997).

[19] M. E. Adel, O. Amir, R. Kalish, and L. C. Feldman, J. of Appl. Phys. **66,** 3248 (1989).

[20] V. V. Afanas' ev, M. Bassler, G. Pensl, and A. Stesmans, in *Oxidation of silicon carbide: Problems and solutions, Proceedings of the international conf. on Silicon Carbide and Related Materials (2001), Tsukuba, Japan, edited by S. Yoshida, S. Nishino, H. Harima and T. Kimoto* (Trans Tech Publications, UK, 2002), p. 961.

[21] M. Wilde, M. Matsumoto, K. Fukutani, Z. Liu, K. Ando, Y. Kawashima, and S. Fujieda, J. Appl. Phys. **92,** 4320 (2002).

[22] V. V. Afanas' ev and A. Stesmans, Appl. Phys. Lett. **71,** 3844 (1997).

[23] A. Borghesi, A. Sassella, B. Pivac, and L. Zanotti, Solid State Commun. **100,** 657 (1996).

[24] A. Stesmans, Phys. Rev. B **61,** 8393 (2000).

Appendix

I. Hydrogen uptake kinetics

Using a simple uptake rate equation, the D incorporation rate in the oxide at any temperature can be expressed as:

$$\frac{dN}{dt} = k_{+} \qquad (6A.1)$$

where $\frac{dN}{dt}$ is the rate of D uptake [atoms cm^{-2} s^{-1}]; and k_{+} represents the rate constant [atoms cm^{-2} s^{-1}] .

The temperature dependence of k_{+} can be expressed as an Arrhenius function

$$k_{+}(T) = Ae^{-\frac{E_a}{K_B T}} \tag{6A.2}$$

where the pre-exponential A is a constant, E_a is the activation energy for the uptake process, K_B is the Botlzmann's constant (8.617 x 10^5 eV K^{-1}) and T is the temperature [K^{-1}]

Solving equation (6A.1) and equating the solution to (6A.2) gives us

$$-\frac{E_a}{k_B}\frac{1}{T} + const. = \ln N_t \tag{6A.3}$$

where N_t represents the areal density of D in the oxide for fixed anneal time (1 h in our case). Equation (6A.3) can be plotted as shown in Fig. 6.6(b) to determine E_a.

II. Hydrogen desorption kinetics

Using a first order desorption kinetics model, the desorption rate can be expressed as :

$$\frac{dN}{dt} = -k\_.N(t) \tag{6A.4}$$

where $\frac{dN}{dt}$ is the desorption rate [atoms cm^{-2} s^{-1}];

$N(t)$ represents areal density of D in the sample [atoms cm^{-1}];

$k\_$ is the desorption rate constant at any temperature T having units [s^{-1}]

Equation (6A.1) has the well known solution :

$$k\_ = \frac{1}{t_0}.\ln\frac{N_0}{N(t_0)} \tag{6A.5}$$

where t_0 represents the desorption anneal time , N_0 and $N(t_0)$ are D content at t=0 and $t = t_0$ respectively. (in our case t_0 =15 mins)

Temperature dependence of the rate constant can be expressed in a similar manner as equation (6A.2) :

$$k\_(T) = Be^{-\frac{E_{des}}{K_B T}} \tag{6A.6}$$

where the pre-exponential term B is a constant, E_{des} is the activation energy for desorption, K_B is the Botlzmann's constant (8.617 x 10^5 eV K^{-1}) and T is the temperature [K^{-1}]

Equating (2) and (3) and taking logarithm of both sides yields:

$$-\frac{E_{des}}{k_B}.\frac{1}{T} + const = \ln(\ln\frac{N_0}{N_{15\,\min}}) \tag{6A.7}$$

$\frac{N_0}{N_{15\,\min}}$ at different temperatures are known quantities from Fig. 6.8(a). Thus, equation (6A.7) can be plotted to determine the desorption activation energy E_a as shown in Fig. 6.8(b).

CHAPTER VII

SUMMARY AND CONCLUSIONS

Silicon Carbide is a wide band-gap semiconductor that possesses attractive properties for electronic applications in high temperature and high power environments. Among the available polytypes, 4H-SiC is the most promising for metal-oxide-field-effect-transistors (MOSFETs). In any MOS system, the quality of the interface between the oxide and the semiconductor has a great impact on the performance of the device. In the case of SiO_2/4H-SiC, imperfections such as the presence of carbon clusters, silicon sub-oxides and Si and C dangling bonds at the interface result in a high density of electrically active defects. These defects trap and scatter carriers in the inversion layer of the MOSFET resulting in a severe degradation of the inversion layer mobility. Reduction of these defects is critical for the realizing SiC MOS devices that operate to their full potential.

This dissertation work focuses on understanding the effects of atomic scale modification of the SiO_2/4H-SiC interface to produce interfaces with lower defect densities and improved electronic properties. The main new findings of this work are the following:

- Nitridation via post-oxidation annealing in NO results in significant reduction of interface trap densities near the conduction band-edge of 4H-SiC. Nitrogen incorporated at the interface by this process has a key role in the trap passivation process. Presence of nitrogen susceptible defects has been observed for the first

time for interfaces formed on different crystal faces ((0001) Si, $(11\bar{2}0)$ a-face and the $(000\bar{1})$ C-face); crystal faces that have significantly different oxidation rates.

- Anisotropy in nitridation rates have been observed for the first time at SiO_2/4H-SiC interfaces. Nitridation kinetics among the $(000\bar{1})$ C-face, $(11\bar{2}0)$ a-face and (0001) Si-face follow the same trend as in their oxidation rates: C-face ≥ a-face > Si-face. Interfacial N incorporation by post-oxidation annealing in NO occurs by the interplay of two processes – N enrichment by NO and a competing O_2 related N removal process. An ad hoc model based on these two mechanisms has been proposed to explain the experimental nitridation kinetics.

- Annealing nitridated interfaces in hydrogen results in a further reduction of trap densities. Presence of a catalytic metal like Pt during the hydrogen anneals results in kinetically favorable conditions for hydrogen uptake at the SiO_2/4H-SiC interface. Hydrogen passivation is found to be a relatively smaller effect compared to nitrogen passivation, which suggests a lower density of hydrogen susceptible defects at the SiO_2/4H-SiC interface.

- Record low interface trap densities have been achieved on the (0001) Si face and $(11\bar{2}0)$ a-face by using the combination of nitrogen and hydrogen passivation. Excellent field effect mobilities have been demonstrated in lateral test MOSFETs passivated by this process.